

SYNTHESIS OF A CFD BENCHMARK EXERCISE BASED ON A TEST IN THE PANDA FACILITY ADDRESSING THE STRATIFICATION EROSION BY A VERTICAL JET IN PRESENCE OF A FLOW OBSTRUCTION

**Michele Andreani^{*(1)}, Avinash J Gaikwad⁽²⁾, Sunil Ganju⁽³⁾, Bhuvaneshwar Gera⁽³⁾,
Sergey Grigoryev⁽⁴⁾, Luis Enrique Herranz⁽⁵⁾, Risto Huhtanen⁽⁶⁾,
Vivek Kale⁽²⁾, Anton Kanaev⁽⁴⁾, Ralf Kapulla⁽¹⁾, Stephan Kelm⁽⁷⁾,
Jongtae Kim⁽⁸⁾, Takeshi Nishimura⁽⁹⁾, Domenico Paladino⁽¹⁾,
Sidharth Paranjape⁽¹⁾, Berthold Schramm⁽¹⁰⁾, Medhat Sharabi⁽¹⁾,
Feng Shen⁽¹¹⁾, Bai Wei⁽¹¹⁾, Daqiang Yan⁽¹¹⁾, Rongjin Zhang⁽¹¹⁾**

⁽¹⁾ Paul Scherrer Institut (PSI), Switzerland

⁽²⁾ Atomic Energy Regulatory Board (AERB), India

⁽³⁾ Bhabha Atomic Research Center (BARC), India

⁽⁴⁾ Nuclear Safety Institute, IBRAE, Russian Federation

⁽⁵⁾ Centro de Investigaciones Energéticas, Medioambientales y Tecnológicas (CIEMAT), Spain

⁽⁶⁾ VTT Technical Research Centre of Finland Ltd, Finland

⁽⁷⁾ Forschungszentrum Jülich (FZJ), Germany

⁽⁸⁾ Korea Atomic Energy Research Institute (KAERI), Korea

⁽⁹⁾ Regulatory Standard and Research Department,
Secretariat of Nuclear Regulation Authority (S/NRA/R), Japan

⁽¹⁰⁾ Gesellschaft für Anlagen- und Reaktorsicherheit (GRS), Germany

⁽¹¹⁾ State Power Investment Corporation Research Institute (SPICRI), People's Republic of China

* Corresponding author: Michele Andreani

Laboratory for Scientific Computing and Modelling

Paul Scherrer Institut, Forschungsstrasse 111, 5232 Villigen PSI, Switzerland

Tel.: ++41 56 310 2687

Fax: ++41 56 310 4481

E-Mail: michele.andreani@psi.ch

Abstract

1
2 The benchmark exercise discussed in this paper was conducted within the OECD/NEA project
3
4 HYMERES. The specific experiment in the PANDA facility chosen for the present benchmark
5
6 addresses the stratification erosion induced by a vertical steam jet, which originates from the exit of a
7
8 circular pipe located below the bottom of the helium-rich layer. The mixing is somewhat slowed
9
10 down by a small circular plate above the jet source. The exercise consisted of a blind phase, and an
11
12 open phase. Two sets of blind simulations were requested: one set obtained using a “common model”,
13
14 and a second set produced by a “best estimate” model. For the “common model”, a list of
15
16 recommendations was given, whereas for the “best estimate” model, each participant was free to
17
18 choose the modelling approach. The submitted results for the erosion times were in a large band, and
19
20 especially the large differences in the results with the “common model” were not expected. The
21
22 results of the best estimate simulations showed that the combination of mesh and modelling approach
23
24 can lead to a wide spread of results. The most important difficulty in interpreting the results and
25
26 finding the reason of the large deviations was the lack of information on the velocity field
27
28 downstream of the obstruction. Therefore, for the open phase extended data from auxiliary, “zero”
29
30 tests (for similar conditions but without helium layer) were provided to the participants to permit a
31
32 more basic validation of their models, using a “multi-step approach”. The step-by-step validation
33
34 permitted some progress with respect to some of the items identified in the blind benchmark.
35
36 However, large discrepancies with data in the final analyses of the test are observed, which cannot be
37
38 easily attributed to specific model deficiencies or insufficient detail of the mesh. These results raised
39
40 some questions in relation to best practice guidelines for the use of CFD codes for containment
41
42 analysis and indicated needs for further CFD-grade experiments.
43
44
45
46
47
48
49
50
51


52 **Keywords:** Containment, stratification erosion, buoyant jet, benchmark, PANDA
53
54
55
56
57
58
59
60
61
62
63
64
65


1
2
3
4
5
6
7
8
9
10
11
12
13
14
15
16
17
18
19
20
21
22
23
24
25
26
27
28
29
30
31
32
33
34
35
36
37
38
39
40
41
42
43
44
45
46
47
48
49
50
51
52
53
54
55
56
57
58
59
60
61
62
63
64
65

Highlights:


- A benchmark on gas stratification erosion was conducted using a test in the PANDA facility
- A large spread of results was observed in the blind calculations.
- The open phase was multi-step, using complementary tests with enhanced information on velocity field
- Progress was achieved, but several contributions still exhibited large discrepancies
- Results are strongly affected by the modeling of radiation heat transfer from and within the steam

1. INTRODUCTION


Hydrogen generated during a stulated) severe accident with core degradation is a major safety issue (Karwat et al., 1999; Breitung and Royl, 2000; Bentaib et al., 2015; Lopez-Alonso et al., 2017), because deflagration or detonation might challenge the structural integrity of the containment. The concern about hydrogen risk and the demand for additional research on accident scenarios and on mitigation measures grew after the Fukushima accident (Liang et al, 2015; Gupta, 2015; Nishimura, et al, 2015). In particular, hydrogen stratification can substantially increase the risk, as this could lead to local pockets of mixtures with high concentration of this flammable gas (Choi et al., 2001). A special concern is thus the build-up and persistence of stratification of hydrogen in certain regions, which has to be addressed by dedicated experimental research and accurate analyses (Smith, 2009). Various experimental programmes (Allelein et al., 2007; Deri et al., 2010; OECD/NEA THAI Project, 2010; Allelein et al., 2012; Studer et al., 2012; Paladino et al., 2013; Kapulla et al., 2014) and code validation activities (Schwarz et al., 2011; Kelm et al., 2016a; Andreani et al., 2016a; Sarikurt and Hassan, 2017; Abe et al., 2018) have included in-depth investigations on stratification formation and break-up/erosion processes. This research included, among others, the investigation on the interaction of a gas plume or jet with a density interface in an open space, typical of the situation in the dome of the containment. However, since the multi-compartment geometry of many containment designs is quite complex, it is necessary to assess the capability of the codes to simulate the effect of various structures on the evolution of the distribution of gases in the presence of flow obstructions. In particular, the effect on mixing of an obstruction at short distance from the origin of the efflux is of general interest (e.g., Noutsopolos and Yannopoulos, 1989), but only a few investigations with light gases exist in open literature (e.g., Chan and Jones, 1997). A first series of experiments in PANDA addressing this issue have been conducted within the HYMERES project.

HYMERES (HYdrogen Mitigation Experiments for REactor Safety) is the acronym for an OECD/NEA project (2013-2016), which is supported by thirteen countries and centered around experiments performed in the PANDA and MISTRA facilities, located at PSI in Switzerland and CEA in France, respectively (Paladino et al., 2012). The project includes various series of experiments (with helium used as simulant for hydrogen), where the mixing of a stratified atmosphere is controlled by jets or energy sinks/sources (such as heaters, coolers, etc.). In PANDA, stratified conditions, with a helium-rich layer at the top of one steam-filled vessel, are either initially prescribed or built during the transient. One of these experiments in PANDA 1_6_2) was chosen for the present benchmark, which is similar to the recent OECD/NEA PANDA Benchmark (Andreani et al., 2016a). It addresses again the stratification erosion induced by a vertical jet, but in this new test, with injection of steam instead of air, and with an obstruction above the pipe exit. The OECD /NEA PANDA benchmark indicated that even for simple conditions the successful application of CFD to containment flows is

1 still hindered by the special feature of the typical problems, i.e. long transients in very large fluid
2 domains. Under these conditions, the application of Best Practice Guidelines (Mahaffy et al., 2015)
3 proves to be very demanding, and often nearly impossible with the available project times and
4 computing resources. Benchmarking activities (especially based on blind predictions) are therefore
5 very important to reveal the weaknesses of modelling strategies established on the base of previous
6 experience when a new problem has to be tackled and sensitivity studies must be limited to a few
7 runs.
8
9

10
11
12
13 In order to enhance the interpretation of the comparison of the calculated results with the experimental
14 data, for the blind benchmark the participants were requested to submit two sets of results: one set
15 should be obtained using a “hmon model”, and a second set produced by a “best estimate” model.
16 For the “common model”, a list of recommendations was given with respect to initial and boundary
17 conditions (e.g., homogeneous initial vertical gas and wall temperatures, modelling of the injection
18 pipe), as well as concerning model selection (no condensation, no radiative heat transfer, standard k- ϵ
19 turbulence model). For the “best estimate” model, each participant was free to choose the modelling
20 approach that was considered to be the best suited to the physical problem investigated, also on the
21 base of previous experience, and to use refined representation of initial and boundary conditions. Each
22 participant was expected to submit only one set of results for each of the two models. The participants
23 were encouraged to use Best Practice Guidelines (BPG) to provide the most trustworthy set of results,
24 but only few participants could afford more than a mesh sensitivity study using two meshes.
25
26
27
28
29
30
31
32
33
34

35 Both sets of submissions, i.e. those using a “Common Model” (CM) and those using a “Best Estimate
36 Model” (BEM) model produced a large variety of results, leaving open a number of questions. The
37 open phase of the benchmark was then considered necessary to provide more information on the
38 importance of some physical effects and the capability of the various modelling strategies adopted by
39 the participants to address them.
40
41
42
43
44

45 The present paper reports the outcome of the benchmark. Results for the entire set of variables
46 requested are collected and discussed in Andreani and Paladino (2018), which will be referred to as
47 the Benchmark Report (2018). Here, only the main aspects of the benchmark are discussed. Since the
48 results of the id phase were already illustrated in Andreani et al. (2016b), the paper focuses on the
49 open phase of the benchmark.
50
51
52
53
54
55
56
57
58
59
60
61
62
63
64
65

2. THE EXPERIMENT

Only the essential information necessary for comparing the test results and the simulations is provided in this chapter. A complete presentation of the tests and of the main experimental results is included in a project report (Kapulla, et al., 2015a).

2.1 Configuration and test conditions

The PANDA facility (Paladino and Dreier, 2012) is a multi-compartment, large-scale thermal-hydraulics test rig located at the Paul Scherrer Institute (PSI), Switzerland. For these series of tests only the two upper vessels were used (Fig. 1, where the large manholes at the top of the vessels are also visible), which are 8 m in height and 4 m in diameter. In Fig. 1, the nominal conditions of the test are indicated. The PANDA vessels and the major internal penetrations/flanges are made of stainless steel. All external surfaces are insulated, and the heat losses have been experimentally determined over a broad range of temperatures. The experiment mainly addresses the evolution of the thermal-hydraulic variables in the vessel (injection vessel, on the left in the figure) where the initial stratification was created and the steam was injected. In the injection vessel (Vessel 1), a steam jet originates from a circular pipe located on the axis of the vessel and with an exit located 2 m below the bottom of the helium-rich layer (which starts at 6 m). The mixing is somewhat slowed down by a small circular plate (20 cm in diameter) also centered on the axis and positioned 1 m above the jet exit. The vessels are kept at approximately constant pressure (1.3 bar) during the test by venting the fluid to the atmosphere through a nozzle at the top of Vessel 2.

Prior to the test, saturated steam was injected in the vessels, and the fluid and vessel walls (as well as the obstruction plate) were thus heated to the target temperature, which was set to avoid wall condensation during the transient. Stratified steam/helium conditions then have been created in the test vessel by injecting helium above 6000 mm (Fig. 1). Just before the beginning of the test, a helium-rich layer occupies the region above the elevation of 5000 mm (measured from the lowest point on the inside of the vessel), the molar fraction of helium increasing non-linearly to about 0.22 at 8000 mm and above into the manhole space. The region of Vessel 1 below this layer and Vessel 2 are filled with steam. The air concentrations were between 0.1 and 0.2%. The measured helium molar fraction at time $t = 0$ as a function of elevation is also displayed in Fig. 1. All concentration measurements are subject to total combined uncertainties of <1%. The measured gas and wall temperatures immediately before the start of the transient were between 105 and 108 °C (nominal value: 108 °C). These values ensure that condensation (if any) could not play a role during the transient. All temperature measurements are subject to an uncertainty of ± 0.7 K.

1 The test was started by injecting superheated steam, the flow rate and the temperature being 60 g/s
2 and 150 °C, respectively. During the test, gas and wall temperatures at several locations were
3 measured, and helium concentration was measured at 6 elevations above the injection. Moreover, PIV
4 measurements in a zone of fluid initially immersed in the helium-rich layer (far above the plate)
5 provide average velocities and turbulent quantities, and thus some information on the interaction
6 between the jet and the stratified ambient (see below).
7
8
9

10 11 12 13 **2.2 Main results**



14 In the experiment, the **time histories** of gas temperatures and helium concentrations above the
15 injection describe the progression of the erosion process (Fig 2), **which** is characterized, at each
16 elevation, by helium concentration drop and temperature increase as a result of the rise of the leading
17 edge of the steam jet and associated mixing **unstable** zone to that height. Since the test was rather
18 fast (within 600 s the fluid in Vessel 1 was fully mixed), and the scanning rate of the mass
19 spectrometer is necessarily low, the time history of the erosion at the various elevations (which will be
20 used to get a representative measure of the global success of the simulations) was obtained from the
21 temperature measurements (scanning rate 0.5 Hz), using a **threshold of 120 °C** (T_{lim} in Fig. 2). This
22 procedure for defining the “erosion times” and comparing the measurements with code predictions at
23 the various locations is clearly not accurate, especially at elevations (notably the highest at 8 m) where
24 **temperature** has a slow and non-uniform increase. **Another option would have been to use the**
25 **times of the inflection points (maximum time derivatives of the temperature curves), but the results**
26 **would differ from those obtained with the used procedure at most by 50 s (at the highest elevation).**

27 The experimental values will be shown together with the results of the simulations in the next section.
28
29
30
31
32
33

34 Mean velocity measurements were obtained by PIV in a Field of View (FOV) located between the
35 elevations of 6300 and 7000 mm. Measurements and discussion of statistical errors are included in the
36 project report (Kapulla et al., 2015a). Since the averaging period was of 409 s (centred around $t_c =$
37 326.6 s), the use of this information for comparing the simulations with the data at specific times is
38 questionable. The use of the velocity measurements for assessment purposes is reconsidered in the
39 open phase of the benchmark, for which additional data for similar conditions over a larger region
40 above the plate (between 5000 and 7000 mm) are made available. Therefore, for the sake of the open
41 benchmark, results for velocities will not be discussed.
42
43
44
45
46
47
48
49
50
51
52
53
54
55

56 **3. RESULTS OF THE SIMULATIONS FOR THE BLIND BENCHMARK**




57 It was mentioned above that the participants in the benchmark were requested to submit two sets of
58 results, one using the “common model” (CM) and one with the “best estimate model” (BEM). The
59
60
61
62
63
64
65

1 specifications for the CM (Andreani et al, 2016b)  luded geometry, treatment of heat transfer at the
2 walls (heat losses, no radiation and no condensation), initial and boundary conditions, and prescribed
3 use of the  ndard high-Reynolds number k-ε turbulence model.

4
5
6 The participants were expected to deliver the times of the erosion progression, the time histories of
7 helium concentrations and gas temperatures at selected locations, as well as axial and transversal
8 profiles of gas temperature and velocity at various elevations, at selected times. Moreover, the
9 organisations delivered an accompanying document with some information on physical and numerical
10 models.
11

12
13
14
15 Not all organisations submitted both sets, and two organisations submitted results with two different
16 codes. There were thus 13 contributions with the CM and 10 with the BEM. Table 1 summarises the
17 submissions. In table 1, only the code used the total number of cells in the mesh, the main deviations
18 of the CM from the specifications and the differences between CM and BEM are listed.
19
20
21
22
23
24

25 **3.1 Results with the Common Model (CM)**

26
27 Table 1 shows that various codes (mostly commercial CFD codes) have been used, with a broad
28  etrum of meshes, from 20000 cells to more than 1 million. The CM simulations were mostly
29 performed with models complying with the specifications, the only important deviations being those
30 referring to initial and boundary conditions. The non-obvious effect of small differences in boundary
31 and initial conditions was not anticipated by some users. This is a good example of the importance of
32 the benchmarking activities for establishing CFD modelling strategies to be used for the analysis of
33 new problems. Therefore, the comparison with data of the simulations using inaccurate values of
34 steam injection temperature and initial helium concentration profiles is somewhat affected by this
35 deviation in the test conditions. For these contributions, the discrepancies with the data and other
36 simulations are easy to explain. However, also for the other contributions, a very broad variety of
37 results has been obtained. Figure 3 shows the time history of the erosion progression and, as example
38 of gas temperature time histories, the results for one elevation. It can be observed that the mixing time
39 (600 s in the experiment) is well predicted in only three simulations (AERB, IBRAE2 and PSIF),
40 whereas most submissions exhibit either a strong underprediction or overprediction. Considering the
41 essential elements of the setups for the simulations (Table 1), but also the additional information
42 provided, it is not obvious how to associate the success of the predictions to any specific difference
43 between models. Since the physical models (and their implementation in the codes) must be very
44 similar for all simulations, the differences in the prediction can  y be due to the mesh (refinement in
45 certain regions and mesh topology), numerical methods, and other effects and modelling options not
46 considered in the specifications (e.g. wall treatment).  therefore surprising that models with largely
47
48
49
50
51
52
53
54
55
56
57
58
59
60
61
62
63
64
65

1 different number of cells lead to comparable predictions, and, vice versa, the use of detailed models
2 with similar number of cells result in very large differences. Although post-test analyses (see below)
3 shed light on some of these apparently puzzling results, the observed spread suggests that the set-up of
4 a CFD simulation for a new problem is not a trivial task, and requires a careful evaluation of the
5 applicability of previous experience for different geometrical configurations and physical conditions.
6
7

8
9 Another interesting observation concerns the temperature rise: in all simulations (and at all elevations)
10 this is sharper than in the experiment, with the asymptotic temperature being much higher than the
11 measured value. The temperature trend therefore reveals a systematic difficulty to predict the erosion
12 process, which is not shown in most concentration histories (Fig. 4) where, because of the low data
13 frequency, the calculated sudden drop seems to be always in agreement with the experimental results.
14 The temperature distribution above the plate is, in general, reasonably well predicted in most
15 simulations, where the horizontal profiles, in agreement with the experiment, show low peaks along
16 the axis. Figure 5 shows, for example, the profile at some distance downstream the plate (Level G,
17 $z=5.63$ m). However, with the exception of one simulation, the profiles are systematically shifted
18 towards higher values, indicating that some mixing and/or heat transfer mechanism (convective or
19 radiative heat transfer) is not well predicted.
20
21
22
23
24
25
26
27
28

29 Indeed, it seems that most simulations over predicted the gas temperatures already in the region below
30 the plate. Figure 5 shows the temperature horizontal profile just below the plate (Level H, $z=4.97$ m)
31 at 150 s: the temperature drop between the pipe outlet and the plate along the axis is underpredicted.
32 This discrepancy, in principle, could be due to the fact that the codes predict perfectly symmetric
33 flow, whereas in the experiment the jet was not perfectly centred due to flow non-symmetry at the
34 pipe outlet, and thus the measured temperature does not represent the value (the maximum) at the jet
35 impingement point. On the other hand, the deviation could reveal unexpected difficulties in predicting
36 the broadening of the free jet. This question has been tackled in the open phase of the benchmark
37 (Section 4).
38
39
40
41
42
43
44
45
46

47 **3.2 Results with the Best Estimate Model (BEM)**



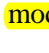
48
49 The simulations with the CM provided two main results: 1) even using very similar models (apart
50 from the mesh) very different results can be obtained, in spite of the use of meshing strategies that
51 could be considered “qualified” on the basis of previous experience with various tests in PANDA; 2)
52 large discrepancies between calculated and experimental results were obtained. With respect to this
53 second result, the agreement was expected to improve with the use of the BEM, where the participants
54 could make use of the best modelling approach according to their experience. This mostly resulted
55 (Table 1) in the use of a different turbulence model, the consideration of radiation heat transfer, and
56
57
58
59
60
61
62
63
64
65

1 initializing the simulations with the experimental gas and wall temperature distribution. It is here
2 appropriate to note that the steam in the mixture (absorbing, scattering and emitting infrared radiation)
3 behaves as a participating medium (Abu-Romia and Tien, 1967; Howell, 1988), and therefore the
4 radiation models consider not only heat transfer between solid surfaces, but also between gas and wall
5 and within the gas.
6
7

8
9 Figure 6 shows the results for the erosion progression (calculated from the temperature rise) and the
10 time history of the helium concentration at the highest elevation. Comparing results with those shown
11 in Figs. 3 and 4 for the simulations with the CM, it can be noted that in a few cases the BEM results
12 are better than the CM results (especially in the case with the largest discrepancy the use of different
13 models produce a dramatic improvement, which was discussed in Andreani et al., 2016b), but in some
14 cases the discrepancies are larger than using the CM. Three results are rather surprising: 1) the spread
15 of results is still quite large; 2) the “best” results are obtained with a rather coarse mesh (163000
16 cells); 3) two simulations with identical code and very similar models (GRS and FZJ), which using
17 the CM exhibited very different results, are now nearly coincident. This shows that the effect of the
18 mesh possibly depends on the interaction with other modelling choices (turbulence model, numerical
19 methods, boundary conditions, etc.).
20
21
22
23
24
25
26
27


28
29 It is also interesting to observe that the three simulations where radiation heat transfer was modelled
30 result in a noticeable speed-up of the erosion process, due to the generation of additional convective
31 motions in the upper part of the vessel, which enhance the mixing (Kelm et al. 2016b). For one
32 simulation (CIEMAT), the faster mixing is uniquely due to radiative heat transfer, since the
33 turbulence model was not changed in the BEM with respect to the CM. Considering radiative heat
34 transfer helped in improving the prediction of the gas temperatures at some elevations but not at other
35 ones. Moreover, the results for wall temperatures are somewhat contradictory, because the simulations
36 using radiative heat transfer show qualitatively different results. This indicates that the simulation of
37 radiation heat transfer (in combination with other models, first of all turbulence) requires additional
38 investigations. The possible role played by radiation heat transfer in the process of gas mixing has,
39 among others, also been recently suggested by Filippov et al. (2017).
40
41
42
43
44
45
46
47
48
49

50 **3.3 Conclusions and open questions originating from blind simulations**

51
52
53
54  h sets of submissions, i.e. those using a  mmon model” (CM) and those using a “best estimate”
55  model (BEM), produced a large variety of results. Especially the large differences in the results with
56 the CM were not expected because, in order to establish some means for comparing the results, a
57
58
59
60
61
62
63
64
65

1 comprehensive set of specifications have been recommended. The open phase of the benchmark was
2 then considered necessary to provide more information on effect of meshing strategies.
3

4
5 The comparison between predicted and experimental results, as well as between simulations, raised a
6 few questions about the actual importance of considering radiative heat transfer, the relation between
7 mesh topology and other modelling aspects (turbulence model, numerical methods, boundary
8 conditions, etc.), and the effect of some test conditions that were not modelled (e.g. non-symmetry of
9 the flow at the outlet of the pipe).
10

11
12
13
14
15 The most important difficulty in interpreting the results and finding the reason of the large deviations
16  the lack of information on the velocity field downstream of the obstruction. In fact, the
17 interaction between the jet and the density stratification is expected to be controlled by the velocity
18 distribution at the interface between the rising jet and that interface. Since the velocity field changes
19 in time, due to the upwards movement of the leading edge of the jet, a meaningful comparison would
20 require a time-dependent experimental information. Unfortunately, due to the short duration of the
21 test, only long-term averages (on the time scale of the experiment) can be generated, and the
22 comparison between the requested calculated instantaneous velocity profiles and these averaged
23 values could not provide any hint on the fidelity of the simulation. One of the main difficulties to
24 interpret the large spread of the erosion times is thus the lack of experimental information on the flow
25 field, not only because of the problems discussed above but also because this is only available for a
26 limited PIV area, which is at large distance from the obstruction. Therefore, an open benchmark using
27 only the experimental information of test HP1_6_2 would lead to little progress in the understanding
28 of the erosion process above an obstruction. The availability of velocity information under quasi-
29 steady state conditions collected in auxiliary tests (Section 4.1) without helium (“zero” tests), but with
30 the same geometrical configuration, permitted, however, to obtain new information to be used in the
31 evaluation of the calculations. In fact, although, in principle, one would need information on flow
32 patterns and temperature field below and above the plate for the specific test, some progress in the
33 analyses could be expected from the use of information on the extended region above the plate
34 provided in these “zero” tests.
35
36
37
38
39
40
41
42
43
44
45
46
47
48

49
50 It was then agreed that a meaningful open benchmark could be run, but this should include the
51 analyses of the data on flow obtained in auxiliary tests, and should be organized in a number of steps
52 (see next chapter), to gradually build confidence in the models used.
53
54
55
56
57
58
59
60
61
62
63
64
65

4. THE OPEN BENCHMARK

To help resolve the questions resulting from the blind phase, an open phase of the benchmark was conducted, where the extended data from the auxiliary “zero” tests (for similar conditions but without helium layer) were provided to the participants to permit a more basic validation of their models, by comparing the results for the flow downstream of the obstruction, which, in turn, are affected by the accuracy in simulating the free jet below the obstruction. A “cascade” of simulations was thus proposed, which aimed to separate the validation of the modelling approach for representing pure fluid dynamic phenomena from the application of the selected methodology to test HP1_6_2, where also heat/mass transfer effects play an equally (or even more) important role.

For each step, a summary of the contributions will be presented in tables, which include only the main information on the mesh and modelling options. The tables include the equivalent CPU time using one processor to provide a unified estimate of the computational overhead. A more complete list of aspects considered in the simulations and details on model selection is included in the Benchmark Report (2018).

4.1 The “zero” tests

The two configurations (and PIV windows) for the tests with obstruction are shown in Fig. 7. In the complementary, “zero”, tests, the geometry was exactly the same as for Test HP1_6_2, the only difference being the initial and boundary conditions. Additionally, it is noted that for the “zero” tests the zone covered by PIV measurements spans a much larger zone, extending 2 m above the obstruction.

These tests were conducted injecting a constant steam flow rate in initially steam-filled vessels. In two tests (HP1_6_0 and HP1_7_0), pure steam was injected in steam-filled vessels, and the pressure was kept constant. The only difference was the flow rate.

These two tests, which were expected to deliver complementary information with respect to Test HP1_6_2, were used for the benchmark. A third test (HP1_8_0), which was performed with air and steam, and rising pressure was not used. For the two tests HP1_6_0 and HP1_7_0, the following nominal conditions apply:

- Pressure: 1.3 bar

- Initial steam and wall temperature: 108 °C
- Injected steam temperature: 150 °C
- Steam flow rate: 60 g/s (HP1_6_0); 30 g/s (HP1_7_0)

Although test HP1_6_0 was the only with the same boundary conditions as HP1_6_2, the analysis of second test was also included, because in test HP1_6_0 temperatures were not recorded.

The open phase of the benchmark thus consisted of a number of steps, aiming to separate the qualification of the fluid-dynamic models from the validation of the full models for test HP1_6_2, for which the success of the predictions also depend on the appropriate representation of heat and mass transfer processes. The open phase of the benchmark was thus composed of four sets of results:

1) prediction of vertical velocity and turbulent kinetic energy (TKE) distributions for Test HP1_6_0 using a “common model” (CM);

2) prediction of vertical velocity distributions and temperatures for test HP1_7_0 using a “best-estimate model” (BEM);

3) prediction of vertical velocity, turbulent kinetic energy and temperatures (although not measured) for test HP1_6_0 using the BEM;

4) post-test simulation of test HP1_6_2 with BEM, including the same mesh for the plate region used for Step 3

Additionally, also the analysis of SETH-2 test ST1_2_2 (Erkan et al., 2009; Paladino et al., 2013), with the same initial and boundary conditions as for test HP_6_2, but without obstruction, was included as Step 5, to verify the capability of the models to properly predict the erosion process in absence of the obstacle. This step was optional for participants.

Step 1 (analysis with CM of test HP1_6_0, where temperatures were not measured)

The first step of the open benchmark was the analysis of test HP1_6_0 (with the same flow rate, 60 g/s, as in test HP1_6_2), using the CM model, i.e., using a common set of recommendations regarding modelling selection and initial and boundary conditions:

- In order to isolate possible spurious sources of deviations in the final Step 4 (post-test calculation of Test HP1_6_2), also test HP1_6_0 had to be run using the full geometrical model, including the straight portion of the inlet pipe

- 1
2
3
4
5
6
7
8
9
10
11
12
13
14
15
16
17
18
19
20
21
22
23
24
25
26
27
28
29
30
31
32
33
34
35
36
37
38
39
40
41
42
43
44
45
46
47
48
49
50
51
52
53
54
55
56
57
58
59
60
61
62
63
64
65
- Use of prescribed I.C. and B.C.:
 - Initial fluid and wall temperature: 107 °C; Pressure and inlet flow rates: experimental curves. Flat pipe outlet velocity profile. Pipe exit turbulence intensity: 4%.
 - Fluid temperature at pipe outlet: 142 °C (precise value not critical, but important)
 - Obstruction plate heat capacity included.
 - Heat losses, condensation and radiative heat transfer neglected. Wall heat transfer to be considered: inner surface wall temperature to be prescribed (constant, at 107 °C)
- Standard high-Re k-ε turbulence model with Standard wall functions
- Value of y_+ in the cells below the plate between $R=3$ and 10 cm around 30.
- Recommended simulation time: 500 s

The summary of contributions is listed in Table 2

It is noted that most organizations contributed results using a finer mesh than that used for the blind benchmark, two used the same mesh, and one used a coarser mesh. Some of these choices are justified in the Benchmark Report (2018). None of the submitted contributions was based on a comprehensive sensitivity study aiming to obtain mesh-insensitive results.

The first variables to be considered in the comparison between data and calculated results are horizontal and vertical profiles of vertical velocity, extracted from the velocity field. Figure 8 shows the experimental information (averaged over 205 s), along with the elevation of the selected horizontal profiles. Figure 8 also includes the experimental profiles of axial velocity, maximum of the vertical velocity and difference between the maxima in the left and right half-plane in the PIV window (this last being an indicator of the non-symmetry of the flow past the obstruction). Y_1 and Y_2 are the elevations where the vertical velocity changes sign and the maximum coincides with the axial value, respectively. The former is the height of the recirculation zone (bubble) downstream of the obstruction; the latter indicates the position where the flow recovers the structure of a full jet (with maximum in the centre).

Figure 9 shows the calculated results for the vertical profiles of the axial velocity and the maximum vertical velocity. The comparison of the axial profile below the plate (between 4000 and 5000 mm), although no data are available for evaluating the quality of the predictions, is of some interest because it shows that very large differences (also qualitative) exist between the simulations of CIEMAT and BARC and the other ones. However, the differences are substantially reduced in the region downstream of the plate, with maximum values being in a band of 0.25 m/s, which indicates a

1 relatively small effect of the predictions below the plate and that most differences above the plate
2 originate from the representation of the flow obstruction region. In fact, simulations showing the same
3 flow development below the plate (S/NRA/R, KAERI and FZJ), diverge above the plate. The
4 simulation of FZJ produced the highest values of the velocity at the top of the measurement region. It
5 is also interesting to observe that the velocities are still growing with distance at the top of the
6 measurement region, whereas the experimental values reach the maximum at lower elevation
7 (between 6000 and 6500 mm). Finally, the module of the minimum velocity in the “bubble” above
8 the plate is underpredicted in all simulations. The vertical distribution of the maximum velocity also
9 shows a similar spread of results, with all calculations underpredicting the distance from the plate
10 where the maximum attains its highest value. Two calculations also overpredict the highest values.

11
12
13
14
15
16
17 The comparison of the velocities is to some extent affected by the still slowly evolving flow field in
18 some calculations, which is well recognized in the time history of the maximum velocity shown in the
19 Benchmark Report (2018), which is not constant at the end of the simulation. In the experiment,
20 however, the overlapping of the long-time average central profile using the entire data set with results
21 using sub-sets indicates a practically steady-state condition. The reason for the evolving flow field is
22 the slow fluid temperature increase, possibly due to the underprediction of heat transfer with the
23 structures.
24
25
26
27
28

29
30 However, considering that some differences in the velocity distribution originate from the way the
31 experimentally unknown temperature field is predicted, the agreement between predictions is
32 reasonably good. The differences are larger for the Turbulent Kinetic Energy (TKE) in the
33 recirculation zone (Fig. 10), whereas in the developed flow region the simulations converge to the
34 experimental value. The large (also qualitative differences) in the distributions are thus confined to the
35 recirculation region, and decay with distance from the obstruction.
36
37
38
39
40

41 An important feature of the transient that could not be investigated in test HP1_6_2, but could have an
42 effect on the interaction of the jet with the density interface, was the symmetry of the flow structure
43 and the flow evolution downstream of the plate. Asymmetric flow could either be produced by the
44 impingement or directly originated at the outlet of the pipe. Whereas the flow below the obstruction
45 cannot be observed also in the “zero” tests, its structure above the plate could be characterized, and it
46 is reasonable to assume that it is representative of that produced in the reference test with helium.
47 Therefore, an important aspect of the assessment of the models using the data from the zero tests is to
48 verify whether the models correctly predict non-symmetries (if any) in the flow. For Step 1, since the
49 recommendations included the modelling of the straight section of the pipe only, the verification only
50 regards the production of non-symmetries in presence of axis-symmetric injection conditions.
51
52
53
54
55
56
57

58 Figure 11 shows the difference between the maxima in the two half-planes of the PIV window, which
59 has a maximum in the zone close to the obstruction and vanishes within half a meter downstream of it.
60
61
62
63
64
65

1 st simulations do not display any substantial asymmetry in the flow field past the plate. Only the
2 contributions from AERB and BARC present a qualitatively important deviation from symmetry, the
3 former in the recirculation zone, the latter a slowly increasing difference with distance from the plate.
4 Figure 11 also shows the elevation where the flow recovers the jet structure (with maximum velocity
5 in the centre). It can be observed that the predictions, although obtained with the same turbulence
6 model, are in a large band. Considering the 2-D velocity maps provided by the participants
7 (Benchmark Report, 2018), however, it is presumed that at least a part of the differences could be due
8 to the different criterion used to determine the condition of “equality” between axial and maximum
9 vertical velocity.
10

11 It has already been observed that large discrepancies exist in the recirculation zone between
12 calculations and experiments, and between the calculated results. This is more evident from the time
13 history of the minimum velocity (Fig. 12), which shows underprediction in all simulations. It is
14 surprising, however, that, in spite of the large differences in the velocity profile, the height of the
15 recirculation zone is well predicted in all calculations.
16

17 Finally, the horizontal profiles of velocity and TKE at the two elevations indicated in Fig. 10 are
18 shown in Figs. 13 and 14, respectively. With respect to velocities, at the elevation of the middle of the
19 recirculation zones, with the exception of a narrow region around the axis, the simulations are in
20 agreement with each other, and also in agreement with the measurements. A large spread of results,
21 however, is exhibited by the turbulent kinetic energies, as regards both maximum values and profiles.
22

23 Similar considerations also apply to the elevation at large distance from the obstruction, where the
24 velocities are in good agreement (especially outside the jet core), but the calculated TKE shows a
25 large variety of values and horizontal profile shapes.
26

27 These profiles indicate that even using the same turbulence model, the results can be quite different,
28 depending on other modelling choices. Large difference between the results obtained with GOTHIC
29 and those produced by CFD codes had to be expected because of the large differences in mesh detail
30 (Table 2). The differences between CFD codes, however, are more difficult to justify, also because no
31 correlation can be easily established between number of cells and main features of the calculated
32 profiles. These results suggest that the mesh topology (and possibly details of the numerical model)
33 could play an important role.
34

35 The general remark on the results of Step 1 is that even for the simplified conditions of HP1-6-0,
36 important differences are observed, which are not related to turbulence modelling (the same standard
37 k-ε for all) or radiation heat transfer (not considered), but probably originating mostly from the mesh
38 (and topology) and, to a lesser extent, heat transfer and implemented boundary conditions.
39
40
41
42
43
44
45
46
47
48
49
50
51
52
53
54
55
56
57
58
59
60
61
62
63
64
65

1
2
3
4
5
6
7
8
9
10
11
12
13
14
15
16
17
18
19
20
21
22
23
24
25
26
27
28
29
30
31
32
33
34
35
36
37
38
39
40
41
42
43
44
45
46
47
48
49
50
51
52
53
54
55
56
57
58
59
60
61
62
63
64
65

Another observation, important for the interpretation of the results for the benchmark test (HP1_6_2), is that the differences in the erosion rates are likely to originate from a different prediction of the fluid dynamics below the density interface, and not related to the representation of the interaction region.

4.3 Step 2 (analysis with BEM of test HP1_7_0, where temperatures were measured)

Since temperatures were not recorded for Test HP1_6_0, and models constructed for best estimate simulations of the benchmark test should be validated also for their capability to properly predict fluid temperatures, the analysis of test HP1_7_0 is considered, although the steam mass flow rate was the half of that in test HP1_6_2 (30 g/s instead of 60 g/s).

In this test, the Reynolds number was thus 13500 instead of 27000. Since the effects of the Re number, at least on free jet flow development, are significant up to Reynolds numbers around 10000, and the TKE decay downstream of the plate is similar in the two tests, HP1_7_0 could be used for developing the BEM modelling approach to be used for HP1_6_0 (and HP1_6_2). In particular, in the multi-step approach for the open benchmark, the comparison of the results with test HP1_7_0 was intended to provide the validation of the models with respect to representation of heat transfer.


Table 3 reports the main features of the simulations contributed to the benchmark. Unless otherwise noted (FZJ and VTT), the mesh used is the  same as that used for Step 1. Most users adopted the SST turbulence model, one the RNG model and some retained the standard turbulence model choice. With respect to Step 1, other important model modifications in some contributions were the consideration of radiation and the velocity profile at the pipe exit pipe (obtained by representing the straight section of the pipe or prescribed on the base of off-line calculations of the flow inside the entire pipe)

Figure 15 shows the experimental flow field and the vertical velocity profiles to be used for the comparison. It is noted that both the height of the recirculation bubble and the height at which the flow recovers the full-jet structure are smaller than for Test HP1_6_0.

Figure 16 shows two vertical profiles of vertical velocity: the distribution along the axis and the profile of the maximum velocity. The general agreement between the various simulations is similar to that observed for Step 1, and, in the region above the plate, better for the simulations that exhibit a close agreement below the plate (KAERI, S/NRA/R and FZJ). However, the flow evolution below the plate has a minor effect on the velocity field above the plate. These results suggest that actually the jet “loses the memory” above the plate.

1 Underpredictions in the far-field velocity larger than for Step 1 are observed in the results of
2 CIEMAT. Worse results were also obtained by VTT. Although the changes in modelling certainly
3 play a prevailing role, and some mesh modifications with respect to Step 1 complicate the picture, this
4 result possibly indicates that the disagreement between simulations does not depend on the jet
5 Reynolds number. Moreover, the interpretation of the results is complicated by certain
6 instabilities and large asymmetries in the velocity field which were exhibited by some
7 simulations, but not observed in the experiment (Benchmark Report, 2018). Some of the calculated
8 asymmetries appeared already at the pipe outlet, produced by bent in the lower part of the
9 injection pipe (Figs. 1 and 7). However, PIV measurements immediately above the pipe exit
10 performed in other HYMERES experiments for similar conditions (Paranjape et al., 2018)
11 indicated that a well-developed turbulent pipe profile existed at the pipe exit. Although at the higher
12 velocity of Test HP1_6_2 the effect of the bent could in principle be larger, the considerations above
13 related to test HP1_7_0 suggested that one of the open issues of the blind benchmark, namely the
14 effect of possible non-symmetries at the pipe exit the flow development above the obstruction,
15 could be considered of minor importance for the evaluation of the results of the benchmark test.
16 Detailed discussions on these and other aspects of the flow are discussed in the Benchmark Report
17 (2018).

18 Concerning the fluid temperatures, the time histories are presented and discussed in the
19 Benchmark Report (2018). Here, we just mention that the two simulations including radiation heat
20 transfer (FZJ and BARC) correctly predict the short time required for the fluid to reach equilibrium
21 values with the structures, whereas the other predictions show still increasing temperatures at
22 1000 s. It can be observed that these two simulations exhibit the most accurate predictions for
23 the axial temperature profile (Fig. 17). The largest deviations occur at the position close to the plate,
24 due to the difficulty to correctly predict the details of the flow within the recirculation zone
25 (Benchmark Report, 2018).

26 Concerning the radial profile at Level D (only this one was required in the benchmark specifications),
27 both simulations show a too narrow profile (but this is true for all simulations) and underprediction of
28 the temperatures at some distance from the axis (Fig. 17). Although the results of BARC are
29 probably somewhat biased by a large (and difficult to explain) temperature drop below the plate and
30 the radial distribution at 1000 s calculated by FZJ is affected (Benchmark Report, 2018) by a plume
31 oscillation (still of small amplitude at level D), it can be concluded that the two simulations agree
32 with each other with respect to the effect radiation heat transfer can have. Globally, these
33 simulations can also be regarded as the most successful, since the contribution of VTT (which does
34 not model radiation) also shows good agreement above the plate, but these good results are
35 due to the lower injection temperature (it can be noted in the axial temperature profile, Fig. 17).

4.4 Step 3 (analysis with BEM of Test HP1_6_0)


Step 3 was intended, in the multi-step approach of the open benchmark, to provide the participants the opportunity to validate the model selection made for test HP1_7_0 for the same flow as used in Test HP1_6_2, and to refine the mesh, if needed. In Step 3, additional horizontal profiles of velocity and TKE at low elevations were requested.

The overview of contributions for Step 3 is presented in Table 4.

Figure 18 shows the axial and maximum velocity vertical profiles. For convenience, the results obtained for Step 1 are also displayed using the same scales.

Two participants (BARC and CIEMAT) used the same mesh as for Step 1, whereas the other four users used slightly finer meshes, adopting modifications that were suggested by the simulation of Step 2. Four participants used the same model settings as for Step 2, but CIEMAT and VTT used different turbulence model (or corrections).

Figure 18 shows that differences in injection velocity for five participants (not considering the contribution of CIEMAT, which for Step 1 used a too low value) are now more pronounced than for Step 1, due to the different assumptions for steam injection temperature (prescribed or calculated) and, possibly, details of the mesh used for the pipe. The development of the flow immediately above the pipe is also affected by the use of a velocity profile at the pipe exit, so that the profiles below the plate diverge more than for Step 1.

In the region above the plate, results of BARC, CIEMAT, FZJ, and VTT are very similar to those obtained using the common model, and the results of S/NRA/R only show a noticeable difference for the maximum velocity. These results possibly indicate that the selection of the turbulence model, for these conditions,  a small impact on the prediction of the global features of the flow. The largest differences between Step 1 and Step 3 regard the simulations of PSI and CIEMAT, where, in both cases, the pipe exit conditions were strongly modified with respect to the calculations with the common model. The calculations of PSI with the “CFD like” GOTHIC code were “worse” than with the common model, but, due to the more physical representation of the pipe exit conditions (pipe exit velocity and temperature profiles are considered), are the best suitable to be compared with CFD codes in this benchmark.

The axial profiles of TKE (Benchmark Report, 2018) also show that the selection of the turbulence model (different from the standard k-ε model in all calculations but that of PSI) has a strong influence in the region immediately above the plate, but its effect is substantially reduced already at relatively short distance from the top of the recirculation zone.

1 This consideration is especially true for the calculations of BARC, where the results with both
2 standard and RNG model are nearly coincident. This is not expected, because the RNG model was
3 developed to handle this kind of flows. The results of CIEMAT display the largest change, but for this
4 simulation are not clear whether the large difference in mesh and inlet velocity were the most
5 important effects. Finally, the radial profiles show that also the predicted axial values of S/NRA/R
6 (for which no axial profile was provided) are less sensitive to the turbulence model selection than
7 expected.
8
9

10
11
12 Obviously, these considerations cannot lead to the conclusion that the selection of turbulence model is
13 immaterial for the representation of the flow past the obstruction and for the erosion process in
14 transient test HP1_6_2, since an apparently small difference in the velocity and TKE distribution can
15 have a large influence on the turbulent diffusivity distribution.
16
17

18
19
20 Indeed, the details of the results for Step 3 are also interesting in view of their prospective importance
21 for the prediction of the benchmark test. Both velocity and TKE horizontal profiles show a large
22 spread between the various simulations, and this suggests that the differences in the flow predictions
23 could result in large differences in the erosion rate.
24
25

26
27
28 Finally, some considerations can be made on the predictions of fluid temperatures, although no
29 experimental values have been recorded. It is observed that large differences exist in the free jet
30 temperature decay (Fig. 19), although the steam injection temperature is the same, apart from the
31 calculation of VTT. Moreover, the radial profiles, similarly to the results for Step 2, show that
32 radiation heat transfer has a strong effect on temperature spatial evolution. It is also interesting to
33 mention that the time to reach a quasi-steady-state condition is very different in the various
34 predictions (Benchmark Report, 2018) and, for some simulations, do not appear consistent with the
35 results (also experimental) obtained for test HP1_7_0 (Step 2). In consideration of similar differences
36 between the various simulations observed for test HP1_7_0 (where experimental values were
37 available), it can tentatively be concluded that the modeling of radiation also permits a better
38 representation of the time development of the temperature field.
39
40
41
42
43
44
45
46
47
48


49 5 (analysis with BEM of test ST1_2_2, without plate)

50
51
52
53
54 Before the post-test results for the benchmark test are discussed, the analyses of test ST1_2_2 are
55 briefly illustrated. The analyses of this test (conducted with the same configuration used for HP1_6_2,
56 with the only difference that no obstruction was present), were expected to offer the opportunity to
57
58
59
60
61
62
63
64
65

1 validate/improve the mesh outside the region of the obstruction plate, also taking advantage of the
2 PIV measurements at short distance from the pipe exit.
3

4 The configuration of test ST1_2_2 (Erkan et al., 2009; Paladino et al., 2013) is shown in Fig. 20,
5 where the initial distribution of helium in the injection vessel is compared with that present at the start
6 of test HP1_6_2. Figure 20 also shows the comparison of the other important boundary conditions, i.e.
7 steam flow rate and temperature. The maximum helium concentration was slightly higher than in the
8 benchmark test, whereas the steam injection temperature was lower. As for the steam mass flow rate,
9 differences can be regarded as negligible.
10
11
12
13

14 It will be seen below that these conditions and the absence of the obstruction resulted in an about 30%
15 faster stratification break-up.
16
17
18

19 Table 5 presents an overview of the four calculations contributed to this part of the benchmark 
20

21 Figure 21 shows the progression of the erosion, based on the gas temperature threshold of 115 °C.
22 This limit is lower than for HP1_6_2 because the steam injection temperature was lower (Fig. 20).
23
24
25

26 The simulations of the three organizations that submitted results also for the other steps (AERB, FZJ
27 and PSI) accurately predict the erosion process, with some differences appearing only towards the end
28 of the transient. The good predictions of these three contributions are also confirmed by the time
29 histories of the helium gas concentration (Fig. 22).
30
31
32

33 The only notable discrepancy in the three simulations are the delayed helium concentration drop
34 calculated by FZJ at level D ($z=6.3$ m), which, however, may be due to a graphical representation
35 effect, because (see Benchmark Report, 2018) the frequency of the required data (every 5 s) does not
36 permit to display the calculated drop and recovery of the helium concentration during the time interval
37 between two measurements.
38
39
40
41
42

43 Figure 23 shows the vertical velocity axial distribution and the horizontal profile at $z=5003$ mm. It is
44 observed that the calculation with GOTHIC (PSI) accurately predicts the maximum velocity at short
45 distance from the pipe exit, whereas the other two simulations strongly overpredict it. The width of
46 the profile instead is better calculated by the simulations of AERB and FZJ. It could be inferred that
47 the velocity decay further up has been properly calculated in all simulations, because otherwise it
48 would not be possible to capture the erosion rate. The analysis of the results of Step 4, however, will
49 lead to different conclusions (see Section 4.6).
50
51
52
53
54

55 As regards the discrepancies at short distance from the pipe exit, although it can be presumed that
56 they can partly be due to the slightly off-center position of the jet (in the third dimension), the results
57
58
59
60
61
62
63
64
65

1
2
3
4 of AERB and FZJ suggest that either the pipe exit conditions or the near-field jet spreading is not
5 properly calculated in their simulations.
6

7
8 This conclusion is supported by the observation of the axial profiles of gas temperature (Fig. 24) at
9 two different times.
10

11
12 In both simulations of AERB and FZJ, the central temperature remains at the value of the injected
13 steam up to above 5 m, whereas the experimental value at that elevation has already dropped by more
14 than 5 K. In the calculation by PSI, however, the gas temperature drops smoothly to the lower
15 measured value. The analyses presented in the Benchmark Report (2018) show that this result is due
16 to the representation of both velocity and temperature profile at the pipe exit, due to the flow
17 development inside the pipe and heat transfer with the pipe walls. In fact, if the velocity and
18 temperature profiles are assumed flat, both axial velocity and temperature do not start decreasing
19 below 5 m.
20

21
22 It can be concluded that in the FZJ and AERB calculations either the entrainment in the free jet is too
23 little, which produces a too small jet broadening, or the pipe exit conditions were not properly
24 accounted for. For FZJ, the good agreement with the measurements for test HP1_7_0 (Step 2, half
25 steam flow rate) with respect to both temperature (Fig. 17) and velocity profiles (Benchmark Report,
26 2018), suggests that the predictions are affected by the Reynolds number. The comparison between
27 simulations for Test ST1_2_2 and HP1_6_2 (shown in the Benchmark Report, 2018) also indicates
28 that the jet spreading below the plate depends on the evolution of the eddy diffusivity.
29
30
31
32
33
34

35 The elevation where the jet is fully developed (central temperature starts decreasing) is thus predicted
36 at about 5000 mm and 5300 mm in the FZJ and AERB calculations, respectively. The
37 underprediction of the jet spreading in the FZJ and AERB simulations can be recognized from the too
38 narrow temperature profile, which is also present in the PSI calculation, although to a lesser extent.
39
40
41

42 This result suggests that also for Step 4 (to be discussed below) the simulations of FZJ and AERB
43 should be affected by inaccuracies in the simulation of flow field and temperatures below the plate.
44
45
46

47 The axial temperature profiles show that only the calculation (FZJ) considering radiation heat transfer
48 captures the correct level of temperature at large distance during the erosion process (time < 500s),
49 although the temperatures drop between the elevation where the jet is fully developed and the bottom
50 of the helium layer is overpredicted. In general, also the horizontal temperature profiles (Fig. 25)
51 show a better success of the FZJ simulation, although not all results seem to offer a consistent picture
52 (Fig. 26).
53
54
55
56
57

58 From the profiles in the mixed region below the tip of the jet (Benchmark Report, 2018) one can
59 conclude that the modelling of radiation heat transfer was necessary to correctly calculate the fluid
60
61
62
63
64
65

1 temperatures. Also at higher levels (Fig. 25 and 26), where the upwards propagation of the jet
2 produced the temperature rise and helium concentration drop, the temperatures before the mixing
3 (Level D) or during or immediately afterwards (Level C) are much better predicted by FZJ. At times
4 after the mixing has occurred (250 s at level D and especially at 500 s at level C), however, the
5 calculation of FZJ shows notable discrepancies, possibly due to the (small) asymmetry in the flow and
6 temperature field appearing shortly before the dissolution of the helium layer is completed
7 (Benchmark Report, 2018).
8
9

10
11
12 Some additional information can be obtained on the gas temperature time histories at the required
13 positions (not shown). First of all, the three simulations of AERB, FZJ and PSI correctly predict the
14 temperatures in vicinity to the pipe exit, which shows that the correct boundary conditions were
15 applied and no numerical diffusion corrupted the simulations from the injection elevation. The best
16 predictions were obtained by FZJ using radiation, although the results of PSI using a coarse mesh and
17 a standard correlation for convective heat transfer are nearly equally successful.
18
19
20
21
22

23 The results for off-axis positions above the initial density interface are somewhat contradictory, with
24 generally better results obtained by PSI, with the effect of radiation being to excessively reduce the
25 temperatures during the entire transient and also after the full dissolution of the helium layer. The
26 discrepancy is especially large at some positions during the erosion process. On the contrary, at lower
27 positions, the calculation with radiation permits to reproduce the correct temperature, whereas the
28 calculation with GOTHIC predicts a strong superheat, the largest differences occurring during the
29 transient compression and erosion of the helium layer, before mixing. Although it cannot be excluded
30 that convective heat transfer could also play a major role in the different predictions (since both
31 turbulence model and meshes were different), it can be presumed that the largest contribution to the
32 divergent behaviour could come from the modelling of radiation in the simulation of FZJ.
33
34
35
36
37
38
39
40


41 Since all positions where the discrepancies are very large are all in regions of slow velocities and even
42 in nearly stagnant zones, these result suggest that the strongest effect of radiation could be observed in
43 the zones where the temperature increase due to compression of the fluid cannot be contrasted by the
44 weak convective heat transfer but is kept low by the effect of radiation heat transfer. Moreover, the
45 results indicate that the effect of radiation heat transfer may show up more distinctly during transients
46 rather under quasi-steady state conditions (such as those established in Test ST1_2_2 after the
47 dissolution of the stratification), which would be justified by the different time scales of the
48 convective heat transfer (which is bound to the finite propagation velocity through the fluid) and
49 radiation heat transfer (which instead has practically an immediate effect).
50
51
52
53
54
55
56
57
58
59
60
61
62
63
64
65

4.6 Step 4 (post-test analysis of benchmark test HP1_6_2)


The last step in the analysis is the post-test simulation of the benchmark test HP1_6_2. In accordance with the rationale for the multi-step approach, mesh around the plate and modelling would be expected to be the same as for Step 3 (HP1_6_0), with some corrections to the mesh in the main domain due to the knowledge gained from the analysis of Test ST1_2_2, featuring helium layer erosion without obstruction. Table 6, where the overview of the contributions is presented, shows that only FZJ and PSI ran all steps and followed this path in building the model used for the final calculation. Also BARC and S/NRA/R submitted results with same mesh and model setting, but opted not to perform the additional Step 5. It is also noted that one organization used a coarser mesh than for Step 3: CIEMAT model reverted to the coarse mesh model used for the blind benchmark.

Also with respect to the turbulence model, in some contributions Step 4 has not been analyzed with the same selection used for the other steps. As regards radiation heat transfer, it is noted that one contribution (VTT) used this model only for Step 4: therefore a preliminary validation using the data of HP1_7_0 an ST1_2_2 (Steps 2 and 5) was not performed.

Figure 27 shows the erosion progression determined using the times at which for each location the gas temperature rises to 120 °C,¹ whereas Fig. 28 shows the helium concentration time history at level B ($z=7.48$ m). In these figures, the results obtained in the open phase are compared with those submitted for the blind benchmark, using the best estimate model. It is noted that VTT did not contribute best estimate results for the blind benchmark, and thus no comparison is possible for this organization.

It is observed (Fig. 28) that several organizations that participated in the blind benchmark could obtain better results (especially BARC, S/NRA/R and GRS, with this third organization, however, supplying the final results with a model that was not verified in Steps 1 to 5). AERB, CIEMAT and , instead, practically obtained the same results as for the blind simulations. This outcome of the multi-step validation of the model for CIEMAT is obvious, because the final step was run with the same mesh and model settings as for the blind exercise. For AERB (Benchmark Report, 2018), the results (using a much finer mesh) have been shown to depend on the mesh around the plate and therefore on an accurate prediction of velocity field near the plate (comparing the results of sensitivity studies for Step 3), overall grid size in the stratification region (Step 5), and numerical scheme. On the other hand, the Realizable k- ϵ was preferred to the standard and the RNG model only for the better convergence obtained with this turbulence model. For FZJ, the results could seem somewhat surprising, because for all other steps the model delivered rather accurate predictions, at least at some

¹ See Section 2.2. Results up to level B (7500 mm) are confirmed by the inspection of the temperature predictions. For level A (8000 mm), the “erosion time” is somewhat underestimated.

1 distance from the pipe exit. It has to be considered, however, that the results of the blind benchmark
2 have not been revised systematically applying the outcome of the other steps, since they used a Best
3  mate Model constructed on the base of a comprehensive validation experience. Numerical effects
4 were also investigated, but showed no considerable importance.
5
6

7 A possible contribution to the discrepancy can be due to the underprediction of the jet broadening
8 below the plate, as suggested by the results of Step 5, and/or the slightly larger maximum velocity and
9 TKE at high elevations (observed in Step 3). The difference in the results can be explained neither by
10 the modelling of radiation alone (also considered by BARC, CIEMAT, GRS, and VTT), nor by mesh
11 or turbulence model or injection conditions. It is likely that a combination of all these elements finally
12 produced the large differences observed in the final results of FZJ for the transient test. Especially
13 interesting is the comparison between the calculations of FZJ and BARC, because for Step 3 the
14 results of both simulations were close to each other, the only important differences being the TKE
15 magnitude at some distance from the plate, and the elevation of the full jet recovery.
16
17
18
19
20
21
22

23 This suggests that the results for the erosion progression are strongly affected by the turbulence
24 model, and wall layer treatment of the jet impingement zone (including the best choice for the size of
25 the cell adjacent to the plate). Some additional elements to partly explain similarities and differences
26 between results will be provided by the analyses of the flow variables (see below), but only further
27 analyses and sensitivity studies by the individual organizations could bring some light on the role
28 played by mesh and modelling choice.
29
30
31
32
33

34 As for other simulations, the concentrations time histories confirm that FZJ and CIEMAT (and at late
35 times also VTT) overpredict the erosion rate, whereas the others either capture or slightly
36 underpredict the mixing rate. It is also observed that in the simulation of VTT, the erosion is initially
37 slower (Level F, at $z=6$ m), probably due to the delay in the reattachment of the flow above the plate
38 (see below), which was observed for Step 2, but not for Step 3 (Benchmark Report, 2018).
39
40
41
42

43 As for the effect of modelling radiation (which, in the case of BARC lead to very accurate results, but,
44 for FZJ resulted in too fast mixing), Fig. 29 shows the comparison of the results obtained by GRS
45 (Schramm et al., 2017). For this simulation, the accelerating effect of radiation is very large. In other
46 investigations (e.g. Kelm et al., 2016b) for similar conditions, radiation was shown to promote mixing
47 due to its influence on temperature (and density) fields, although its effect was not as substantial as in
48 the simulations shown here. Additional studies on the effects of radiation are presented in the
49 Benchmark Report (2018).
50
51
52
53
54
55
56
57
58
59
60
61
62
63
64
65

1 The apparently excellent global results obtained with GOTHIC and coarse meshes are probably
2 affected by compensation of errors, as indicated by the comparison for the velocity.
3

4 Due to the large averaging time of the available velocity measurements, the comparison between the
5 calculated axial and horizontal velocity profiles (Fig. 30) has to be taken with some caution, as shown
6 by the large fluctuations in the measurements over a 10 s period around the central time (300 s) of the
7 averaging period. Nevertheless, it can be recognized that the velocity in the PIV window calculated by
8 PSI is far too low, which suggests that the good predictions for the erosion result from the
9 compensation of errors between the lower velocities in the far field above the plate and numerical
10 diffusion. Since the results for Step 5 in the near field (without plate) were excellent and the results
11 for Step 3 (without helium layer) were reasonably good, it can be concluded that the complexity of the
12 transient test HP1_6_2 lead to overprediction of the velocity decay between the plate and the density
13 interface. It can also be observed that the same order (from faster to slower) in the erosion timing
14 displayed by concentration and temperature traces can be found in the magnitude of the velocity: the
15 simulation of FZJ, which predicts fast erosion, also predicts the largest velocity in the PIV window.
16 Vice versa, the simulation of AERB, which underpredicts the velocity, also slightly underpredicts the
17 erosion rate.
18

19 A special attention deserves the simulation of VTT, which used a very detailed mesh and calculated
20 (as result from the detailed modeling of the injection pipe) an asymmetric velocity and temperature
21 profile at the pipe exit. The evolution of the calculated flow field (Benchmark Report, 2018) shows
22 for about 200 s a splitting of the velocity field above the plate, and only at about 220 s the plume/jet
23 structure is recovered. Since for the same flow rate (Step 3) this delay was not observed (but it was
24 observed in test HP1_7_0, Step 2), the results suggest that the density interface produced the same
25 effect as a lower mass flow rate. No conclusive explanation could be found so far for the results
26 concerning the recirculation zone above the plate. On the other hand, the simulation of BARC (taken
27 as example, but similar behavior is displayed by FZJ and CIEMAT) also show an "open" flow
28 structure at early times, but already after 100 s the full jet/plume is recovered. This behavior does not
29 depend on the steam injection temperature (constant at 150 °C in the BARC calculation).
30

31 The observation related to the VTT simulation is particularly important, because it suggests that the
32 set-up of a model based on the good results for simplified conditions can prove not to be equally
33 successful when applied to the more complex situation of a test featuring transient behavior and
34 strong density differences.
35

36 Some important observations can be made on the axial and horizontal temperature distributions (Figs.
37 31 and 32), Generally, the most accurate axial temperature distributions are obtained by the models
38 including radiation heat transfer, but also the simulation with GOTHIC, which accurately accounts for
39 the temperature drop between the pipe exit and the plate, displays a quite remarkable agreement. The
40
41
42
43
44
45
46
47
48
49
50
51
52
53
54
55
56
57
58
59
60
61
62
63
64
65

1 initially too large temperature difference between the elevations below and above the plate calculated
2 by VTT is related to the delay in the re-attachment of the flow (see above).
3

4 Due to the complexity of the phenomena, it is not possible to draw any conclusions, but it is simply
5 observed that no obvious correlation seem to exist between accuracy in the calculation of the
6 temperatures and mixing rate. The horizontal temperature profile immediately below the plate (Level
7 H) shows that all simulations predict a too narrow peak, with rather flat profile at some distance from
8 the axis. At this elevation, the most distinct difference between some simulations including radiation
9 (CIEMAT, FZJ and VTT) and those not representing this heat transfer mode is the larger temperature
10 drop between the centre of the jet/plume and the periphery of the flow. This, however, is not observed
11 in the calculation of BARC.
12
13
14
15
16

17 For the region above the plate, the results are obviously affected by the different progression of the
18 stratification erosion. It can be observed, however, that at intermediate elevations (Levels G and D)
19 most of the simulations including radiation predict better the temperature profiles, especially the
20 temperatures near the wall.
21
22
23
24

25 The results obtained with the models with radiation at the bottom of the dome (Level C) seem to be
26 less accurate than those neglecting this heat transfer mode. In fact, whereas at 250 s the top of the jet
27 has already reached that elevation in the simulations of CIEMAT, FXJ and BARC, and therefore the
28 temperature profiles are not comparable, at 500 s in all simulations the mixing has been completed at
29 level C, and one can observe large discrepancies with data in the simulations with radiation (again,
30 excluding BARC), of the same magnitude, though opposite in sign, as the other simulations.
31
32
33
34
35

36 The simulation of FZJ at 150 s, moreover, is affected by asymmetry, similar to that observed for test
37 ST1_2_2. In this case, it is easy to explain this profile with the bending and fluctuation of the plume,
38 as shown by the temperature field at various times (Benchmark Report, 2018). It is interesting to note
39 that the presence of a density interface acts on the plume as a lower flow rate. In fact, large-scale
40 oscillations were predicted for HP1_7_0 (30 g/s), but not for HP1_6_0 (60 g/s).
41
42
43
44
45

46 The comparisons of the gas temperature time histories at various positions (Benchmark Report, 2018)
47 permitted a better evaluation of the role played by radiation. Especially interesting is the consideration
48 of the temperature level reached during the transient, the temperature after the stratification moved
49 above a specific location, and the temperature rise time at the various locations.
50
51
52

53 An example of temperatures at higher locations is shown in Fig. 33. At the position along the axis
54 (Fig. 33 left), the calculations can be divided in three groups: 1) the simulations with radiation are the
55 most accurate with respect to the final values, but underpredict the times of the rise (erosion), with the
56 exception of BARC; 2) the CFD simulations without radiation overpredict the temperature; 3) the
57
58
59
60
61
62
63
64
65

1 results of PSI with GOTHIC are in between. Concerning the slopes of the temperature increase, the
2 results are rather sparse, with GOTHIC obtaining better results at intermediate levels, and only CFD
3 simulations with radiation (especially BARC) being able to predict the sudden rise at higher
4 elevations.
5

6
7 As regards the off-axis positions initially immersed in the helium layer (Fig. 33, right), the two CFD
8 simulations without radiation clearly overpredict the temperatures at all positions, whereas four of the
9 CFD simulations with radiation (CIEMAT, FZJ, GRS and VTT) underpredict the temperatures to
10 various extent. In general, the BARC simulation (also with radiation) is the most successful. The
11 calculation of PSI, however, is nearly equally accurate.
12
13
14
15

16
17
18
19 Finally, the temperatures at two positions off-axis below the initial bottom of the helium layer are
20 considered (Fig. 34). Close to the centre (325 mm from the axis), at the elevation of the recirculation
21 bubble above the plate (GH_19, $z=5.3$ m) the results are in a band of 15 K, with the PSI results being
22 the most accurate. Further off-axis (about 900 mm from the centre), and at the level of the injection,
23 therefore at a position weakly affected by convective motions, the CFD simulations with radiation
24 show substantially better results than the other calculations. At this position (K_17, $z=4$ m), and this
25 was the case also for test ST1-2-2 (Benchmark Report, 2018), the role played by radiation in nearly
26 stagnant region appear more clearly. It can also be shown that in these regions, where the heat-up is
27 initially mainly caused by compression, radiation is the only effective heat transfer process, since it
28 does not require the development of the boundary layer, which affects instead convective heat transfer
29 (Filippov et al., 2017)
30
31
32
33
34
35
36
37

38 It must also be remarked that the various predictions including radiation heat transfer produced
39 different results, as expected from the use of different models and methods to calculate the steam
40 absorptivity. The differences, also connected to the different time progression of the erosion, are large
41 during the mixing process, and vanish at many locations after the helium layer has been dissolved.
42
43
44
45
46
47
48
49
50
51


52 **5. CONCLUSIONS**

53
54
55 The experiment in the PANDA facility chosen for the present benchmark, test HP1_6_2, addresses
56 the stratification erosion induced by a vertical steam jet, which originates from the exit of a circular
57 pipe located below the bottom of the helium-rich layer. The mixing is somewhat slowed down by a
58 small, horizontal, circular plate above the jet source. The benchmark consisted of two phases: blind
59
60
61
62
63
64
65

1 and open. The results of the blind benchmark exhibited a large spread of results, some showing very
2 large discrepancies with the measured data, which was not expected, especially for the part addressing
3 the use of a “common” model. The results of the blind simulations made evident that further
4 investigations and validation studies were necessary to separate different sources of errors and avoid
5 their mutual elimination (compensating errors) in a complex model.
6
7

8
9 It was recognized that the most important difficulty in interpreting the results and finding the reason
10 of the large deviations was the lack of information on the velocity field downstream of the
11 obstruction, since only long-time averaged velocities were available in the region of the initial density
12 interface, above 6 m. It was therefore agreed that valuable information on the flow produced by the
13 interaction of the free jet with the obstruction could be obtained from auxiliary tests without helium
14 (“zero” tests), but with the same geometrical configuration and featuring an extended region above the
15 plate where velocity measurements were available.
16
17
18
19
20
21

22 Therefore, the open benchmark included the analyses of the data on the flow structure above the plate
23 obtained in these auxiliary tests: a “cascade” of simulations was thus proposed, which aimed to
24 separate the validation of the modelling approach for representing pure fluid dynamic phenomena
25 (using the data of the “zero” tests HP1_6_0 and HP1_7_0) from the application of the selected mesh
26 and models to the more complex test HP1_6_2, for which the success of the predictions also depend
27 on the appropriate representation of heat and mass transfer processes
28
29
30
31
32

33 The open phase of the benchmark thus consisted of  steps. Additionally, also the analysis of
34 SETH-2 test ST1_2_2, with the same initial and boundary conditions as for test HP1_6_2, but without
35 obstruction, was included as Step 5, to verify the capability of the models to properly predict the
36 erosion process in absence of the obstacle, and therefore test their basic capabilities to represent the
37 global features of the transient in the entire flow domain. Finally, also the velocity measurements at
38 the pipe exit in two other test series were used in some comparisons to verify the appropriate
39 representation of the injection conditions.
40
41
42
43
44
45


46 Since each participant was requested to submit one set (best estimate) of final results for each step and
47 only the main sensitivity studies of some organisations were contributed to the final report, only
48 general conclusion will be discussed, leaving the detailed answers to the questions to future
49 publications of the individual organisations.
50
51
52

53 The simulations with a common model for the quasi-steady state conditions of test HP1_6_0 without
54 helium (step 1) were expected to provide the opportunity to investigate the effect of mesh on the
55 simulation of the interaction of the jet with the plate. The final results submitted exhibited notable
56 differences, especially in relation to transversal distributions and flow development downstream of the
57
58
59
60
61
62
63
64
65


1
2
3
4
5
6
7
8
9
10
11
12
13
plate. Although the simulations could be affected by numerics and the spurious effects of the
calculated slow change of the thermal field, the analysis indicate that meshing strategies could not
converge to produce similar results and setting an adequate mesh for representing the flow
modification due to an obstacle poses a real challenge. It can be inferred that the variety of results
later obtained for the full test are strongly affected by the meshes used in this region. This is somehow
confirmed by the observations that the few simulations of test ST1_2_2 (Step 5) without obstacle
were all reasonably successful, although performed with largely different meshes and model
selections.

14
15
16
17
18
19
20
21
22
23
24
25
26
As regards the interaction of mesh and model selection (which produced in the blind benchmark
astonishingly different results using a turbulence model but not a different one), no new information
could be generated within this benchmark, due to the lack of systematic analysis and the use of similar
turbulence models (all variants of k- ϵ and k- ω models). However, comparing results for test HP1_6_0
with the “common” model and the “best-estimate” model (Steps 1 and 3, respectively), it was
observed that the selection of models had a smaller effect than expected, and was seemingly less
important than the mesh.

27
28
29
30
31
32
33
34
35
36
37
38
39
40
41
42
43
44
Thermal radiation heat transfer was confirmed to have an accelerating effect on the progression of the
erosion process, independently of the specific model used, and a substantial part of the information
obtained from the temperatures indicates that this heat transfer mode should be modelled to get the
correct spatial and temporal evolution of the thermal field. However, since various simulations with
radiation were only performed for the final step, some results appear to be contradictory, and
inaccuracies (possibly compensated or enhanced by radiation) are certainly associated with the use of
meshes not optimised for the flow investigated (see above) and with the possible interaction with
other models and effects, no firm conclusion could be reached on the necessity and approach to model
radiation heat transfer. This issue will certainly require further investigations, both experimental and
numerical.

45
46
47
48
 definite conclusion could be reached with respect to best choice for turbulence model, as the
meshing appeared to be a more important issue for the conditions investigated in this benchmark.

49
50
51
52
53
54
55
56
57
58
59
60
61
62
63
64
65
The velocity and temperature distributions in the jet at the pipe exit have some effect on flow and
thermal variables, but this is mostly confined to the region below the obstruction. Finally, the effect of
numerical methods has been reported from some participants and for some contributions it can be
suspected to be responsible for some anomalous results and the submission of the final results with
meshes not optimised. However, the absence of systematic studies in most contributions show how
difficult is to implement in the analyses of transients requiring hundreds hours of CPU a rigorous
approach to guarantee mesh and time step independence.

1 The main conclusion of the open benchmark is that the step-by-step validation permitted some
2  gress with respect to some of the items identified above. However, large discrepancies with data in
3 the final analyses of the test are observed, which cannot be easily attributed to specific model
4 deficiencies. The uncertainty is partly due to the difficulty to perform exhaustive analyses for each
5 step including all effects, partly to the physical model limitations (e.g. use of RANS models for
6 turbulence), and partly to specific features of the reference test that cannot be tackled in simulations of
7 simplified conditions. On the one hand, even for the simpler fluid conditions of the tests without
8 density interface, mesh and models could not be fully assessed. On the other hand, it is clear that the
9 complexity of the physical conditions prevailing in the selected test, where the modification of the
10 flow produced by the obstacle interacts with the stratification erosion process, rendered the splitting of
11 the problem in hydrodynamic and heat/mass transfer components of lesser use than anticipated.

12 A few general considerations should be added in relation to the blind benchmark and the large,
13 unexpected, differences in the results. The spread of the results was similar, for instance, to the recent
14 OECD/NEA-PSI CFD benchmark without obstruction, although specifications for the “common”
15 model were given, which covered various aspects of the simulation (geometry, turbulence modelling,
16 initial, and boundary conditions, some fluid and flow properties, etc.). Since other aspects of the
17 simulation were not considered in the specifications (e.g. wall treatment), and therefore some of the
18 differences could be due to specific code inputs as well as to the numerical methods used, and the
19 level of validation (including mesh convergence studies and application of BPG) was different for the
20 various contributions, it is difficult to draw any conclusions from the comparison of the requested
21 results. However, it can be observed that, similarly to previous exercises for similar flows and
22 configurations (but without obstruction), the present results suggest that whenever a new problem is
23 tackled, established modelling strategies must be evaluated again. The outcome of the exercise
24 reinforced the awareness of the spread of results that can be obtained if the adequacy of the mesh is
25 solely evaluated on the base of previous experience and limited mesh refinement studies. In this
26 respect, the fact that some of the best results were obtained with rather coarse meshes should not be
27 used as argument in favour of this approach for applications, without appropriate validation.
28 Furthermore, even the use of very detailed meshes, resulting from systematic studies (going close to
29 the full application of the BPG) does not lead necessarily to similar results, which are possibly
30 affected by the topology of the mesh, local refinement, details of the numerics, and other effects.

31 These considerations lead to a few key-findings of this comparison. First of all grid independence
32 must be proven for each physical and geometrical model as well as set of boundary conditions and
33 cannot be simply assumed that this can be concluded from a similar case. Small changes in the
34 flow/setup, here the implementation of a small flow obstruction, may challenge the model validity
35 range. This suggests that continuous validation and a backward assessment of previous results (e.g.
36 those obtained for the OECD/NEA benchmark or other tests addressing stratification break-up) is

1
2
3
4
5
6
7
8
9
10
11
12
13
14
15
16
17
18
19
20
21
22
23
24
25
26
27
28
29
30
31
32
33
34
35
36
37
38
39
40
41
42
43
44
45
46
47
48
49
50
51
52
53
54
55
56
57
58
59
60
61
62
63
64
65

necessary. The results furthermore highlight that the effect of user-defined numerical or physical assumptions is in the order of those of model differences.

In summary, the results highlight, for the sake of more precise conclusions, the need for proper grid convergence studies, beyond the prescriptions of the BPG (not addressing mesh topology), which possibly should be improved by including, for instance, recommendations on mesh structure for an open catalogue of simple flows. Moreover, following the practice of the V&V community (e.g. that organised by ASME), in future benchmarks more attention has to be paid to code inputs and their effects on the numerical solution of the equations.

The results obtained by each participant using the best estimate models show that the combination of mesh and modelling approach again can result in a wide spread of results, with the quality of the results not always being improved using a model selection that proved to be successful for other configurations and test conditions. For instance, the use of refined turbulence models (such as SST) and considering radiative heat transfer did not result in fully satisfactory predictions, and made evident that further investigations and validation studies are necessary to separate different sources of errors and avoid their elimination (compensating errors) in a complex model.

It is important here to stress once more the importance of blind benchmarks, because they disclose the difficulty in tackling new problems for which the modelling strategy must be derived from previous experience. This is true, we believe, in general, but it is more true for containment related problems, because the strict application of BPG is hindered by the long computation times associated with complex geometries, large volumes and long transients.

Finally, considering the specific configuration of the test on which it was based, the present benchmark revealed the (partly unexpected) difficulty to simulate a flow in presence of a simple obstruction. This observation suggests that in the future more experimental data and associated V&V will be required to validate the codes for more complex geometries. These issues are currently addressed in the OECD/NEA project HYMERES-2 (OECD/NEA, 2017).

ACKNOWLEDGMENTS

The experiment was conducted by the Experimental thermal-hydraulic group of PSI, composed by three of the authors - R. Kapulla, S. Paranjape and D. Paladino – and G. Mignot, M. Fehlmann, L. Ryan and S. Suter. The authors gratefully acknowledge the support of all the countries participating in the OECD/NEA HYMERES project and the OECD/NEA secretariat. The authors would like to thank all the members of the Management Board and the Programme Review Group of the HYMERES project for their help in defining the test programme and evaluating the test results.

REFERENCES

Abe, S., Studer, E., Ishigaki, M., Sibamoto, Y., and Yonomoto, T. (2018) “Stratification Breakup by a Diffuse Buoyant Jet: The MISTRA HM1-1 and 1-1bis Experiments and their CFD Analysis”, *Nucl. Eng. Design*, **331**, pp. 162–175.

Abu-Romia, M.M. and Tien, C.L (1967) “Appropriate Mean Absorption Coefficients for Infrared Radiation of Gases”, *Journal of Heat Transfer*, **89**(4), 321-327.

Allelein, H.-J., Fischer, K., Vendel, J., Malet, J., Studer, E., Schwarz, S., Houkema, M., H. Paillère, H., Bentaib, A. (2007). International Standard Problem ISP-47 on Containment Thermal Hydraulics. Nuclear Energy Agency, Committee on the Safety of Nuclear Installations, Final Report NEA/CSNI/R(2007)10, 2007.

Allelein, H.-J., Reinecke, E.-A., Belt, A., Broxtermann, P., and Kelm, S. (2012) “Combined Analytical and Experimental Investigations for LWR Containment Phenomena”, *Nucl. Eng. Technol.*, **44**(3), 249-260.

Andreani, M., Badillo, A., and Kapulla, R. (2016a) “Synthesis of the OECD/NEA-PSI CFD Benchmark Exercise”, *Nucl. Eng. Design*, **299**, 59-80

Andreani, M., Daqiang, Y., Gaikwad, A.J., Ganju, S., Gera., B., Grigoryev, S., Herranz, L.E., Huhtanen, R., Kanaev, A., Kelm, S., Kim, J., Nishimura, T., Schramm, B., Sharabi, M., and Paladino, D. (2016b) “Synthesis of a blind CFD benchmark exercise based on a test in the PANDA facility addressing the stratification erosion by a vertical jet in presence of a flow obstruction”,

1 OECD/NEA 6th Workshop on Computational Fluid Dynamics for Nuclear Reactor Safety
2 (CFD4NRS-6), MIT, Cambridge, MA-USA, 13-15 September, 2016.
3

4 Andreani, M. and Paladino D., (Benchmark Report, 2018), prepared by PSI (with appendices
5 contributed by AERB, FZJ and VTT) (2018) “OECD/NEA HYMERES project: synthesis of results of
6 the benchmark on PANDA test HP1_6_2”, PSI Technical Note AN-42-17-07 Rev.1, Project report
7 HYMERES-P-17-48, May 2018.
8
9

10 Bentaib, A., Meynet, N., and Bleyer, A. (2015) “Overview on Hydrogen Risk Research and
11 Development Activities: Methodology and Open Issues”, *Nucl. Eng. Technol.*, **47**, 26-32.
12
13

14 Breitung, W. and Royl, P. (2000) “Procedure and Tools for Deterministic Analysis and Control of
15 Hydrogen Behavior in Severe Accidents”. *Nucl. Eng. Design*, **202**, 249-268.
16
17

18 Chan, C.K. and Jones, S.C. (1997) “Gas Mixing Experiments in a Large Enclosure”, Proc. of the 18th
19 Annual Conf. of the Canadian Nuclear Society
20
21

22 Choi, Y.-S., Lee, U.-J., and Park, G.-C. (2001) “Study on local hydrogen behaviors in a
23 subcompartment of the NPP containment”, *Nucl. Eng. Design*, **208**, 99-116.
24
25

26 Deri, E., Cariteau, B., and Abdo D. (2010) “Air fountains in the erosion of gaseous stratifications”,
27 *Int. J. Heat and Fluid Flow*, Volume **31**, Issue 5, Pages 935–941.
28
29

30 Erkan, N., Mignot, G., Kapulla, R., Paladino, D., Zboray, R., Strassberger, H.J., Bissels, W. and
31 Fehlmann, M. (2009) “OECD SETH-2 PANDA Test ST1_2_2 Quick-Look Report”, PSI internal
32 technical report TM-42-09-07-0, April 2009.
33
34

35 Filippov, A.S., Grigoryev, S.Yu., O.V. Tarasov, O.V. (2017) “On the possible role of thermal
36 radiation in containment thermal–hydraulics experiments by the example of CFD analysis of
37 TOSQAN T114 air–He test”, *Nucl. Eng. Design*, **310**, 175-186.
38
39

40 Gupta, S. (2015) “Experimental Investigations Relevant for Hydrogen and Fission Product Issues
41 Raised by the Fukushima Accident”, *Nucl. Eng. Technol.*, **47**, 11-25.
42
43
44
45
46
47
48
49
50
51
52
53
54
55
56
57
58
59
60
61
62
63
64
65

1 Howell. J.R. (1988) “Thermal Radiation in Participating Media: The Past the Present, and Some
2 Possible Futures”, *Journal Heat Transfer*, **110**, 1220-1229.

3
4
5 Huhtanen, R. (2018), Private Communication.

6
7 Kapulla, R., Mignot, G., Paranjape, S., Suter, S., Fehlmann, M., and Paladino, D. (2015a)
8 “OECD/NEA HYMERES Project: Jet/Plume interacting with flow obstruction HP1 Series. Test Series
9 Report”, PSI internal report TM-42-15-16, Rev.0, Project report HYMERES-P-15-26, Nov. 2015
10 (report restricted to project participants).

11
12 Kapulla, R., Paranjape, S., Mignot, G., Suter, S., Fehlmann, M., and Paladino D. (2015b)
13 “OECD/NEA HYMERES Project: PANDA Tests HP1_6_0, HP1_7_0, HP1_8_0, and HP1_678_Disk
14 Data Report”, PSI internal report TM-42-15-13 Rev. 0, Project report HYMERES-P-15-25, October
15 2015 (report restricted to project participants).

16
17 Karwat, H. et al. (1999) “State-of-the-Art Report on Containment Thermal-hydraulics and Hydrogen
18 Distribution”, OECD/NEA group of experts, CSNI/R(99)-16 (1999).

19
20 Kelm, S., Ritterath, M., Prasser, H.-M., and Allelein, H.J. (2016a) "Application of the MINIPANDA
21 Test Case ‘Erosion of a Stratified Layer by a Vertical Jet’ for CFD Validation”, *Nucl. Eng. Design*,
22 **299**, 124-135.

23
24 Kelm, S., Müller, H., and Allelein, H.-J. (2106b) “Importance of thermal radiation heat transfer
25 modeling in containment typical flows”, Paper submitted for presentation at the CFD4NRS-6, MIT,
26 Cambridge, MA, USA, September 13-15.

27
28 Liang, R. et al., (2015) “Status Report on Hydrogen Management and Related Computer Codes“,
29 NEA/CSNI/R(2014)8,

30
31 Lopez-Alonso E., Papini D., and Jimenez G. (2017) “Hydrogen Distribution and Passive
32 Autocatalytic Recombiner (PAR) Mitigation in a PWR-KWU Containment Type”, *Annals of Nuclear
33 Energy*, **109**, pp. 600-611.

34
35 Mahaffy, J., et al. (2015). Best Practice Guidelines for the Use of CFD in Nuclear Reactor Safety
36 Applications - Revision” NEA/CSNI/R(2014)11.

37
38
39
40
41
42
43
44
45
46
47
48
49
50
51
52
53
54
55
56
57
58
59
60
61
62
63
64
65

1 Noutsopoulos, G.C. and Yannopoulos, P.C. (1989) “Axial Dilution in Obstructed Round Buoyant Jet”,
2 *Journal of Hydraulic Engineering*, **115**(1), pp. 71-81.
3

4 Nishimura, T., Hoshi, H. and Hotta, A. (2015) “Current Research and Development Activities on
5 Fission Products and Hydrogen Risk after the Accident at Fukushima Daiichi Nuclear Power Station”,
6
7 *Nucl. Eng. Technol.*, **47**, 1-10
8
9

10
11 OECD/NEA HYMERES-2 project (2017-2021).
12

13
14 OECD/NEA THAI Project (2010) “Hydrogen and Fission Product Issues Relevant for Containment
15 Safety Assessment under Severe Accident Conditions” Final Report, 22 June 2010, Report
16
17 NEA/CSNI/R(2010)3.
18
19

20
21 Paladino, D. and Dreier, J. (2012) “PANDA a Multi Purposes Integral Test Facility”, *Science and*
22
23 *Technology of Nuclear Installations*, **2012**, Article ID 239319, doi:10.1155/2012/239319.
24
25

26 Paladino, D., Mignot, G., Kapulla, R., Zboray, R., Andreani, M., Tkatschenko, I., Studer, E., and
27
28 Brinster, J. (2013) “OECD/SETH-2 Project: PANDA and MISTRA Experiments addressing Key
29 Safety Issues for Water Reactor Containment”, Proceedings of the 15th International Topical Meeting
30
31 on Nuclear Reactor Thermal-hydraulics (NURETH-15), paper 106, Pisa, Italy, 12-17 May 12-17,
32
33 2013.
34
35
36

37
38 Paranjape, S., Kapulla, R., Mignot, G. and Paladino D. (2018) “Gas Redistribution Caused by
39 Interacting Heat Sources in the Presence of a Vertical Condenser,” 12th International Topical Meeting
40
41 on Nuclear Reactor Thermal-Hydraulics, Operation and Safety (NUTHOS-12), Qingdao, China,
42
43 October 14-18, 2018.
44
45
46

47 Sarikurt, F.S. and Hassan, Y.A. (2017) “Large Eddy Simulations of Erosion of a Stratified Layer by a
48 Buoyant Jet”, *Int. J. of Heat and Mass Transfer*, Vol. **112**, p. 354-365.
49
50

51
52 Schramm, B., Stewering, J., and Sonnenkalb M. (2017) “Einsatz von CFD-Codes für die Simulation
53 von unfalltypischen Phänomenen im Sicherheitseinschluss: Validierung und gezielte
54
55 Modellerweiterung”, Anschlussbericht RS1526, 2017 GRS-472, ISBN 978-3-946607-55-7.
56
57
58
59
60
61
62
63
64
65

1 Schwarz, S., Fischer, K., Bentaib, A., Burkhardt, J., Lee, J.-J., Duspiva, J., Visser, D., Kytala, J.,
2 Royl, P., Kim, J., Kostka, P. and Liang, R. (2011) “Benchmark on Hydrogen Distribution in a
3 Containment based on the OECD-NEA THAI HM-2 Experiment”, *Nucl. Technol.*, **175**(3), 594–603.
4
5

6
7 Smith B.L. (2009) “Identification and Prioritization of Generic Nuclear Safety Problems Requiring
8 CFD Analysis”, Proc. 17th Int. Conf. on Nuclear Engineering (ICONE-17), Paper 75482, Brussels,
9 Belgium, July 12-16, 2009.
10
11
12

13
14 Studer, E., Brinster, J., Tkatschenko, I., Mignot, G., Paladino, D., and Andreani, M. (2012)
15 “Interaction of a light gas stratified layer with an air jet coming from below: Large scale experiments
16 and scaling issues”, *Nucl. Eng. Design*, **253**, 406-412.
17
18
19
20
21
22
23
24
25
26
27
28
29
30
31
32
33
34
35
36
37
38
39
40
41
42
43
44
45
46
47
48
49
50
51
52
53
54
55
56
57
58
59
60
61
62
63
64
65

1
2
3
4
5
6
7
8
9
10
11
12
13
14
15
16
17
18
19
20
21
22
23
24
25
26
27
28
29
30
31
32
33
34
35
36
37
38
39
40
41
42
43
44
45
46
47
48
49
50
51
52
53
54
55
56
57
58
59
60
61
62
63
64
65

LIST OF TABLES

Table 1: Summary of submissions for the blind benchmark


 Table 2: Overview of contributions for Step 1 of the open benchmark

Table 3: Overview of contributions for Step 2 of the open benchmark

Table 4: Overview of contributions for Step 3 of the open benchmark

Table 5: Overview of simulations performed for Step 5 of the open benchmark


Table 6: Overview of contributions for Step 4 of the open benchmark

Table 1: Summary of submissions for the blind benchmark

	CM			BEM
Organi- sation Contri- bution*	Code	Mesh cells $\times 10^3$	Main deviations from specifications	Differences from CM
AERB	FLUENT 16	163	-	RNG k- ϵ
BARC	CFD- ACE+	164	Injected steam temperature	RNG k- ϵ
CIEMAT	FLUENT 15	135	-	radiative heat transfer included
FZJ	CFX-15	565	Constant pressure	SST, condensation and radiative heat transfer included. Initial gas and wall T distribution.
GRS	CFX-15	1412	-	Slightly refined mesh (1.7 million cells), SST, radiative heat transfer included
IBRAE <i>IBRAE</i>	CFX-12	110	No man-hole, injected steam temperature	Different code (CABARET)
IBRAE <i>IBRAE2</i>	FLUENT 14.5.7	355	No man-hole, plate thickness=0	RSM
KAERI	OpenFOAM 2.3.1	158	Square pipe and plate	
S/NRA/R	FLUENT 15	655	-	SST, pre-conditioning phase (He injection) simulated
PSI <i>PSIF</i>	FLUENT 15	560	Half vessels, no man-hole	
PSI <i>PSIG</i>	GOTHIC 8.1	20	Square plate	Initial gas and wall T distribution. Enhanced HTC at the walls
SPICRI	CFX-13	1284	Initial T and X_{He} . No wall heat capacity	SST
VTT	FLUENT 16	2872		

*for multiple contributions from the same organisation

Table 2: Overview of contributions for Step 1 of the open benchmark

Organi- sation	Code	 Cells x10 ³ (Nr. Cells for Blind simulations) (U=unstructured mesh)	Reported deviations from specifications	Size of cells below obstruction (m)	Equivalent CPU time on one core (h)
AERB	FLUENT V.16	240 <i>(163)</i>	Constant Pressure B.C.	0.03 y+=40-125	1500
BARC	CFD-ACE+ Version 2011	690 (U) <i>(164)</i>	Constant Pressure B.C.	0.03 y+=30-50	848
CIEMAT	FLUENT 16.2	256 (U) <i>(135)</i>	350 s transient time	(V=9.4e-7 m ³) ³ √V~0.01	24
FZJ	CFX-17	570 <i>(565)</i>	-	0.005 y+~30	1606
KAERI	OpenFOAM 2.4X	260 <i>(158)</i>	-	0.04	375
S/NRA/R	FLUENT V15.0	843 (U) <i>(655)</i>	-	0.0036	696
PSI	GOTHIC 8.1	41 <i>(20)</i>	-	0.01 y+~17-38	768
VTT	FLUENT V16.0	2214 <i>(2872)</i>	Enhanced wall treatment	0.0125	2500

1
2
3
4
5
6
7
8
9
10
11
12
13
14
15
16
17
18
19
20
21
22
23
24
25
26
27
28
29
30
31
32
33
34
35
36
37
38
39
40
41
42
43
44
45
46
47
48
49
50
51
52
53
54
55
56
57
58
59
60
61
62
63
64
65

Table 3: Overview of contributions for Step 2 of the open benchmark

Organisa- tion	Code	Nr. Cells $\times 10^3$ (Step 1)	Turbulence model	Heat transfer	Annotations	Equivale nt CPU time on one core (h)
AERB	FLUENT V.16	240 (240)	Standard k- ϵ Standard wall functions	Heat loss: heat flux B.C. No Rad	Constant pressure B.C. Lower steam injection temperature	1500
BARC	CFD-ACE+ Version 2011	690 (690)	RNG k- ϵ Non-equil. wall function	Heat losses: considered (heat flux B.C.) Rad.: Discrete Ordinate(DO) Method	Constant pressure B.C.	1536
CIEMAT	FLUENT 16.2	256 (256)	Standard k- ϵ Standard wall functions	Heat losses: considered No radiation	Lower steam injection temperature Constant pressure B.C.	44
FZJ	CFX-17	660 (570)	SST, production limiter for TKE, Low Re corrections Automatic wall treatment	Heat losses: considered using effective HTC on outer surface and average steel T. Rad: Monte Carlo method with $\kappa=1 \text{ m}^{-1}$ (gray gas)	Cell size below plate: 0.0005 m; $y^+ \sim 4$ (Mesh refined around plate to match requirement of SST turbulence model) Inlet V profile Different from Step 1 due to modelling straight part of pipe	2932

1
2
3
4
5
6
7
8
9
10
11
12
13
14
15
16
17
18
19
20
21
22
23
24
25
26
27
28
29
30
31
32
33
34
35
36
37
38
39
40
41
42
43
44
45
46
47
48
49
50
51
52
53
54
55
56
57
58
59
60
61
62
63
64
65

KAERI	OpenFOAM 2.4X	260 (260)	Standard k-ε Standard wall functions	No Rad. No heat losses. Fix wall temperature	Flat V profile at pipe exit	672
S/NRA/R	FLUENT V15.0	843	k-ω SST, Kato-Lauder, Low Re corrections	No Rad. Constant Wall temp.	Constant Pressure B.C. Inlet V profile	928
PSI	GOTHIC 8.2a	42 (41) Injection pipe modelled	Standard k-ε Standard wall functions	Heat losses: heat flux B.C. No Rad.	Inlet V and T profiles obtained modelling the injection pipe (tuning the vessel inlet T) New version of the code (8.2)	444
VTT	FLUENT V16.0	2388 (2872) Finer than for Step 1	k-ω SST, Production Kato-Lauder, Production Limiter, low-Re correction Near-wall treatment	No Rad Constant Wall temp.	Grid includes injection pipe with heat structures. Experimental Mass inflow and temperature defined into the inlet pipe.	N/A

1
2
3
4
5
6
7
8
9
10
11
12
13
14
15
16
17
18
19
20
21
22
23
24
25
26
27
28
29
30
31
32
33
34
35
36
37
38
39
40
41
42
43
44
45
46
47
48
49
50
51
52
53
54
55
56
57
58
59
60
61
62
63
64
65

Table 4: Overview of contributions for Step 3 of the open benchmark

Organi- sation	Code	Nr. Cells $\times 10^3$ (used for steps 1 and 2)	Turbulence model (choice for Step 2)	Heat transfer	Annotations	Equi- valent CPU time on one core (h)
BARC	CFD- ACE+ Version 2011	690 (690/ 690)	RNG k- ϵ Non-equil. wall function (same)	Heat losses: considered (heat flux B.C.) Rad: DO method	Constant pressure B.C.	904
CIEMAT	FLUENT 17.1	429 (256/ 256)	SST k- ω Standard wall functions (Standard k- ϵ)	Heat losses: Considered Rad: DO method	Mesh refined Min/Maximum volume (m^3): 1.1424e-07/ 1.4587e-02 cell below plate $\approx 7.3e-07$ New version of the code used	412
FZJ	CFX-17	660 (570/ 660)	SST Automatic wall treatment. (same)	Radiative heat transfer considered. Gray gas. Absorption coefficient: $1 m^{-1}$	Cell size below plate: 0.0005 m; $y^+ \sim 4$ (same as for Step 2)	2882
S/NRA/R	FLUENT V15.0	843 (843/ 843)	SST, Kato- Launder, low Re corrections (same)	No Rad. Constant Wall temp.	Cell size below plate: 0.0036 m. No Cond./Rad. Inlet V profile	480

1
2
3
4
5
6
7
8
9
10
11
12
13
14
15
16
17
18
19
20
21
22
23
24
25
26
27
28
29
30
31
32
33
34
35
36
37
38
39
40
41
42
43
44
45
46
47
48
49
50
51
52
53
54
55
56
57
58
59
60
61
62
63
64
65

PSI	GOTHIC 8.2	42 (41/42)	Standard k-ε Standard wall functions (same)	Heat losses: heat flux B.C. No Radiation		755
VTT	FLUENT V16.0	2311 (2214, 2378)	SST k-ω, Production Kato-Launder, Production Limiter, low Re corrections Near wall treatment (same)	No Radiation Constant Wall temp.	Grid includes injection pipe with heat structures. Experimental Mass inflow and temperature defined into the inlet pipe	N/A

1
2
3
4
5
6
7
8
9
10
11
12
13
14
15
16
17
18
19
20
21
22
23
24
25
26
27
28
29
30
31
32
33
34
35
36
37
38
39
40
41
42
43
44
45
46
47
48
49
50
51
52
53
54
55
56
57
58
59
60
61
62
63
64
65

Table 5: Overview of simulations performed for Step 5 of the open benchmark

Organi- sation	Code	Nr. Cells $\times 10^3$ (Steps 2/3)	Turbulence model (Steps 2/3)	Heat transfer	Annotations	Equivalent CPU time on one core (h)
AERB	FLUENT V.16	895 (240)	Realizable k- ϵ Non- equilibrium wall functions (Standard k- ϵ , standard wall functions))	Heat loss: heat flux B.C. No Radiation	Straight part of Injection pipe modelled to get velocity profile. Constant pressure B.C.	2160
FZJ	CFX-16.1	560 (660)	SST Automatic wall treatment	Heat loss: heat flux B.C. Radiative heat transfer considered. Gray gas. Absorption coefficient: 1 m^{-1}	Straight part of Injection pipe modelled to get velocity profile (w/o heat transfer) Constant pressure B.C.	2660
PSI	GOTHIC 8.2a	42	Standard k- ϵ Standard wall functions	Heat losses: heat flux B.C. No Radiation	Same mesh as for other steps (including denser mesh at 5 m)	755
SPICRI	cosCYCAS 1.0	5.5	Standard k- ϵ Standard wall functions	Wall heat transfer considered	Axis- symmetric model	27.9

Table 6: Overview of contributions for Step 4 of the open benchmark

Organi- sation	Code	Nr. Cells $\times 10^3$ (Steps 1, 2, 3 and 5)	Turbulence model (steps 2,3,5)	Heat transfer	Annotations	Equiva- lent CPU time on one core (h)
AERB	FLUENT V16.1	899 (240, 240, N/A, 894)	Realizable k- ϵ (standard) Non-equil. wall function (standard)	Heat losses: heat flux B.C. No Rad.	Straight part of Injection pipe modelled to get velocity profile. Constant pressure B.C.	1730
BARC	CFD- ACE+ Version 2011	690 (690. 690, 690, N/A)	RNG k- ϵ Non-equil. wall function (same)	Heat losses: heat flux B.C. No Cond. Rad: DO method	Cell size below plate: 0.03 m; y+ between 30 and 50. Constant pressure B.C.	1536
CIEMAT	FLUENT 17.1	133 (260, 260, 420, N/A)	Standard k- ϵ Standard wall functions (SST)	Heat losses: Considered No Cond. Radiation: DO method	Submitted results using the same model as for BEM blind simulation	188 1920 for the BEM blind simulation
FZJ	CFX-17	660 (570, 660, 660, 550)	SST Automatic wall treatment (same)	Radiative heat transfer: Monte Carlo. Gray gas, absorption coefficient: 1 m^{-1}	Cell size below plate: 0.0005 m; $y^+ \sim 4$	5551

1
2
3
4
5
6
7
8
9
10
11
12
13
14
15
16
17
18
19
20
21
22
23
24
25
26
27
28
29
30
31
32
33
34
35
36
37
38
39
40
41
42
43
44
45
46
47
48
49
50
51
52
53
54
55
56
57
58
59
60
61
62
63
64
65

1
2
3
4
5
6
7
8
9
10
11
12
13
14
15
16
17
18
19
20
21
22
23
24
25
26
27
28
29
30
31
32
33
34
35
36
37
38
39
40
41
42
43
44
45
46
47
48
49
50
51
52
53
54
55
56
57
58
59
60
61
62
63
64
65

GRS	CFX-17	7000	SST, Including buoyancy turbulence terms automatic wall treatment	Radiative heat transfer: DTM (64 rays), gray gas, absorption coefficient $\sim 1 \text{ m}^{-1}$ (from RS1500 correlation)	Straight part of injection pipe modelled to get velocity profile	17700
S/NRA/R	FLUENT V15.0	843 (843, 843, 843, N/A)	SST, Kato- Launder, low Re corrections no wall treatment (same)	No Cond. No Rad. Constant Wall temp.	Cell size below plate: 0.0036 m. Constant P Inlet V profile	208
PSI	GOTHIC 8.2	42 (41.4 2,42,4 2)	Standard k- ϵ Standard wall functions (same)	Heat losses: heat flux B.C. Rad: not considered	Contrarily to BEM simulation for the blind benchmark, the low initial values of the wall temperature at the top of the dome were not used for a large part of the dome, and Standard convective HTC correlation were used (no enhancement factor)	768

1
2
3
4
5
6
7
8
9
10
11
12
13
14
15
16
17
18
19
20
21
22
23
24
25
26
27
28
29
30
31
32
33
34
35
36
37
38
39
40
41
42
43
44
45
46
47
48
49
50
51
52
53
54
55
56
57
58
59
60
61
62
63
64
65

VTT	FLUENT V16.2	3313 (2214, 2378, 2311, N/A)	k- ω SST, Production Kato- Launder, Production Limiter Near wall treatment	Constant vessel wall temperature No Cond Rad: P1 method with WSGG model for gas absorptivity Absorption coefficient between 0.38 and 0.393 m ⁻¹	No low-Re correction Grid used for the other steps is refined in plume area above 5.9m. Boundary-layer cells on walls (2 cells). Grid includes injection pipe with heat structures. Experimental Mass inflow and temperature defined into the inlet pipe. Cell size below plate: 0.0125 m	8400
-----	-----------------	--	--	---	--	------

LIST OF FIGURES

1
2
3
4 Figure 1: Cutaway drawing of the vessels (left), configuration for the experiment (middle), and initial
5 helium concentration vertical profile in Vessel 1 (right).
6

7
8 Figure 2: Time histories of helium concentrations (left) and gas temperatures (right) at various
9 elevations along axis of Vessel 1.
10

11
12 Figure 3: Blind benchmark: Erosion progression (right) calculated with the CM and time history (left)
13 of gas temperature at position B20 ($z=7500$ mm), shown as an example. The dashed line shows how
14 the erosion time at each elevation (e.g. at the elevation of position B20) is derived.
15
16

17
18 Figure 4: Blind benchmark: Helium concentration time histories at elevation A (left) and B (right)
19 calculated with the “Common Model” (CM)
20
21

22
23 Figure 5: Blind benchmark: Gas temperature horizontal profile at level G at 300 s (left) and at level H
24 at 150 s (right) calculated with the CM. Square marks show the experimental data.
25
26

27
28 Figure 6: Blind benchmark: Erosion progression (left) and helium concentration time history at Level
29 B (right) calculated with the BEM.
30

31
32 Figure 7: (top) vertical section (plane 315° - 135°) and horizontal section of Vessel 1 showing the
33 locations of the concentration and gas temperature measurements and the Field of View (FOV) for
34 PIV measurements used for HP1_6_2 (Vessel 2 and IP are not shown); (bottom) position of the
35 combined PIV window used for Tests HP1_X_0.
36
37

38
39 Figure 8: Open benchmark, Step 1: Average experimental flow field (left) measured in Test HP1_6_0,
40 and vertical velocity profiles used in the comparisons with calculated results (right).
41
42

43
44 Figure 9: Open benchmark, Step 1: Axial profile of the vertical velocity (left) and vertical profile of
45 the maximum vertical velocity (right).
46

47
48 Figure 10: Open benchmark, Step 1: Measured distribution of Turbulent Kinetic Energy (left) and
49 comparison between experimental and calculated axial profile
50

51
52 Figure 11: Open benchmark, Step 1: Difference of the maximum velocity in the two half planes (left)
53 and position (Y2) of the full jet recovery (right).
54

55
56 Figure 12: Open benchmark, Step 1: Time history of the minimum vertical velocity (left) and
57 elevation (Y1) of the top of the recirculation zone (right).
58
59
60
61
62
63
64
65

1
2
3
4
5
6
7
8
9
10
11
12
13
14
15
16
17
18
19
20
21
22
23
24
25
26
27
28
29
30
31
32
33
34
35
36
37
38
39
40
41
42
43
44
45
46
47
48
49
50
51
52
53
54
55
56
57
58
59
60
61
62
63
64
65

Figure 13: Open benchmark, Step 1: Horizontal profiles of the vertical velocity at the elevation of the middle of the recirculation zone (left) and at an elevation in the flow developed region (right).

Figure 14: Open benchmark, Step 1: Horizontal profiles of the TKE at the elevation of the middle of the recirculation zone (left) and at an elevation in the flow developed region (right).

Figure 15: Open benchmark, Step 2: Average experimental flow field (left) measured in Test HP1_7_0, and vertical velocity profiles used in the comparisons with calculated results (right).

Figure 16: Open benchmark, Step 2: Axial profile of the vertical velocity (left) and vertical profile of the maximum vertical velocity (right).

Figure 17: Open benchmark, Step 2: Temperature radial profile at 6.276 m (left) and axial temperature distribution (right).

Figure 18: Open benchmark, Step 3: Axial velocity and maximum velocity vertical profiles for Step 3, compared with results for Step 1.

Figure 19: Open benchmark, Step 3: Axial temperature profile and horizontal profile at 6.3 m.

Figure 20: Open benchmark, Step 5: Configuration for SETH-2 test ST1_2_2, and important initial and boundary conditions of test ST1_2 and repetition test ST1_2_2 compared with those used for Test HP1_6_2.

Figure 21: Open benchmark, Step 5: Progression of erosion along the axis in test ST1_2_2, using gas temperature rise times.

Figure 22: Open benchmark, Step 5: Helium concentration time histories at various elevations along the axis of Vessel 1.

Figure 23: Open benchmark, Step 5: Vertical velocity axial profile (left) and horizontal profile at $z=5003$ mm (1 m above pipe exit)

Figure 24: Open benchmark, Step 5: Axial temperature profile at two times.

Figure 25: Open benchmark, Step 5: horizontal profiles at 6.3 m at 150 s (before mixing) and 300 s (after mixing)

Figure 26: Open benchmark, Step 5: horizontal profiles at 6.93 m at 250 s (during mixing or immediately after) and 500 s (after mixing)

Figure 27: Open benchmark, Step 4: Erosion progression calculated in the open phase (left), compared with best estimate results contributed to the blind benchmark.

1
2
3
4
5
6
7
8
9
10
11
12
13
14
15
16
17
18
19
20
21
22
23
24
25
26
27
28
29
30
31
32
33
34
35
36
37
38
39
40
41
42
43
44
45
46
47
48
49
50
51
52
53
54
55
56
57
58
59
60
61
62
63
64
65

Figure 28: Open benchmark, Step 4: Helium concentration time history at $z=6.48$ m calculated in the open phase (left), compared with best estimate results contributed to the blind benchmark.

Figure 29: Open benchmark, Step 4: Example of results obtained using the model for radiation or neglecting it: helium concentration time histories calculated at 8 m (left, GRS, Schramm et al., 2017) and at 7.5 m (right, VTT, Huhtanen, 2018).

Figure 30: Open benchmark, Step 4: Vertical velocity averaged axial and horizontal profiles in the PIV window.

Figure 31: Open benchmark, Step 4: Axial gas temperature distributions at two times

Figure 32: Open benchmark, Step 4: Gas temperature horizontal profiles at various elevations and two times.

Figure 33: Open benchmark, Step 4: Gas temperature time histories at two positions (left: on the axis; right: at 570 mm from the wall) at 6.5 m.

Figure 34: Open benchmark, Step 4: Off-axis ($r: \pm 325$ mm) gas temperature time histories at two positions below the initial bottom of the helium layer ($z: 5301$ and 4000 mm, respectively)

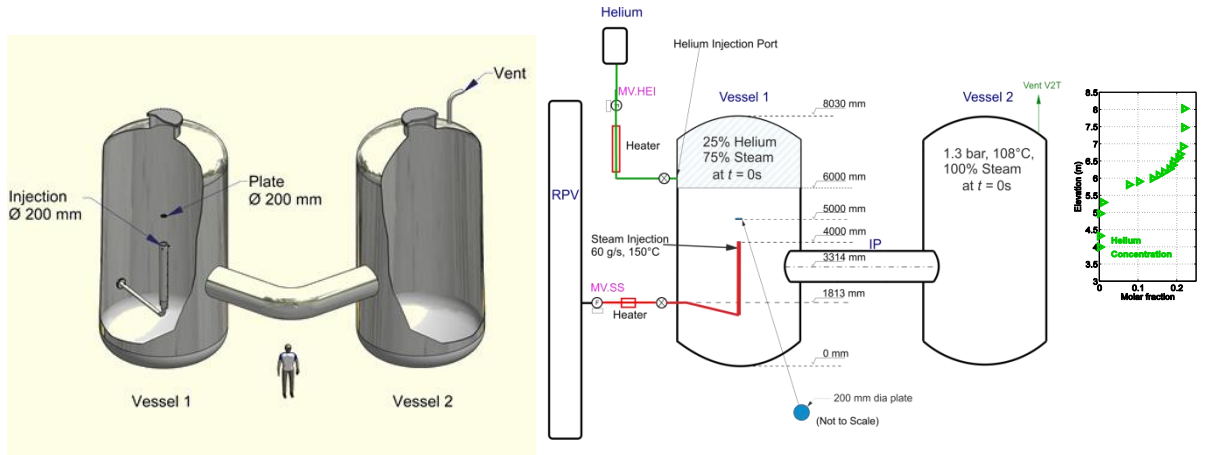


Figure 1: Cutaway drawing of the vessels (left), configuration for the experiment (middle), and initial helium concentration vertical profile in Vessel 1 (right).

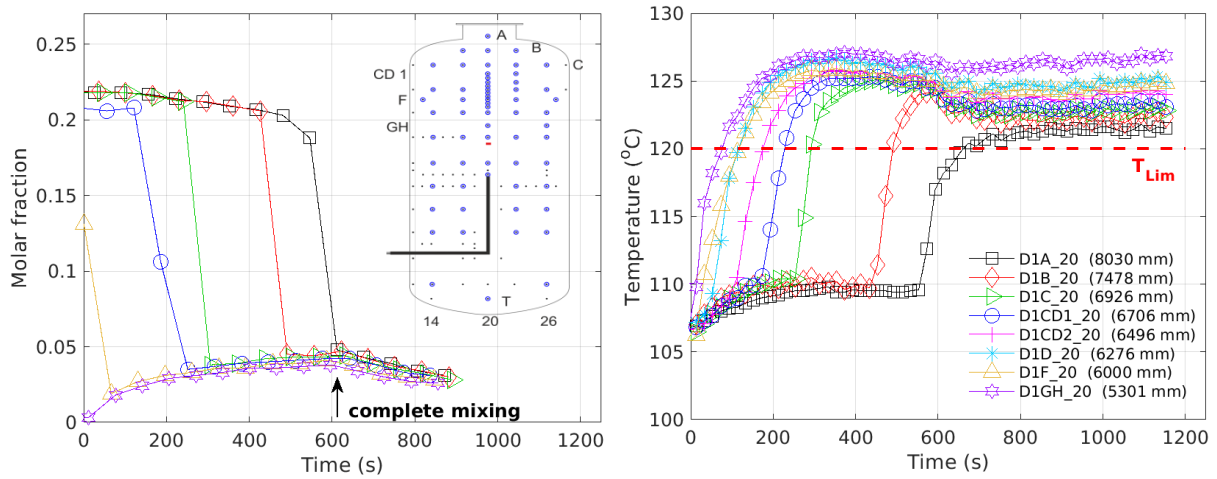


Figure 2: Time histories of helium concentrations (left) and gas temperatures (right) at various elevations along axis of Vessel 1.

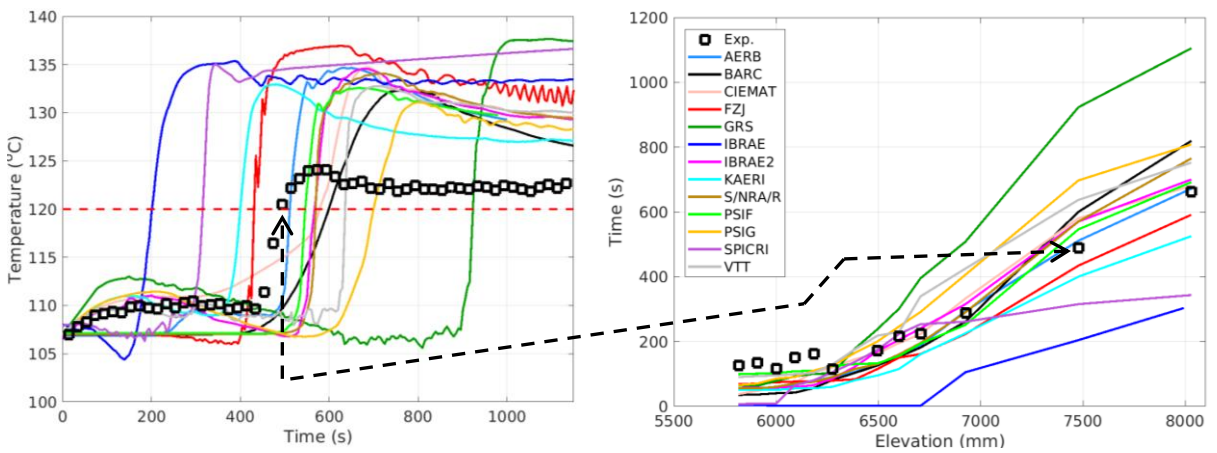


Figure 3: Blind benchmark: erosion progression (right) calculated with the CM and time history (left) of gas temperature at position B20 ($z=7500$ mm), shown as an example. The dashed line shows how the erosion time at each elevation (e.g. at the elevation of position B20) is derived.

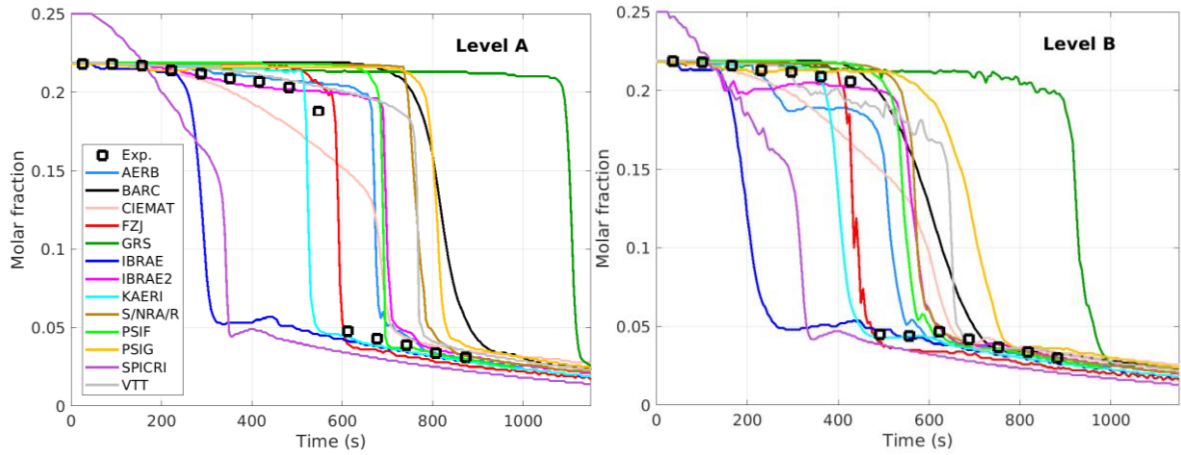


Figure 4: Blind benchmark: Helium concentration time histories at elevation A (left) and B (right) calculated with the “Common Model” (CM).

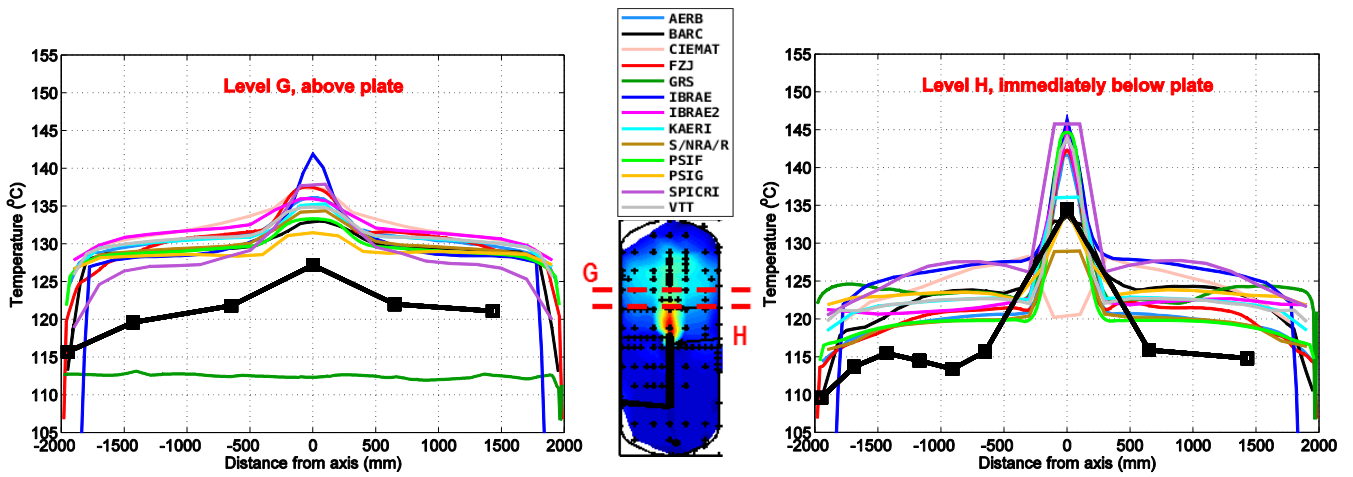


Figure 5: Blind benchmark: Gas temperature horizontal profile at level G at 300 s (left) and at level H at 150 s (right) calculated with the CM. Square marks show the experimental data.

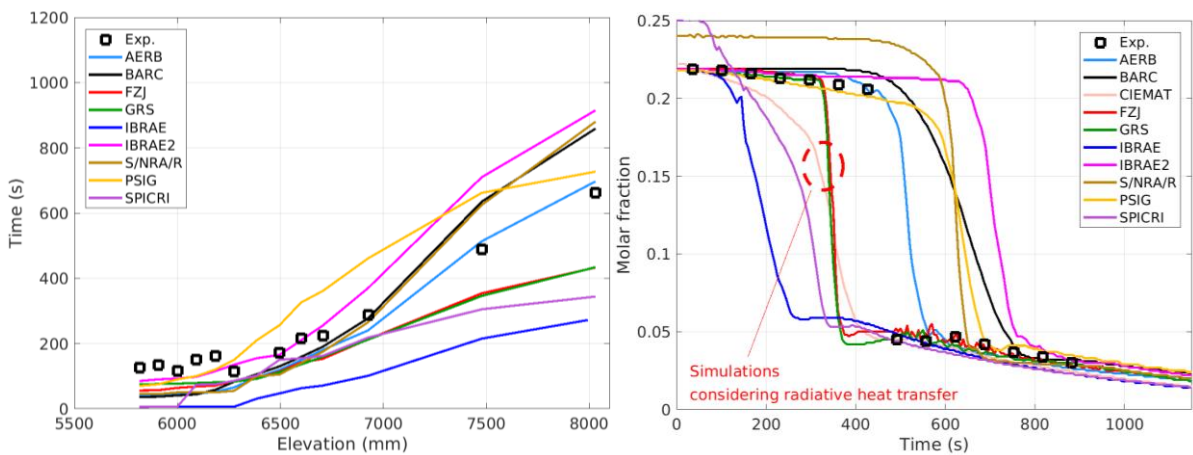


Figure 6: Blind benchmark: Erosion progression (left) and helium concentration time history at Level B (right) calculated with the BEM.

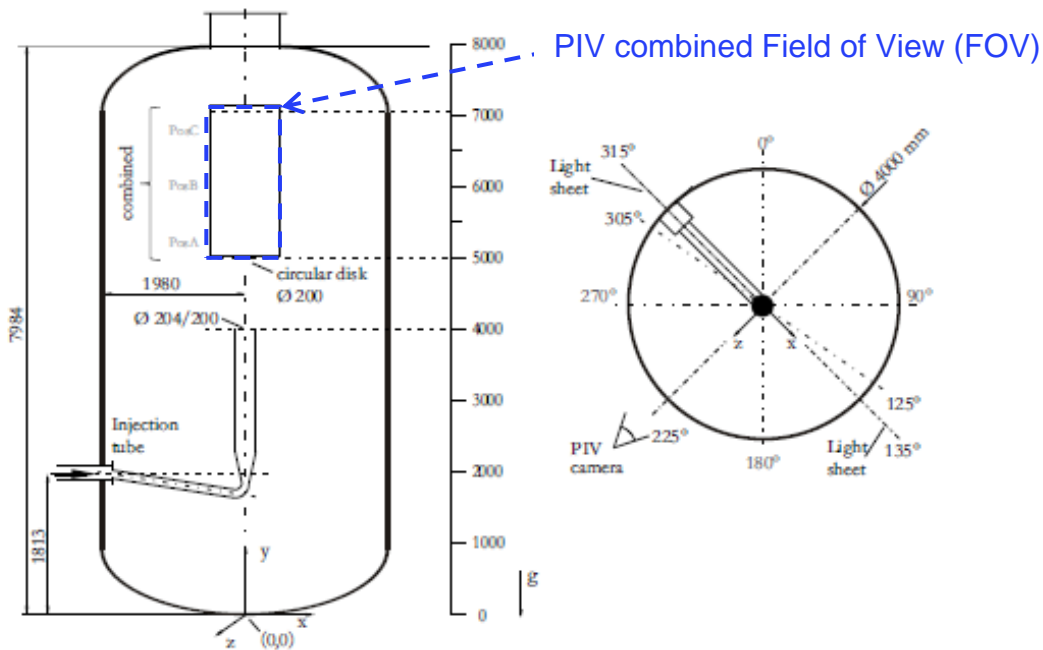
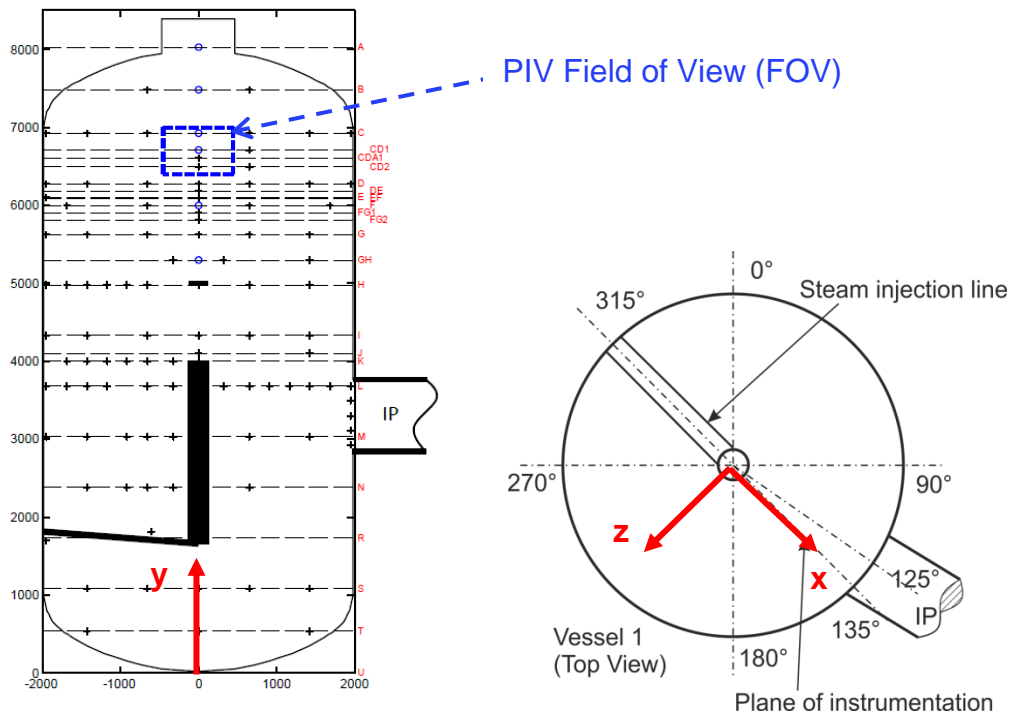


Figure 7: (top) vertical section (plane 315° - 135°) and horizontal section of Vessel 1 showing the locations of the concentration and gas temperature measurements and the Field of View (FOV) for PIV measurements used for HP1_6_2 (Vessel 2 and IP are not shown); (bottom) position of the combined PIV window used for Tests HP1_X_0.

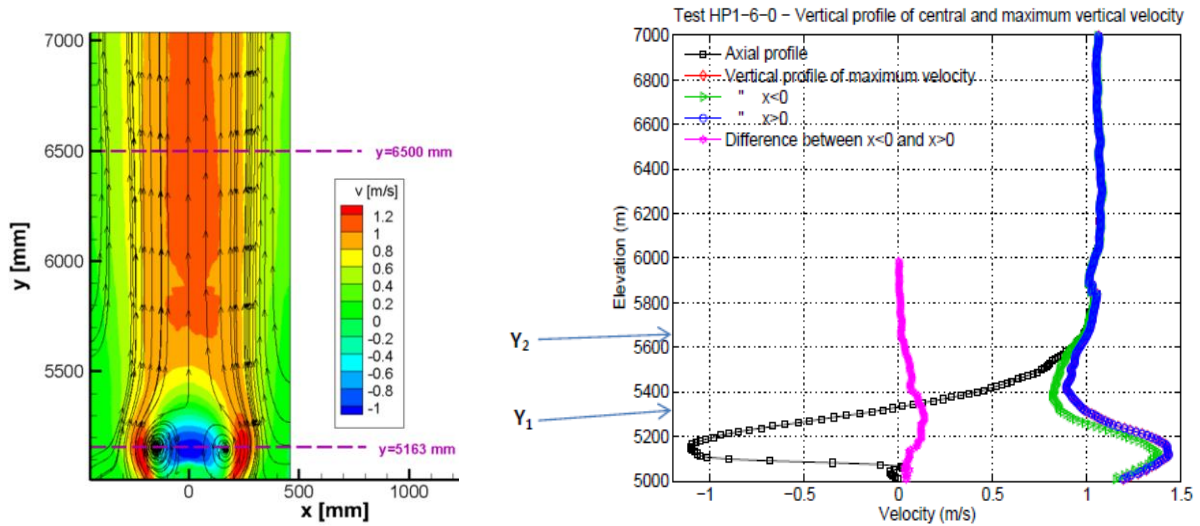


Figure 8: Open benchmark, Step 1: Average experimental flow field (left) measured in Test HP1_6_0, and vertical velocity profiles used in the comparisons with calculated results (right).

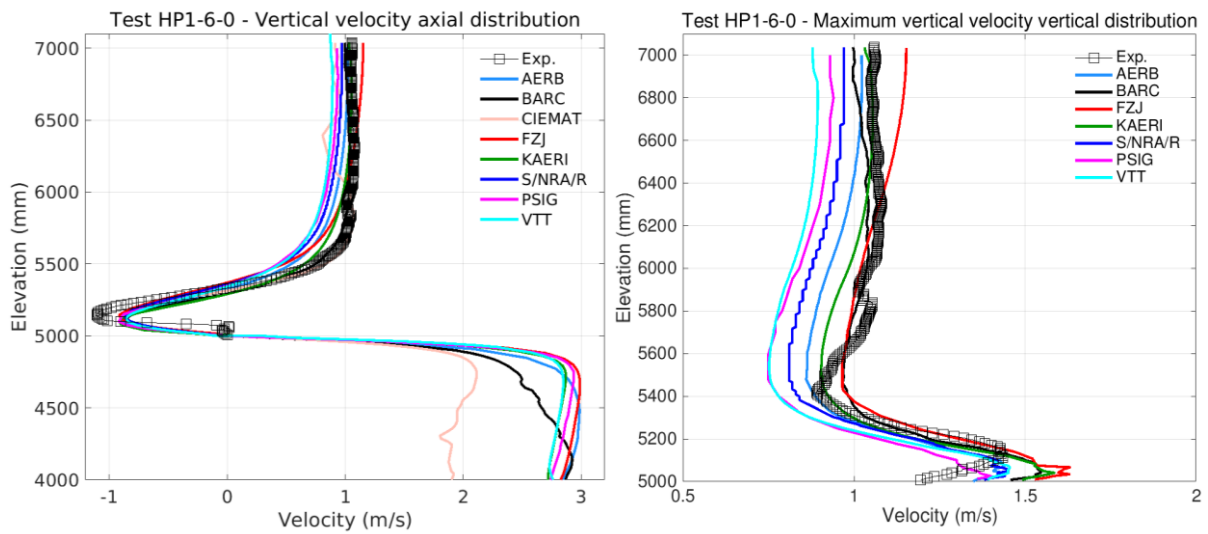


Figure 9: Open benchmark, Step 1: Axial profile of the vertical velocity (left) and vertical profile of the maximum vertical velocity (right).

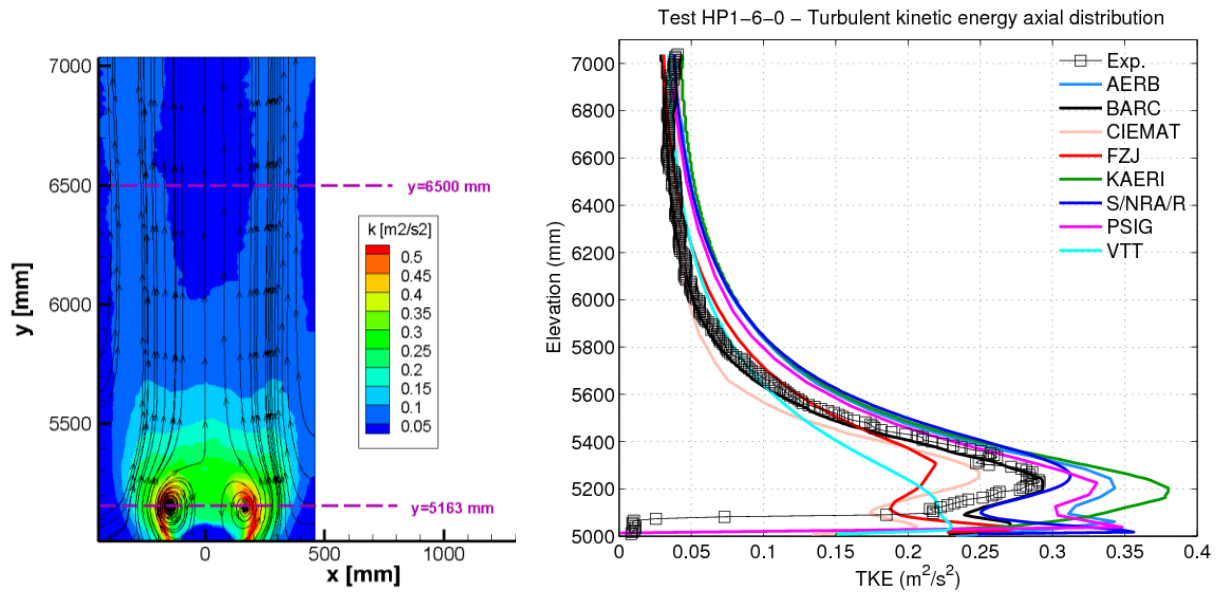


Figure 10: Open benchmark, Step 1: Measured distribution of Turbulent Kinetic Energy (left) and comparison between experimental and calculated axial profile.

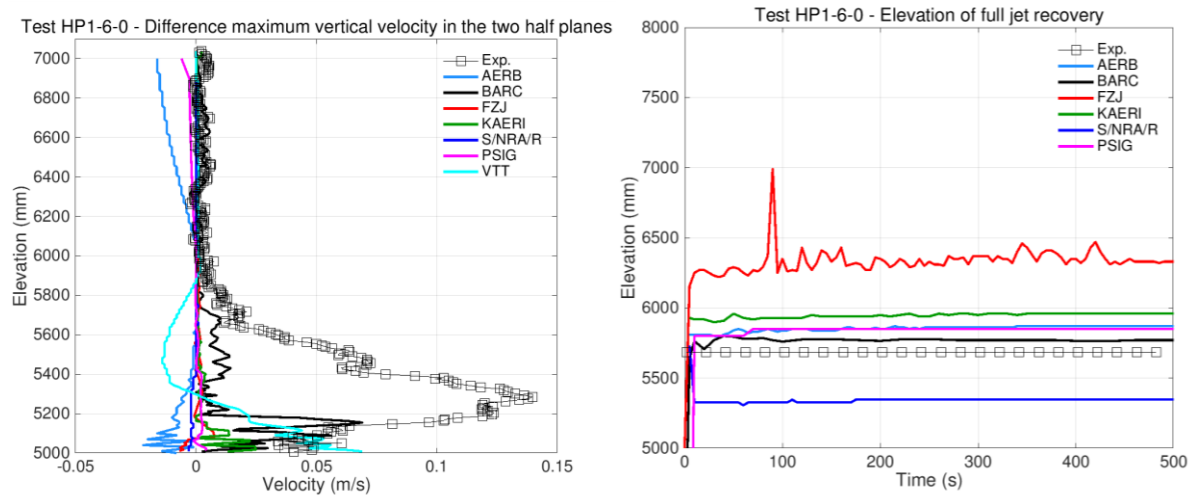


Figure 11: Open benchmark, Step 1: Difference of the maximum velocity in the two half planes (left) and position (Y2) of the full jet recovery (right).

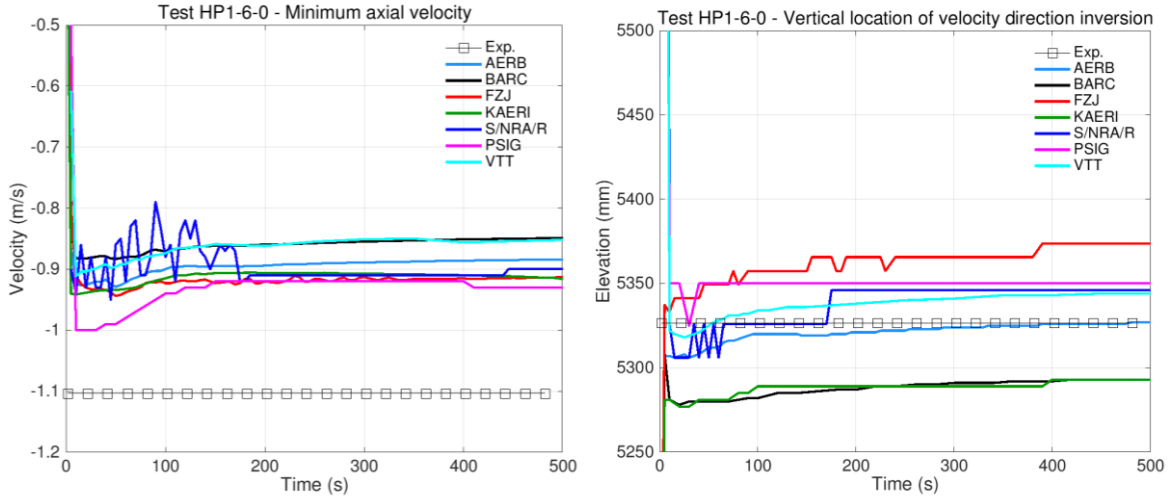


Figure 12: Open benchmark, Step 1: Time history of the minimum vertical velocity (left) and elevation (Y1) of the top of the recirculation zone (right).

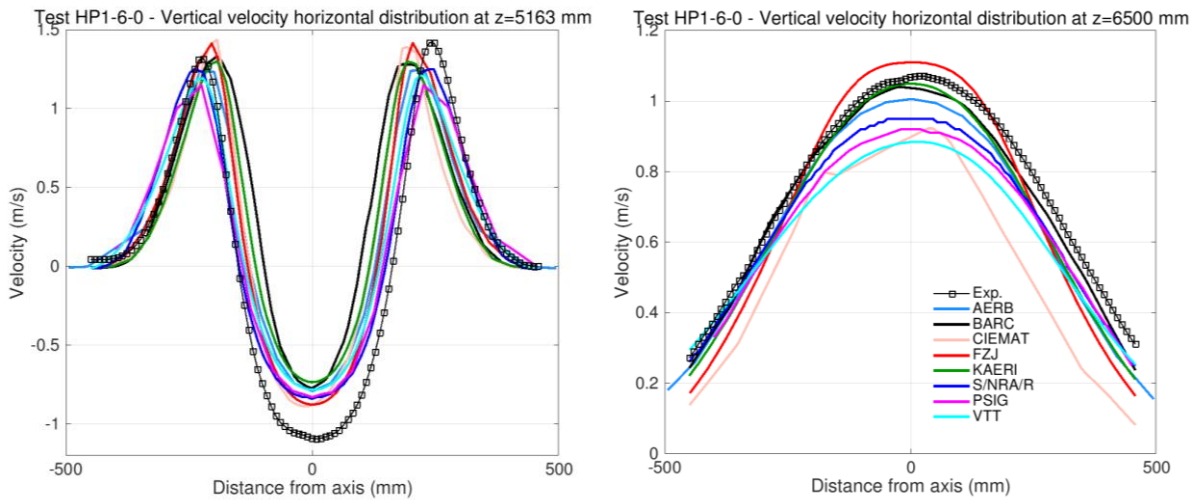


Figure 13: Open benchmark, Step 1: Horizontal profiles of the vertical velocity at the elevation of the middle of the recirculation zone (left) and at an elevation in the flow developed region (right).

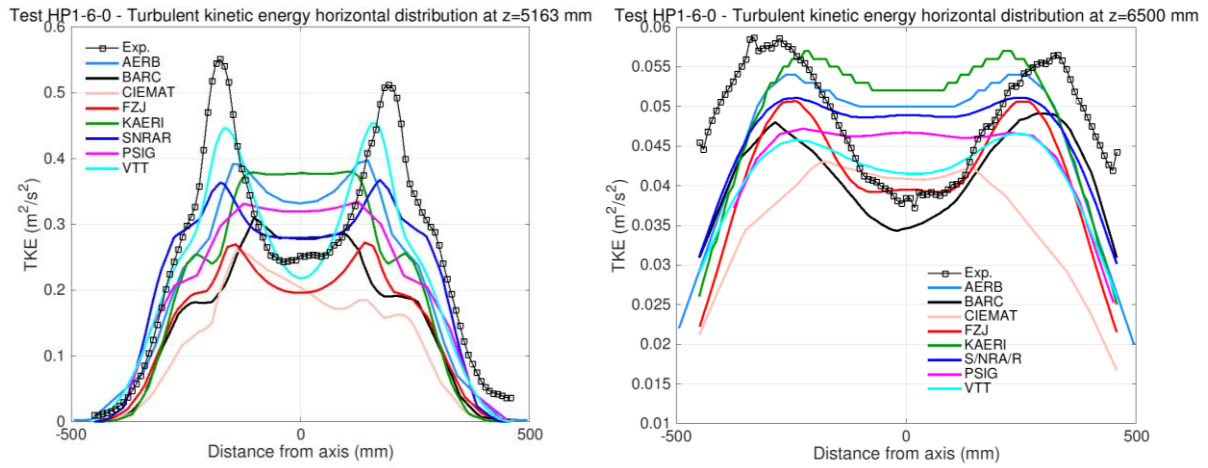


Figure 14: Open benchmark, Step 1: Horizontal profiles of the TKE at the elevation of the middle of the recirculation zone (left) and at an elevation in the flow developed region (right).

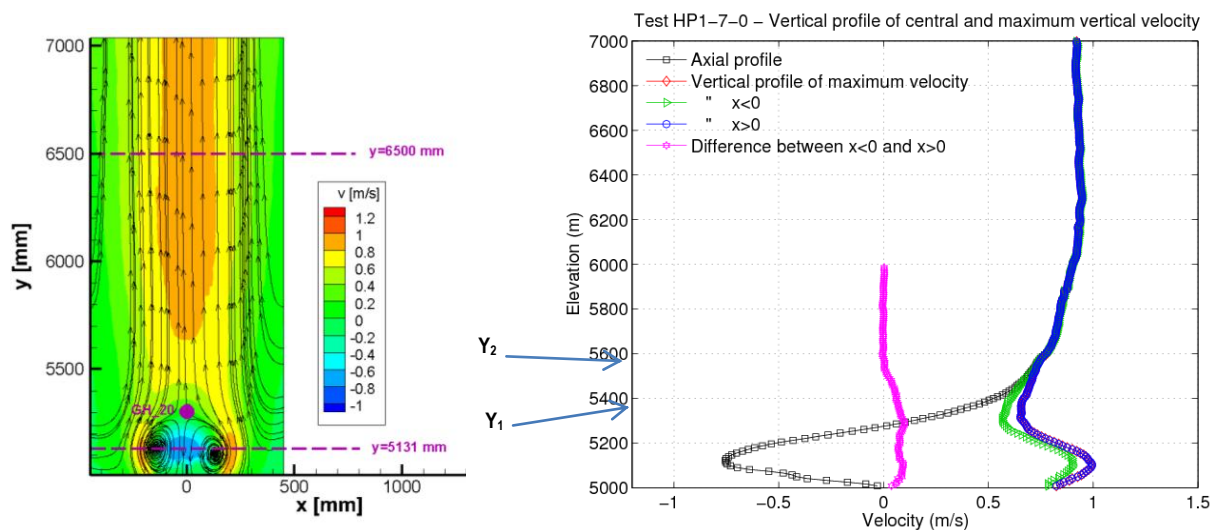


Figure 15: Open benchmark, Step 2: Average experimental flow field (left) measured in Test HP1_7_0, and vertical velocity profiles used in the comparisons with calculated results (right).

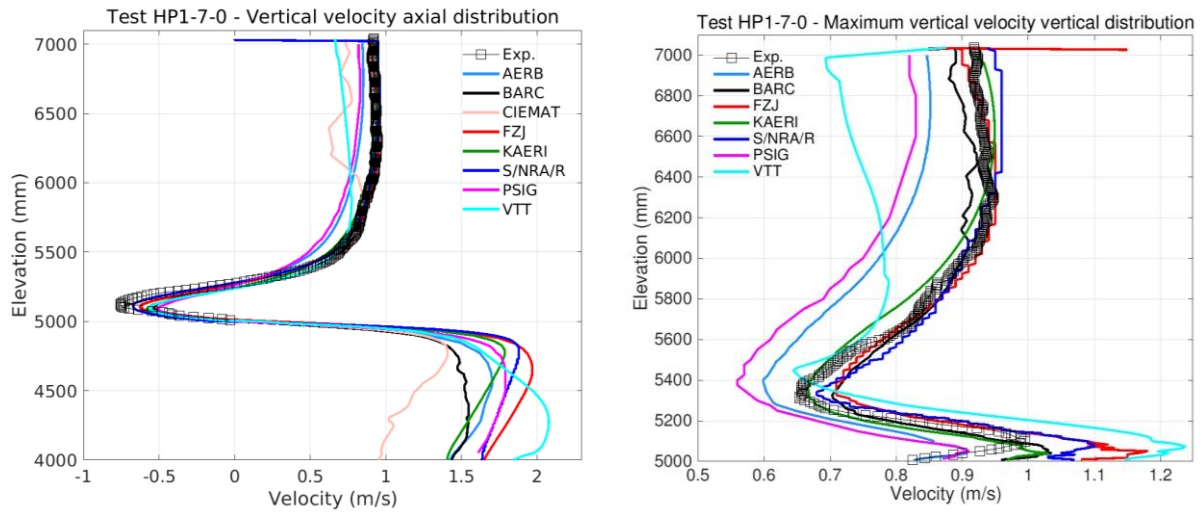


Figure 16: Open benchmark, Step 2: Axial profile of the vertical velocity (left) and vertical profile of the maximum vertical velocity (right).

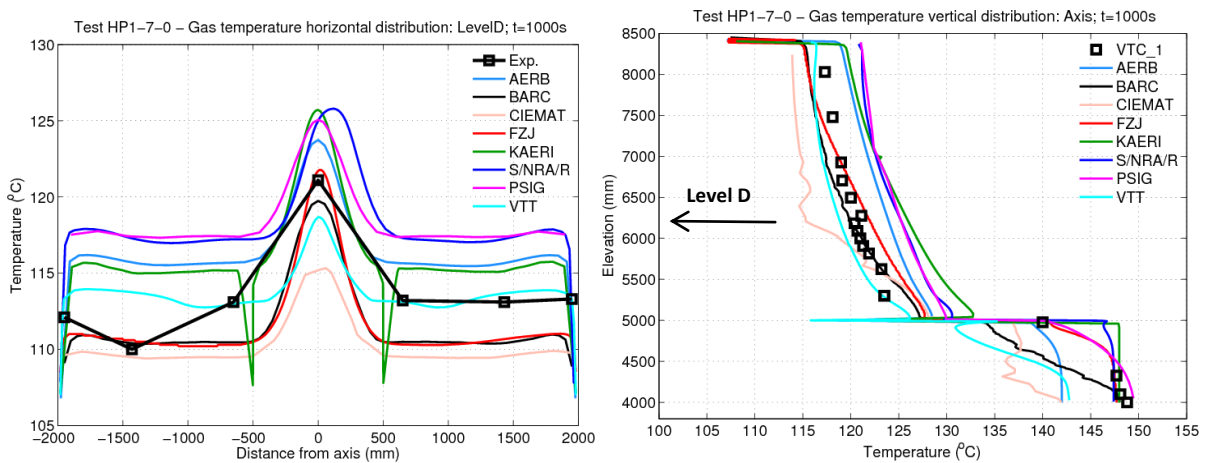


Figure 17: Open benchmark, Step 2: Temperature radial profile at 6.276 m (left) and axial temperature distribution (right).

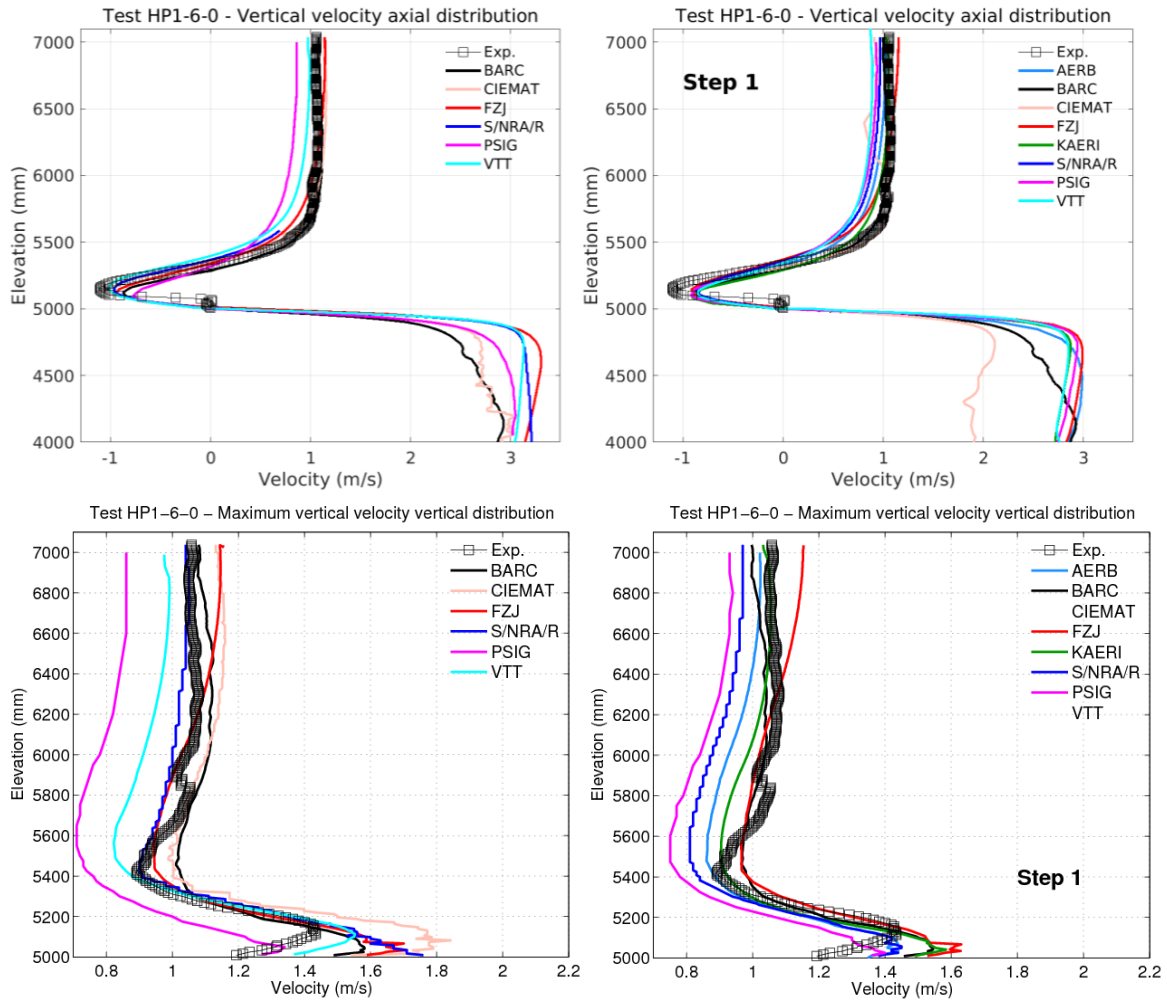


Figure 18: Open benchmark, Step 3: Axial velocity and maximum velocity vertical profiles for Step 3, compared with results for Step 1.

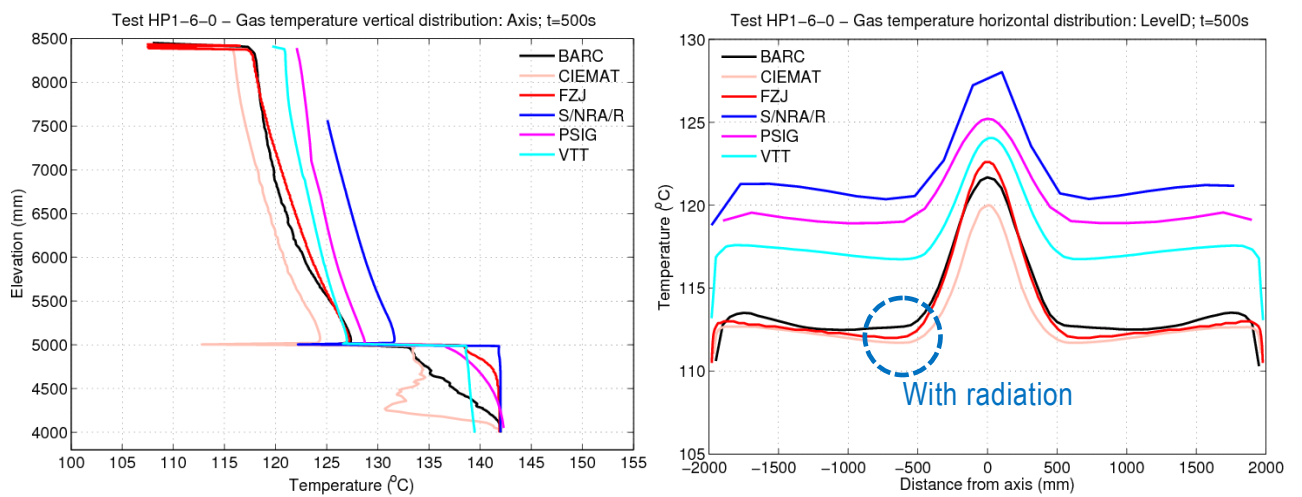


Figure 19: Open benchmark, Step 3: Axial temperature profile and horizontal profile at 6.3 m.

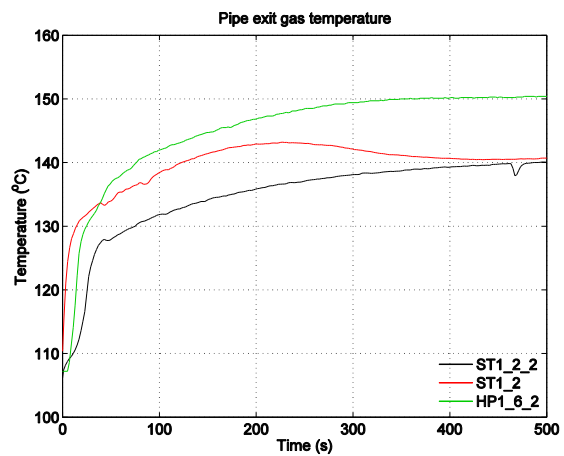
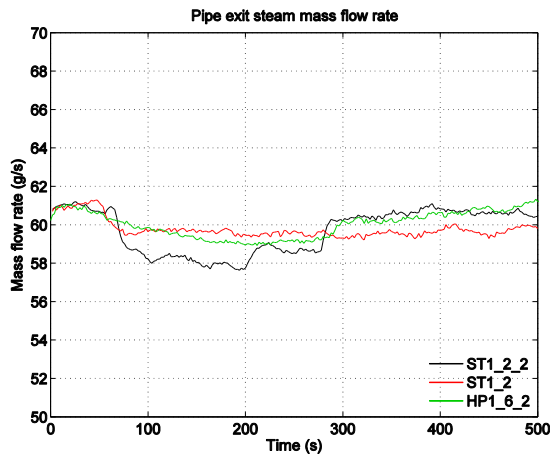
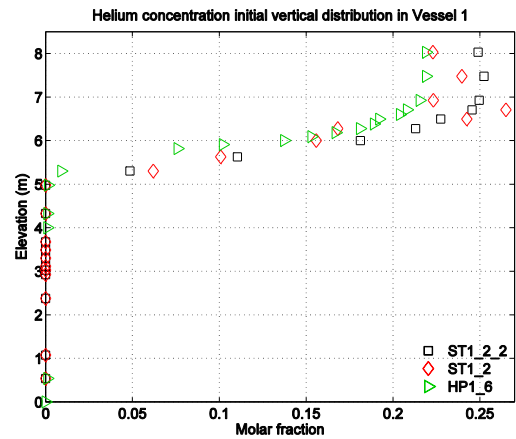
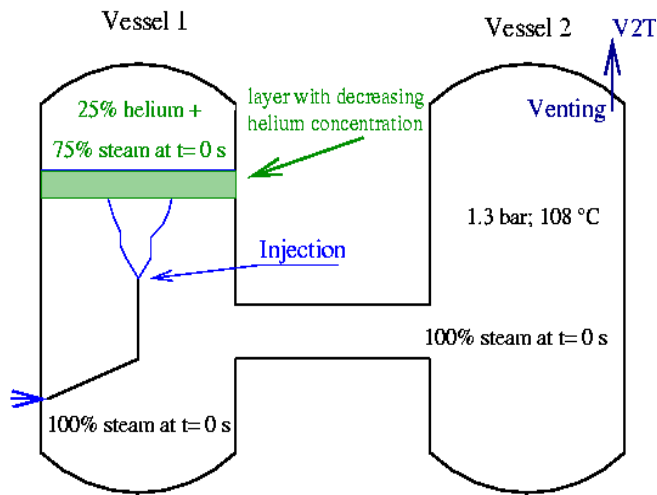


Figure 20: Open benchmark, Step 5: Configuration for SETH-2 test ST1_2_2, and important initial and boundary conditions of test ST1_2 and repetition test ST1_2_2 compared with those used for Test HP1_6_2.

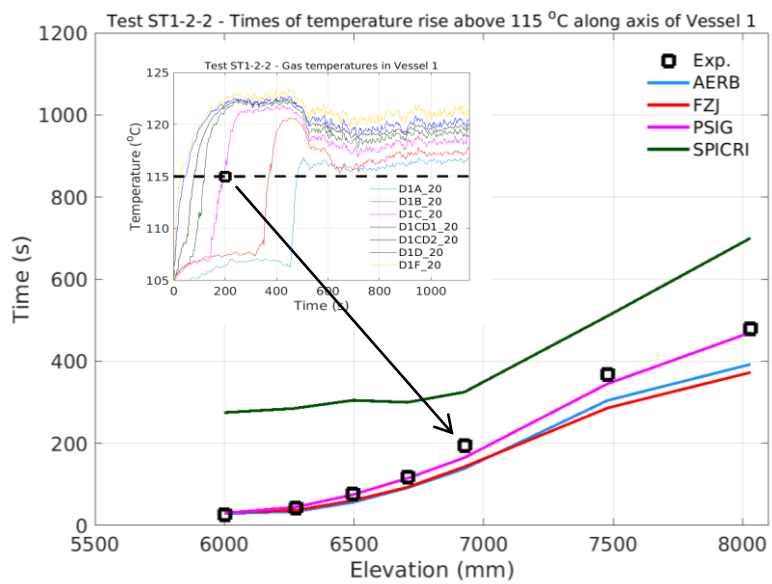


Figure 21: Open benchmark, Step 5: Progression of erosion along the axis in test ST1_2_2, using gas temperature rise times.

1
2
3
4
5
6
7
8
9
10
11
12
13
14
15
16
17
18
19
20
21
22
23
24
25
26
27
28
29
30
31
32
33
34
35
36
37
38
39
40
41
42
43
44
45
46
47
48
49
50
51
52
53
54
55
56
57
58
59
60
61
62
63
64
65

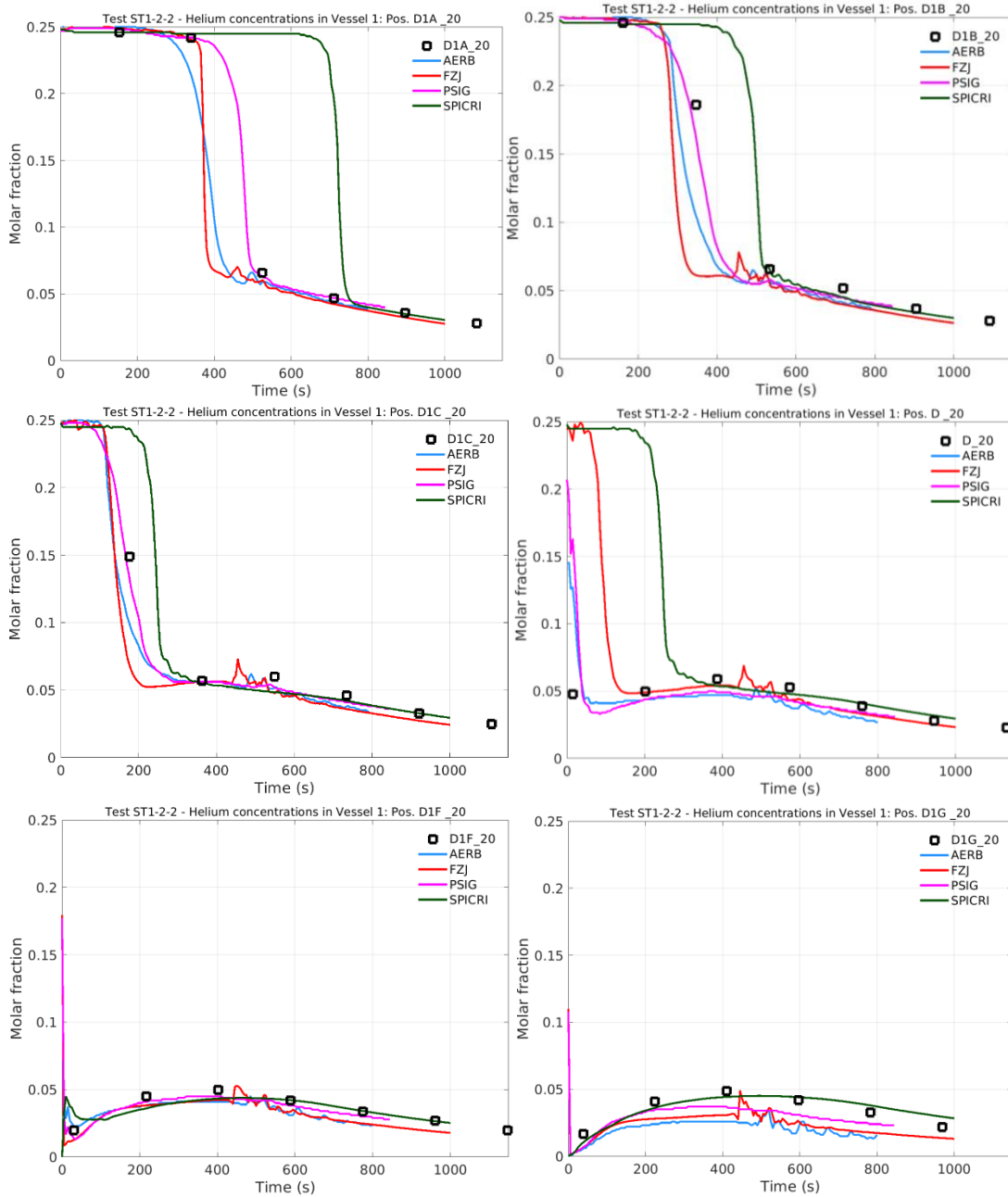


Figure 22: Open benchmark, Step 5: Helium concentration time histories at various elevations along the axis of Vessel 1.

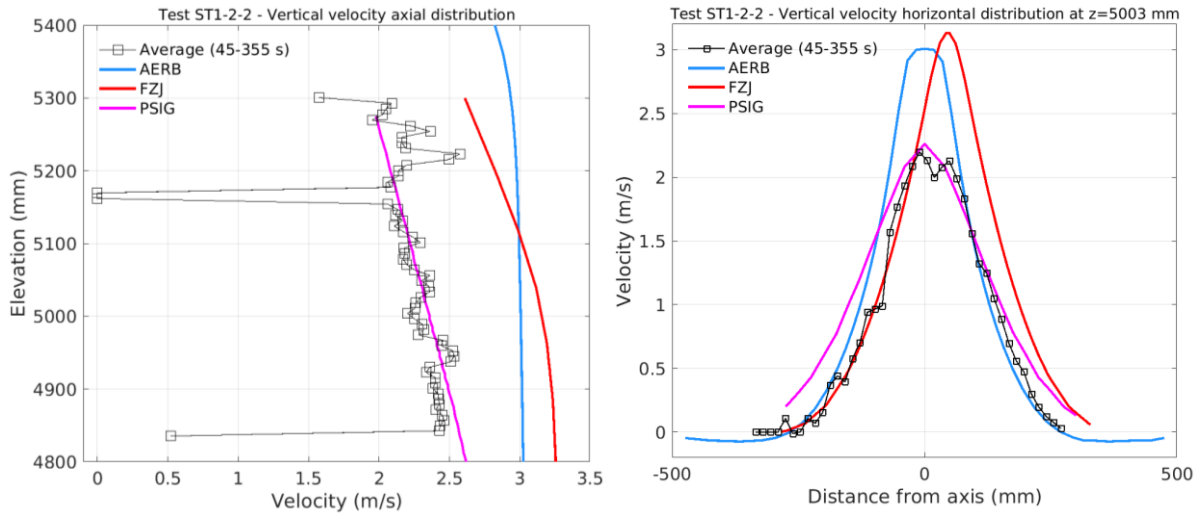


Figure 23: Open benchmark, Step 5: Vertical velocity axial profile (left) and horizontal profile at $z=5003$ mm (1 m above pipe exit)

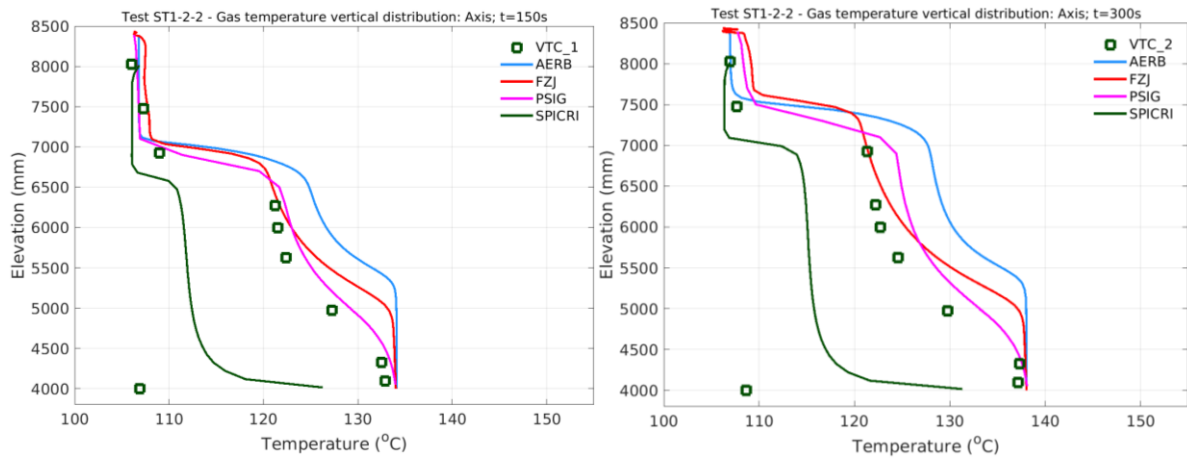


Figure 24: Open benchmark, Step 5: Axial temperature profile at two times.

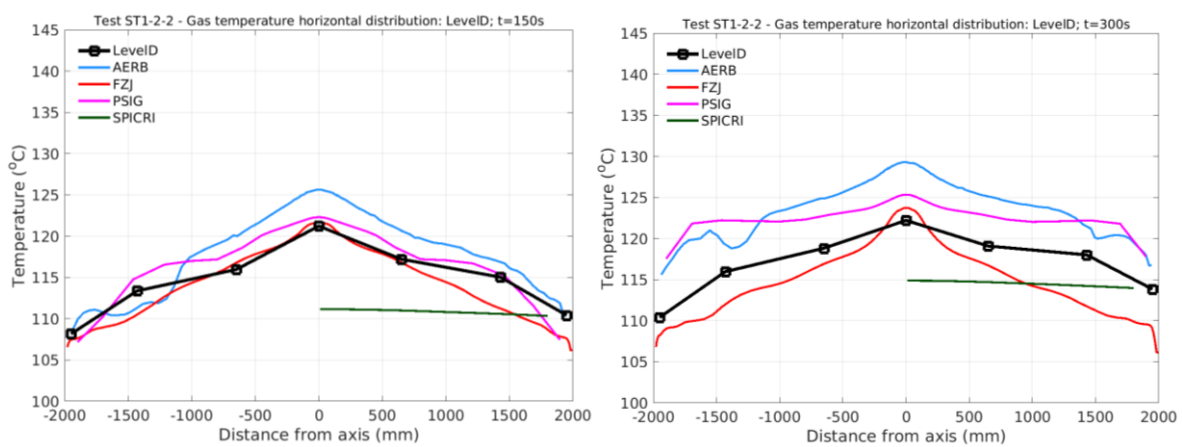


Figure 25: Open benchmark, Step 5: Horizontal profiles at 6.3 m at 150 s (before mixing) and 300 s (after mixing)

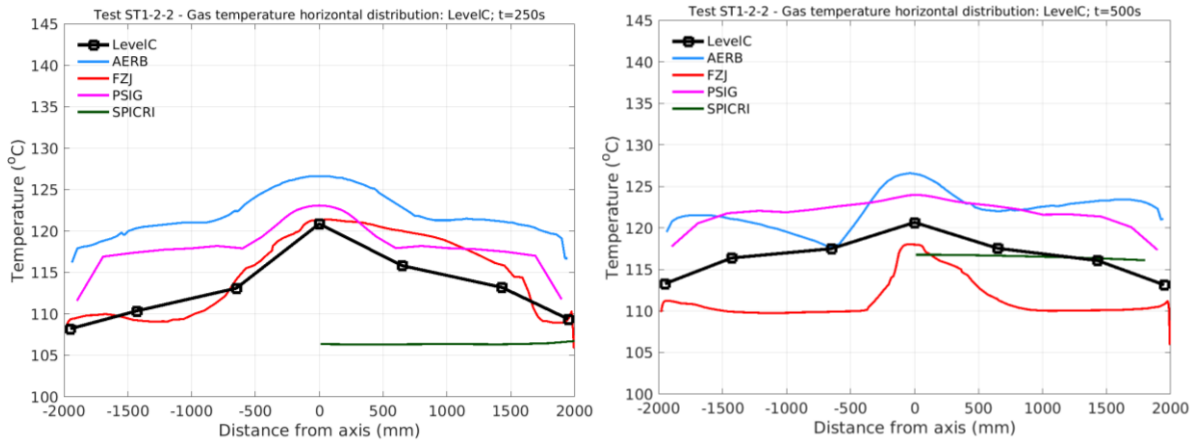


Figure 26: Open benchmark, Step 5: Horizontal profiles at 6.93 m at 250 s (during mixing or immediately after) and 500 s (after mixing)

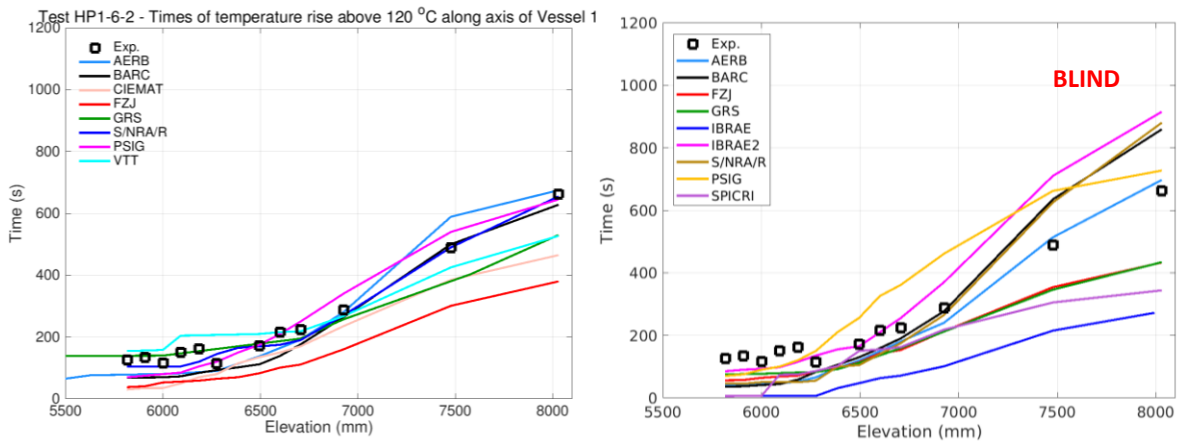


Figure 27: Open benchmark, Step 4: Erosion progression calculated in the open phase (left), compared with best estimate results contributed to the blind benchmark.

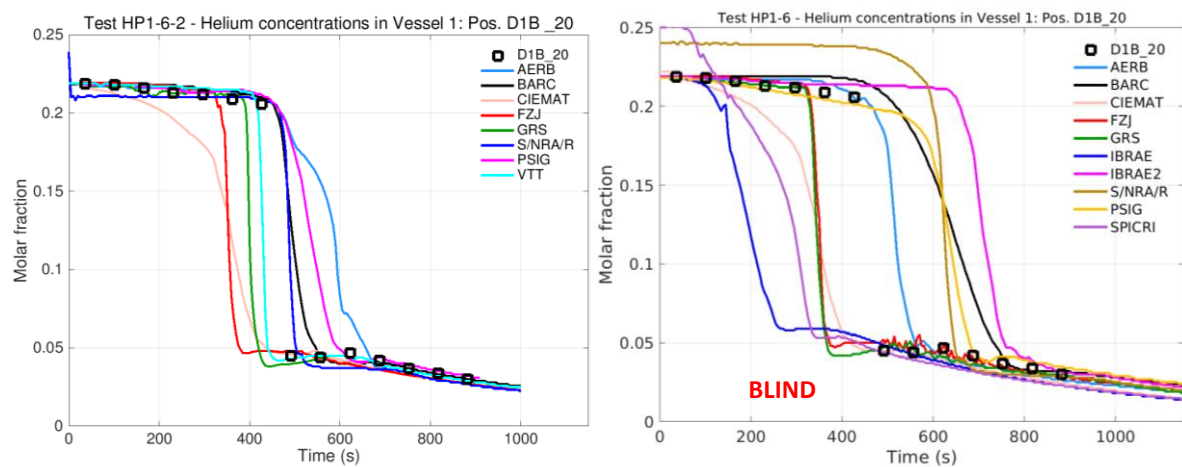


Figure 28: Open benchmark, Step 4: Helium concentration time history at $z=6.48$ m calculated in the open phase (left), compared with best estimate results contributed to the blind benchmark.

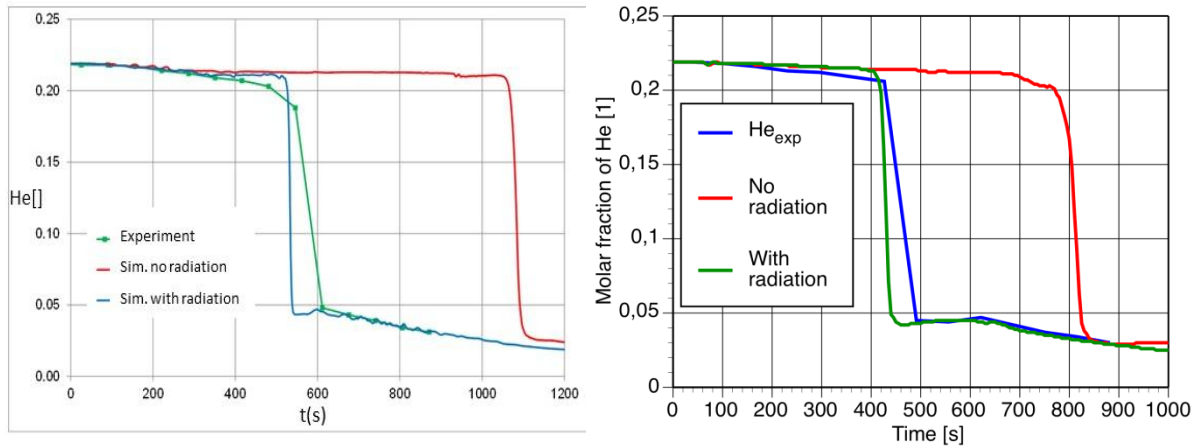


Figure 29: Open benchmark, Step 4: Example of results (helium concentration time histories) obtained at 8 m (left) by GRS (Schramm et al., 2017) and at 7.5 m (right) by VTT (Huhtanen, 2018) using the model for radiation or neglecting it.

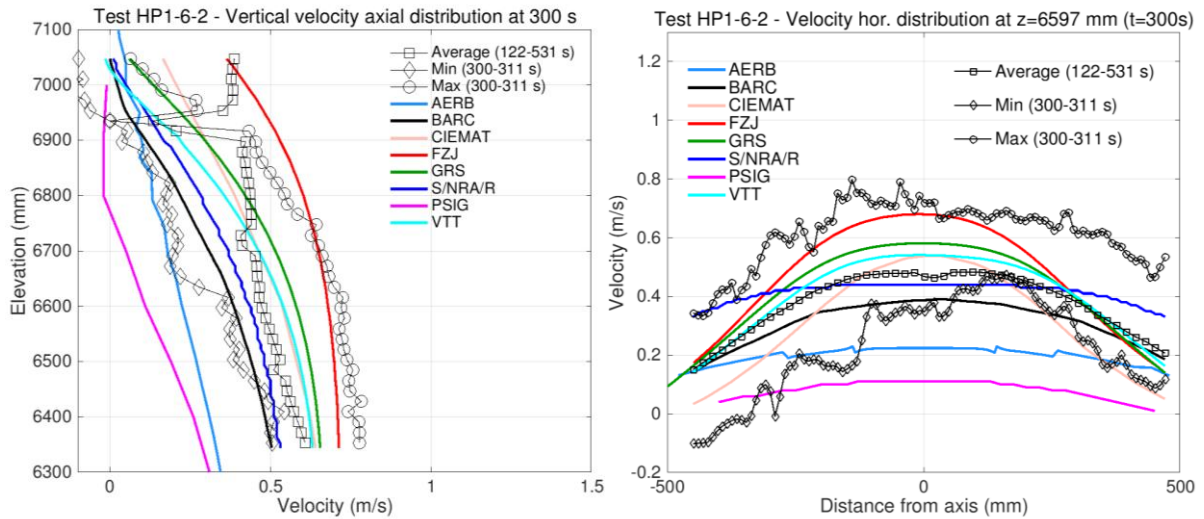


Figure 30: Open benchmark, Step 4: Vertical velocity averaged axial and horizontal profiles in the PIV window.

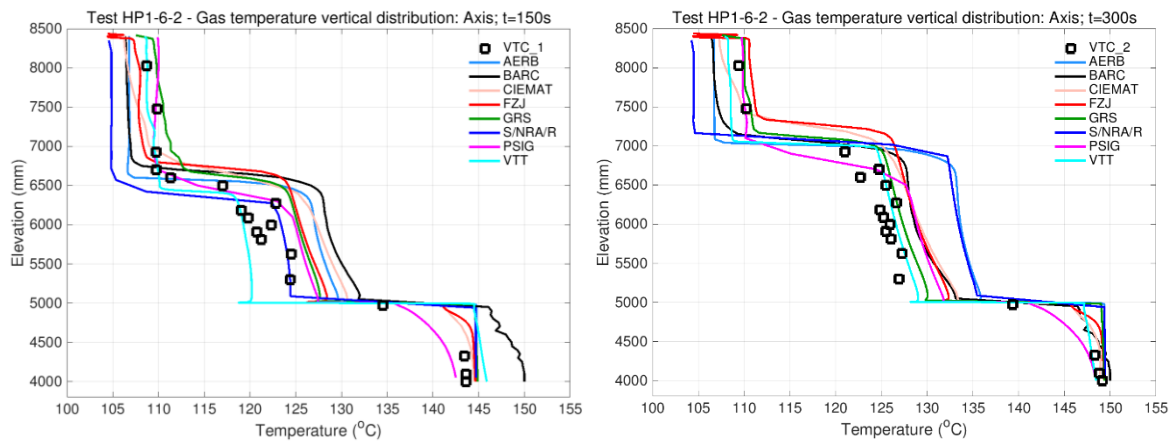


Figure 31: Open benchmark, Step 4: Axial gas temperature distributions at two times.

1
2
3
4
5
6
7
8
9
10
11
12
13
14
15
16
17
18
19
20
21
22
23
24
25
26
27
28
29
30
31
32
33
34
35
36
37
38
39
40
41
42
43
44
45
46
47
48
49
50
51
52
53
54
55
56
57
58
59
60
61
62
63
64
65

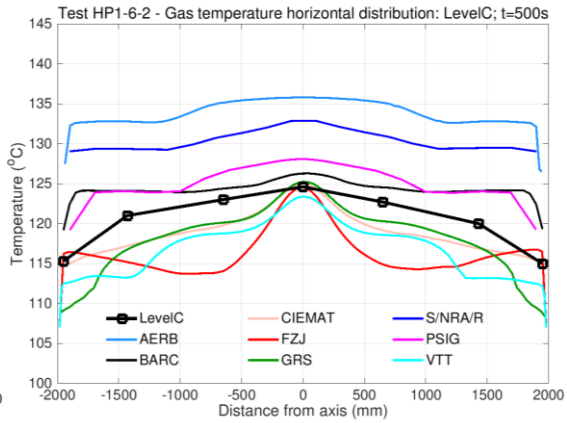
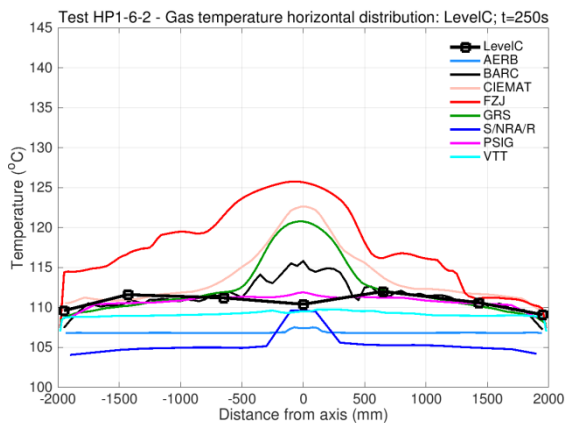
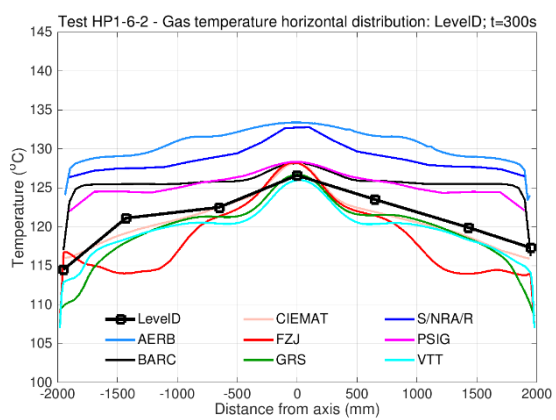
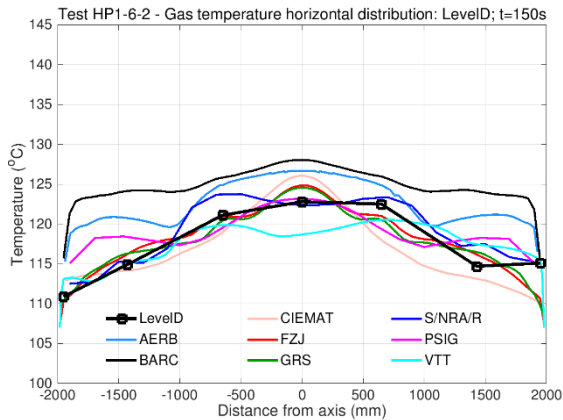
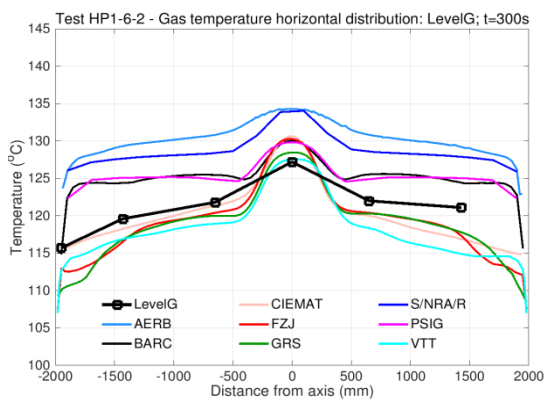
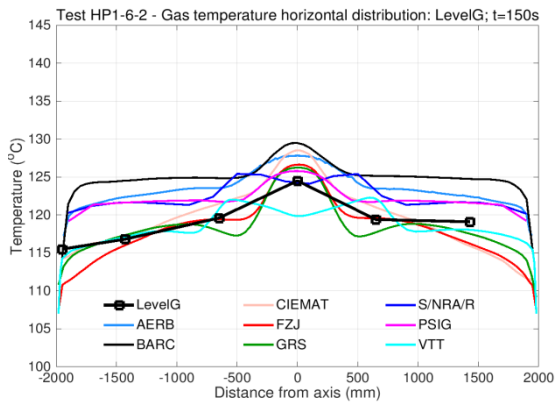
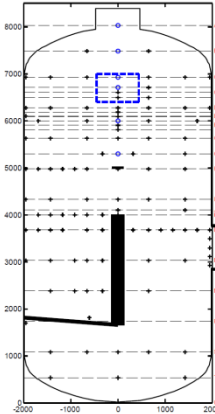
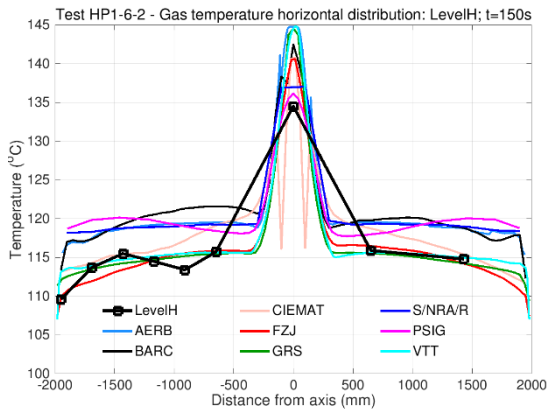


Figure 32: Open benchmark, Step 4: Gas temperature horizontal profiles at various elevations and two times.

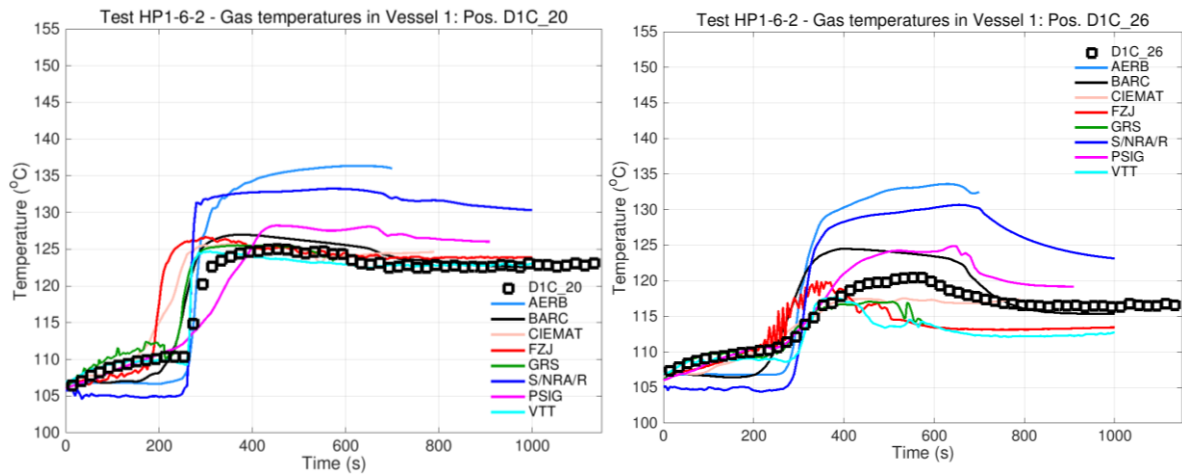


Figure 33: Open benchmark, Step 4: Gas temperature time histories at two positions (left: on the axis; right: at 570 mm from the wall) at 6.5 m.

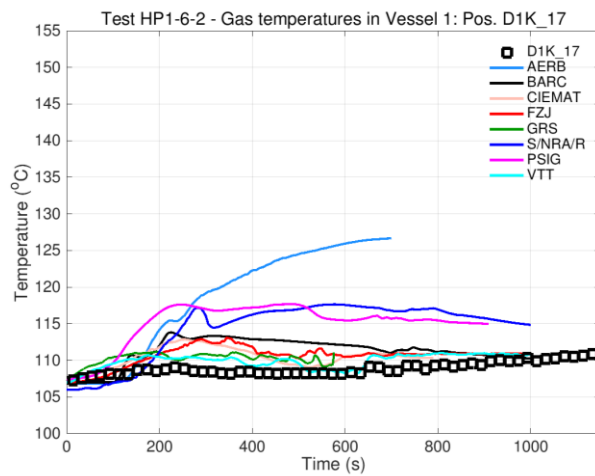
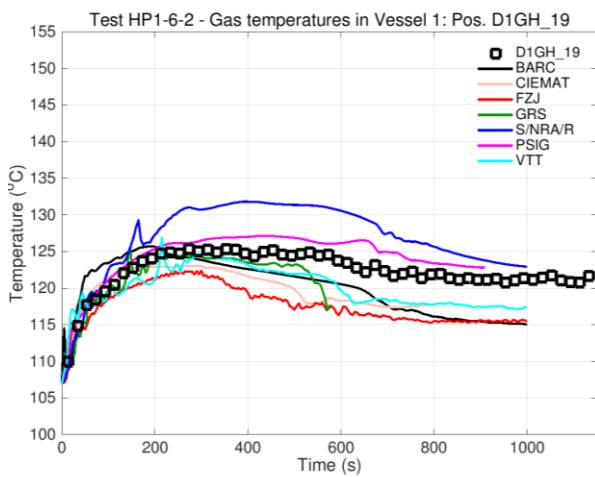


Figure 34: Open benchmark, Step 4: Off-axis ($r: \pm 325$ mm) gas temperature time histories at two positions below the initial bottom of the helium layer ($z: 5301$ and 4000 mm, respectively)

1
2
3
4
5
6
7
8
9
10
11
12
13
14
15
16
17
18
19
20
21
22
23
24
25
26
27
28
29
30
31
32
33
34
35
36
37
38
39
40
41
42
43
44
45
46
47
48
49
50
51
52
53
54
55
56
57
58
59
60
61
62
63
64
65

REFERENCES

Abe, S., Studer, E., Ishigaki, M., Sibamoto, Y., and Yonomoto, T. (2018) “Stratification Breakup by a Diffuse Buoyant Jet: The MISTRA HM1-1 and 1-1bis Experiments and their CFD Analysis”, *Nucl. Eng. Design*, **331**, pp. 162–175.

Abu-Romia, M.M. and Tien, C.L (1967) “Appropriate Mean Absorption Coefficients for Infrared Radiation of Gases”, *Journal of Heat Transfer*, **89**(4), 321-327.

Allelein, H.-J., Fischer, K., Vendel, J., Malet, J., Studer, E., Schwarz, S., Houkema, M., H. Paillère, H., Bentaib, A. (2007). International Standard Problem ISP-47 on Containment Thermal Hydraulics. Nuclear Energy Agency, Committee on the Safety of Nuclear Installations, Final Report NEA/CSNI/R(2007)10, 2007.

Allein, H.-J., Reinecke, E.-A., Belt, A., Broxtermann, P., and Kelm, S. (2012) “Combined Analytical and Experimental Investigations for LWR Containment Phenomena”, *Nucl. Eng, Technol.*, **44**(3), 249-260.

Andreani, M., Badillo, A., and Kapulla, R. (2016a) “Synthesis of the OECD/NEA-PSI CFD Benchmark Exercise”, *Nucl. Eng. Design*, **299**, 59-80

Andreani, M., Daqiang, Y., Gaikwad, A.J., Ganju, S., Gera., B., Grigoryev, S., Herranz, L.E., Huhtanen, R., Kanaev, A., Kelm, S., Kim, J., Nishimura, T., Schramm, B., Sharabi, M., and Paladino, D. (2016b) “Synthesis of a blind CFD benchmark exercise based on a test in the PANDA facility addressing the stratification erosion by a vertical jet in presence of a flow obstruction”, OECD/NEA 6th Workshop on Computational Fluid Dynamics for Nuclear Reactor Safety (CFD4NRS-6), MIT, Cambridge, MA-USA, 13-15 September, 2016.

Andreani, M. and Paladino D., (Benchmark Report, 2018), prepared by PSI (with appendices contributed by AERB, FZJ and VTT) (2018) “OECD/NEA HYMERES project: synthesis of results of the benchmark on PANDA test HP1_6_2”, PSI Technical Note AN-42-17-07 Rev.1, Project report HYMERES-P-17-48, May 2018.

Bentaib, A., Meynet, N., and Bleyer, A. (2015) “Overview on Hydrogen Risk Research and Development Activities: Methodology and Open Issues”, *Nucl. Eng. Technol.*, **47**, 26-32.

Breitung, W. and Royl, P. (2000) “Procedure and Tools for Deterministic Analysis and Control of Hydrogen Behavior in Severe Accidents”. *Nucl. Eng. Design*, **202**, 249-268.

Chan, C.K. and Jones, S.C. (1997) “Gas Mixing Experiments in a Large Enclosure”, Proc. of the 18th Annual Conf. of the Canadian Nuclear Society

Choi, Y.-S., Lee, U.-J., and Park, G.-C. (2001) “Study on local hydrogen behaviors in a subcompartment of the NPP containment”, *Nucl. Eng. Design*, **208**, 99-116.

Deri, E., Cariteau, B., and Abdo D. (2010) “Air fountains in the erosion of gaseous stratifications”, *Int. J. Heat and Fluid Flow*, Volume **31**, Issue 5, Pages 935–941.

Erkan, N., Mignot, G., Kapulla, R., Paladino, D., Zboray, R., Strassberger, H.J., Bissels, W. and Fehlmann, M. (2009) “OECD SETH-2 PANDA Test ST1_2_2 Quick-Look Report”, PSI internal technical report TM-42-09-07-0, April 2009.

Filippov, A.S., Grigoryev, S.Yu., O.V. Tarasov, O.V. (2017) “On the possible role of thermal radiation in containment thermal–hydraulics experiments by the example of CFD analysis of TOSQAN T114 air–He test”, *Nucl. Eng. Design*, **310**, 175-186.

Gupta, S. (2015) “Experimental Investigations Relevant for Hydrogen and Fission Product Issues Raised by the Fukushima Accident”, *Nucl. Eng. Technol.*, **47**, 11-25.

Howell. J.R. (1988) “Thermal Radiation in Participating Media: The Past the Present, and Some Possible Futures”, *Journal Heat Transfer*, **110**, 1220-1229.

Huhtanen, R. (2018), Private Communication.

Kapulla, R., Mignot, G., Paranjape, S., Suter, S., Fehlmann, M., and Paladino, D. (2015a) “OECD/NEA HYMERES Project: Jet/Plume interacting with flow obstruction HP1 Series. Test Series Report”, PSI internal report TM-42-15-16, Rev.0, Project report HYMERES-P-15-26, Nov. 2015 (report restricted to project participants).

Kapulla, R., Paranjape, S., Mignot, G., Suter, S., Fehlmann, M., and Paladino D. (2015b) "OECD/NEA HYMERES Project: PANDA Tests HP1_6_0, HP1_7_0, HP1_8_0, and HP1_678_Disk Data Report", PSI internal report TM-42-15-13 Rev. 0, Project report HYMERES-P-15-25, October 2015 (report restricted to project participants).

Karwat, H. et al. (1999) "State-of-the-Art Report on Containment Thermal-hydraulics and Hydrogen Distribution", OECD/NEA group of experts, CSNI/R(99)-16 (1999).

Kelm, S., Ritterath, M., Prasser, H.-M., and Allelein, H.J. (2016a) "Application of the MINIPANDA Test Case 'Erosion of a Stratified Layer by a Vertical Jet' for CFD Validation", *Nucl. Eng. Design*, **299**, 124-135.

Kelm, S., Müller, H., and Allelein, H.-J. (2016b) "Importance of thermal radiation heat transfer modeling in containment typical flows", Paper submitted for presentation at the CFD4NRS-6, MIT, Cambridge, MA, USA, September 13-15.

Liang, R. et al., (2015) "Status Report on Hydrogen Management and Related Computer Codes", NEA/CSNI/R(2014)8,

Lopez-Alonso E., Papini D., and Jimenez G. (2017) "Hydrogen Distribution and Passive Autocatalytic Recombiner (PAR) Mitigation in a PWR-KWU Containment Type", *Annals of Nuclear Energy*, **109**, pp. 600-611.

Mahaffy, J., et al. (2015). Best Practice Guidelines for the Use of CFD in Nuclear Reactor Safety Applications - Revision" NEA/CSNI/R(2014)11.

Noutsopoulos, G.C. and Yannopoulos, P.C. (1989) "Axial Dilution in Obstructed Round Buoyant Jet", *Journal of Hydraulic Engineering*, **115**(1), pp. 71-81.

Nishimura, T., Hoshi, H. and Hotta, A. (2015) "Current Research and Development Activities on Fission Products and Hydrogen Risk after the Accident at Fukushima Daiichi Nuclear Power Station", *Nucl. Eng. Technol.*, **47**, 1-10

OECD/NEA HYMERES-2 project (2017-2021).

OECD/NEA THAI Project (2010) “Hydrogen and Fission Product Issues Relevant for Containment Safety Assessment under Severe Accident Conditions” Final Report, 22 June 2010, Report NEA/CSNI/R(2010)3.

Paladino, D. and Dreier, J. (2012) “PANDA a Multi Purposes Integral Test Facility”, *Science and Technology of Nuclear Installations*, **2012**, Article ID 239319, doi:10.1155/2012/239319.

Paladino, D., Mignot, G., Kapulla, R., Zboray, R., Andreani, M., Tkatschenko, I., Studer, E., and Brinster, J. (2013) “OECD/SETH-2 Project: PANDA and MISTRA Experiments addressing Key Safety Issues for Water Reactor Containment”, Proceedings of the 15th International Topical Meeting on Nuclear Reactor Thermal-hydraulics (NURETH-15), paper 106, Pisa, Italy, 12-17 May 12-17, 2013.

Paranjape, S., Kapulla, R., Mignot, G. and Paladino D. (2018) “Gas Redistribution Caused by Interacting Heat Sources in the Presence of a Vertical Condenser,” 12th International Topical Meeting on Nuclear Reactor Thermal-Hydraulics, Operation and Safety (NUTHOS-12), Qingdao, China, October 14-18, 2018.

Sarikurt, F.S. and Hassan, Y.A. (2017) “Large Eddy Simulations of Erosion of a Stratified Layer by a Buoyant Jet”, *Int. J. of Heat and Mass Transfer*, Vol. **112**, p. 354-365.

Schramm, B., Stewering, J., and Sonnenkalb M. (2017) “Einsatz von CFD-Codes für die Simulation von unfalltypischen Phänomenen im Sicherheitseinschluss: Validierung und gezielte Modellerweiterung”, Anschlussbericht RS1526, 2017 GRS-472, ISBN 978-3-946607-55-7.

Schwarz, S., Fischer, K., Bentaib, A., Burkhardt, J., Lee, J.-J., Duspiva, J., Visser, D., Kyttala, J., Royl, P., Kim, J., Kostka, P. and Liang, R. (2011) “Benchmark on Hydrogen Distribution in a Containment based on the OECD-NEA THAI HM-2 Experiment”, *Nucl. Technol.*, **175**(3), 594–603.

Smith B.L. (2009) “Identification and Prioritization of Generic Nuclear Safety Problems Requiring CFD Analysis”, Proc. 17th Int. Conf. on Nuclear Engineering (ICONE-17), Paper 75482, Brussels, Belgium, July12-16, 2009.

Studer, E., Brinster, J., Tkatschenko, I., Mignot, G., Paladino, D., and Andreani, M. (2012)

“Interaction of a light gas stratified layer with an air jet coming from below: Large scale experiments and scaling issues”, *Nucl. Eng. Design*, **253**, 406-412.

Highlights:

- A benchmark on gas stratification erosion was conducted using an experiment in the PANDA facility
- A large spread of results was observed in the blind calculations.
- The open phase was multi-step, using complementary tests with enhanced information on velocity field
- Progress was achieved, but several contributions still exhibited large discrepancies
- Results are strongly affected by the modeling of radiation heat transfer from and within the steam

REVISED MANUSCRIPT SUBMITTED TO NUCLEAR ENGINEERING AND DESIGN

SYNTHESIS OF A CFD BENCHMARK EXERCISE BASED ON A TEST IN THE PANDA FACILITY ADDRESSING THE STRATIFICATION EROSION BY A VERTICAL JET IN PRESENCE OF A FLOW OBSTRUCTION

**Michele Andreani⁽¹⁾, Avinash J Gaikwad⁽²⁾, Sunil Ganju⁽³⁾, Bhuvaneshwar Gera⁽³⁾,
Sergey Grigoryev⁽⁴⁾, Luis Enrique Herranz⁽⁵⁾, Risto Huhtanen⁽⁶⁾,
Vivek Kale⁽²⁾, Anton Kanaev⁽⁴⁾, Ralf Kapulla⁽¹⁾, Stephan Kelm⁽⁷⁾,
Jongtae Kim⁽⁸⁾, Takeshi Nishimura⁽⁹⁾, Domenico Paladino⁽¹⁾,
Sidharth Paranjape⁽¹⁾, Berthold Schramm⁽¹⁰⁾, Medhat Sharabi⁽¹⁾,
Feng Shen⁽¹¹⁾, Bai Wei⁽¹¹⁾, Daqiang Yan⁽¹¹⁾, Rongjin Zhang⁽¹¹⁾**

⁽¹⁾ Paul Scherrer Institut (PSI), Switzerland

⁽²⁾ Atomic Energy Regulatory Board (AERB), India

⁽³⁾ Bhabha Atomic Research Center (BARC), India

⁽⁴⁾ Nuclear Safety Institute, IBRAE, Russian Federation

⁽⁵⁾ Centro de Investigaciones Energéticas, Medioambientales y Tecnológicas (CIEMAT), Spain

⁽⁶⁾ VTT Technical Research Centre of Finland Ltd, Finland

⁽⁷⁾ Forschungszentrum Jülich (FZJ), Germany

⁽⁸⁾ Korea Atomic Energy Research Institute (KAERI), Korea

⁽⁹⁾ Regulatory Standard and Research Department,
Secretariat of Nuclear Regulation Authority (S/NRA/R), Japan

⁽¹⁰⁾ Gesellschaft für Anlagen- und Reaktorsicherheit (GRS), Germany

⁽¹¹⁾ State Power Investment Corporation Research Institute (SPICRI), People's Republic of China

* Corresponding author: Michele Andreani

Laboratory for Scientific Computing and Modelling

Paul Scherrer Institut, Forschungsstrasse 111, 5232 Villigen PSI, Switzerland

Tel.: ++41 56 310 2687

Fax: ++41 56 310 4481

E-Mail: michele.andreani@psi.ch

1
2
3
4
5
6
7 **REVISED** MANUSCRIPT SUBMITTED TO NUCLEAR ENGINEERING AND DESIGN
8
9

10
11 **SYNTHESIS OF A CFD BENCHMARK EXERCISE BASED ON A TEST IN THE PANDA**
12 **FACILITY ADDRESSING THE STRATIFICATION EROSION BY A VERTICAL JET IN**
13 **PRESENCE OF A FLOW OBSTRUCTION**

14 **Michele Andreani⁽¹⁾, Avinash J Gaikwad⁽²⁾, Sunil Ganju⁽³⁾, Bhuvaneshwar Gera⁽³⁾,**
15 **Sergey Grigoryev⁽⁴⁾, Luis Enrique Herranz⁽⁵⁾, Risto Huhtanen⁽⁶⁾,**
16 **Vivek Kale⁽²⁾, Anton Kanaev⁽⁴⁾, Ralf Kapulla⁽¹⁾, Stephan Kelm⁽⁷⁾,**
17 **Jongtae Kim⁽⁸⁾, Takeshi Nishimura⁽⁹⁾, Domenico Paladino⁽¹⁾,**
18 **Sidharth Paranjape⁽¹⁾, Berthold Schramm⁽¹⁰⁾, Medhat Sharabi⁽¹⁾,**
19 **Feng Shen⁽¹¹⁾, Bai Wei⁽¹¹⁾, Daqiang Yan⁽¹¹⁾, Rongjin Zhang⁽¹¹⁾**

20
21 ⁽¹⁾ Paul Scherrer Institut (PSI), Switzerland

22 ⁽²⁾ Atomic Energy Regulatory Board (AERB), India

23 ⁽³⁾ Bhabha Atomic Research Center (BARC), India

24 ⁽⁴⁾ Nuclear Safety Institute, IBRAE, Russian Federation

25 ⁽⁵⁾ Centro de Investigaciones Energéticas, Medioambientales y Tecnológicas (CIEMAT), Spain

26 ⁽⁶⁾ VTT Technical Research Centre of Finland Ltd, Finland

27 ⁽⁷⁾ Forschungszentrum Jülich (FZJ), Germany

28 ⁽⁸⁾ Korea Atomic Energy Research Institute (KAERI), Korea

29 ⁽⁹⁾ Regulatory Standard and Research Department,

30 Secretariat of Nuclear Regulation Authority (S/NRA/R), Japan

31 ⁽¹⁰⁾ Gesellschaft für Anlagen- und Reaktorsicherheit (GRS), Germany

32 ⁽¹¹⁾ State Power Investment Corporation Research Institute (SPICRI), People's Republic of China

33
34
35
36
37
38
39
40
41
42 * Corresponding author: Michele Andreani

43 Laboratory for Scientific Computing and Modelling

44 Paul Scherrer Institut, Forschungsstrasse 111, 5232 Villigen PSI, Switzerland

45 Tel.: ++41 56 310 2687

46 Fax: ++41 56 310 4481

47
48
49
50
51 E-Mail: michele.andreani@psi.ch
52
53
54
55
56
57
58
59
60
61
62
63
64
65

1
2
3
4
5
6
7 **Abstract**
8

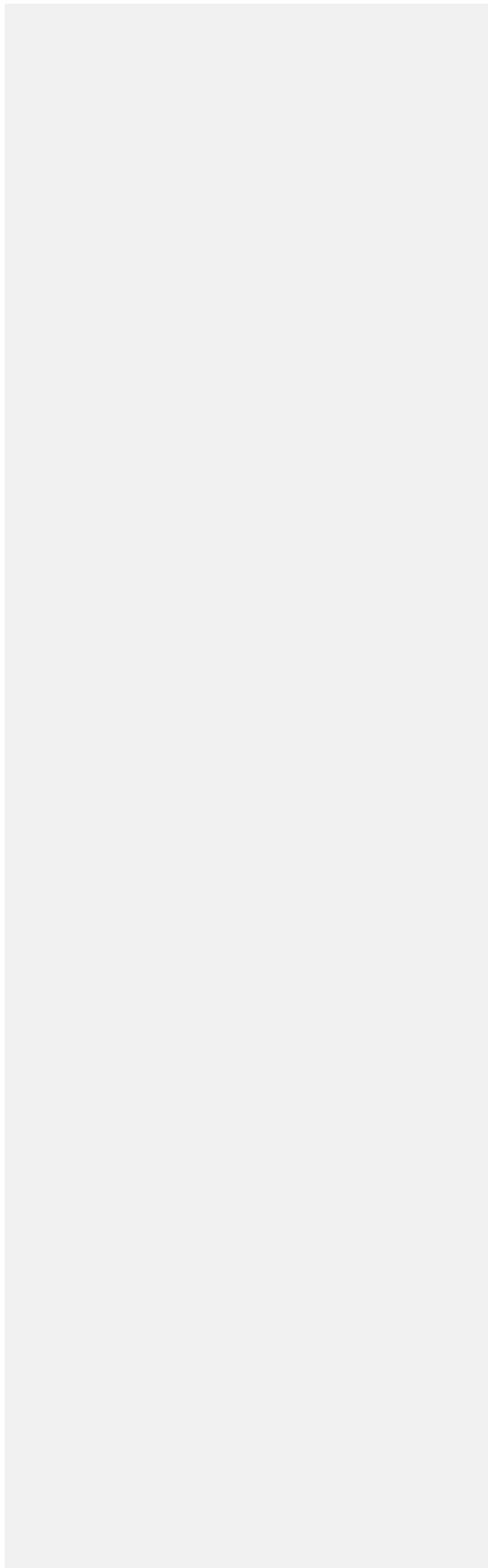
9 The benchmark exercise discussed in this paper was conducted within the OECD/NEA project
10 HYMERES. The specific experiment in the PANDA facility chosen for the present benchmark
11 addresses the stratification erosion in a vessel where the upper region contained initially a mixture of
12 steam and helium, and the remaining volume was filled with steam. The mixing is induced by a
13 vertical steam jet, which originates from the exit of a circular pipe located below the bottom of the
14 helium-rich layer. The stratification erosion process ~~mixing~~ is somewhat slowed down by a small
15 circular plate above the jet source. The exercise consisted of a blind phase, and an open phase. Two
16 sets of blind simulations were requested: one set obtained using a “common model”, and a second set
17 produced by a “best estimate” model. For the “common model”, a list of recommendations was given,
18 whereas for the “best estimate” model, each participant was free to choose the modelling approach.
19 The submitted results for the erosion times were in a large band, and especially the large differences
20 in the results with the “common model” were not expected. The results of the best estimate
21 simulations showed that the combination of mesh and modelling approach can lead to a wide spread
22 of results. The most important difficulty in interpreting the results and finding the reason of the large
23 deviations was the lack of information on the velocity field downstream of the obstruction. Therefore,
24 for the open phase extended data from auxiliary, “zero” tests (for similar conditions but without
25 helium layer) were provided to the participants to permit a more basic validation of their models,
26 using a “multi-step approach”. The step-by-step validation permitted some progress with respect to
27 some of the items identified in the blind benchmark. However, large discrepancies with data in the
28 final analyses of the test are observed, which cannot be easily attributed to specific model deficiencies
29 or insufficient detail of the mesh. These results raised some questions in relation to best practice
30 guidelines for the use of Computational Fluid Dynamic (CFD) codes for containment analysis and
31 indicated needs for further CFD-grade experiments.
32
33
34
35
36
37
38
39
40
41
42
43
44
45
46
47
48
49

50 **Keywords:** Containment, stratification erosion, buoyant jet, benchmark, PANDA
51
52
53
54
55
56
57
58
59
60
61
62
63
64
65

1
2
3
4
5
6
7
8
9
10
11
12
13
14
15
16
17
18
19
20
21
22
23
24
25
26
27
28
29
30
31
32
33
34
35
36
37
38
39
40
41
42
43
44
45
46
47
48
49
50
51
52
53
54
55
56
57
58
59
60
61
62
63
64
65

Highlights:

- A benchmark on gas stratification erosion was conducted using an experiment~~test~~ in the PANDA facility
- A large spread of results was observed in the blind calculations.
- The open phase was multi-step, using complementary tests with enhanced information on velocity field
- Progress was achieved, but several contributions still exhibited large discrepancies
- Results are strongly affected by the modeling of radiation heat transfer from and within the steam



1
2
3
4
5
6
7
8
9
10
11
12
13
14
15
16
17
18
19
20
21
22
23
24
25
26
27
28
29
30
31
32
33
34
35
36
37
38
39
40
41
42
43
44
45
46
47
48
49
50
51
52
53
54
55
56
57
58
59
60
61
62
63
64
65

1. INTRODUCTION

Hydrogen generated during a ~~(postulated)~~ severe accident with core degradation is a major safety issue (Karwat et al., 1999; Breitung and Royl, 2000; Bentaib et al., 2015; Lopez-Alonso et al., 2017), because deflagration or detonation might challenge the structural integrity of the containment. The concern about hydrogen risk and the demand for additional research on accident scenarios and on mitigation measures grew after the Fukushima [Daiichi](#) accident (Liang et al., 2015; Gupta, 2015; Nishimura, et al, 2015). In particular, hydrogen stratification can substantially increase the risk, as this could lead to local pockets of mixtures with high concentration of this flammable gas (Choi et al., 2001). A special concern is thus the build-up and persistence of stratification of hydrogen in certain regions, which has to be addressed by dedicated experimental research and accurate analyses (Smith, 2009). Various experimental programmes (Allelein et al., 2007; Deri et al., 2010; OECD/NEA THAI Project, 2010; Allelein et al., 2012; Studer et al., 2012; Paladino et al., 2013; Kapulla et al., 2014) and code validation activities (Schwarz et al., 2011; Kelm et al., 2016a; Andreani et al., 2016a; Sarikurt and Hassan, 2017; Abe et al., 2018) have included in-depth investigations on stratification formation and break-up/erosion processes. This research included, among others, the investigation on the interaction of a gas plume or jet with a density interface in an open space, typical of the situation in the dome of the containment. However, since the multi-compartment geometry of many containment designs is quite complex, it is necessary to assess the capability of the codes to simulate the effect of various structures on the evolution of the distribution of gases in the presence of flow obstructions. In particular, the effect on mixing of an obstruction at short distance from the origin of the efflux is of general interest (e.g., Noutsopoulos and Yannopoulos, 1989), but only a few investigations with light gases exist in open literature (e.g., Chan and Jones, 1997). A first series of experiments in PANDA addressing this issue have been conducted within the HYMERES project.

HYMERES (HYdrogen Mitigation Experiments for REactor Safety) is the acronym for an OECD/NEA project (2013-2016), which is supported by thirteen countries and centered around experiments performed in the PANDA and MISTRA facilities, located at PSI in Switzerland and CEA in France, respectively (Paladino et al., 2012). The project includes various series of experiments (with helium used as simulant for hydrogen), where the mixing of a stratified atmosphere is controlled by jets or energy sinks/sources (such as heaters, coolers, etc.). In PANDA, stratified conditions, with a helium-rich layer at the top of one steam-filled vessel, are either initially prescribed or built during the transient. One of these experiments in PANDA (HP1_6_2) was chosen for the present benchmark, which is similar to the recent OECD/NEA PANDA Benchmark (Andreani et al., 2016a). It addresses again the stratification erosion induced by a vertical jet, but in this new test, with injection of steam instead of air, and with an obstruction above the pipe exit. [The conditions of the experiment address an idealised accident scenario, where a dry release of pure light gas \(Hydrogen in Light Water](#)

1
2
3
4
5
6
7 reactors) is followed by a phase of steam release. In most postulated scenarios, stratification and
8 mixing would be in competition, due to the continuous efflux into the containment and operation of
9 safety features. The simpler conditions investigated in HYMERES are, however, more suitable for
10 fundamental code validation. In other projects (e.g. ERCOSAM-SAMARA, Paladino et al., 2018),
11 stratification break-up caused by the operation of safety measures was investigated, neglecting the
12 continuous steam release.
13
14

15
16 The OECD /NEA PANDA benchmark indicated that even for simple conditions the successful
17 application of CFD to containment flows is still hindered by the special feature of the typical
18 problems, i.e. long transients in very large fluid domains. Under these conditions, the application of
19 Best Practice Guidelines (Mahaffy et al., 2015) proves to be very demanding, and often nearly
20 impossible with the available project times and computing resources. Benchmarking activities
21 (especially based on blind predictions) are therefore very important to reveal the weaknesses of
22 modelling strategies established on the base of previous experience when a new problem has to be
23 tackled and sensitivity studies must be limited to a few runs.
24
25

26
27 In order to enhance the interpretation of the comparison of the calculated results with the experimental
28 data, for the blind benchmark the participants were requested to submit two sets of results: one set
29 should be obtained using a “common model”, and a second set produced by a “best estimate” model.
30 “The common model” was an attempt to overcome the difficulties to identify merits and limitations of
31 the simulations due to the effect of a large number of parameters, which, for instance, affected the
32 OECD/NEA benchmark (Andreani et al., 2016a). For the “common model”, a list of
33 recommendations was given with respect to initial and boundary conditions (e.g., homogeneous initial
34 vertical gas and wall temperatures, modelling of the injection pipe), as well as concerning model
35 selection (no condensation, no radiative heat transfer, standard k-ε turbulence model). For the “best
36 estimate” model, each participant was free to choose the modelling approach that was considered to
37 be the best suited to the physical problem investigated, also on the base of previous experience, and to
38 use refined representation of initial and boundary conditions. Each participant was expected to submit
39 only one set of results for each of the two models. The participants were encouraged to use Best
40 Practice Guidelines (BPG) to provide the most trustworthy set of results, but only few participants
41 could afford more than a mesh sensitivity study using two meshes.
42
43
44
45
46

47 Both sets of submissions, i.e. those using a “Common Model” (CM) and those using a “Best Estimate
48 Model” (BEM) model produced a large variety of results, leaving open a number of questions. The
49 open phase of the benchmark was then considered necessary to provide more information on the
50 importance of some physical effects and the capability of the various modelling strategies adopted by
51 the participants to address them.
52
53
54
55
56
57
58
59
60
61
62
63
64
65

1
2
3
4
5
6
7
8 The present paper reports the outcome of the benchmark. Results for the entire set of variables
9 requested are collected and discussed in Andreani and Paladino (2018), which will be referred to as
10 the Benchmark Report (2018). Here, only the main aspects of the benchmark are discussed. Since the
11 results of the blind phase were already illustrated in Andreani et al. (2016b), the paper focuses on the
12 open phase of the benchmark.
13
14

15 16 **2. THE EXPERIMENT**

17
18 Only the essential information necessary for comparing the test results and the simulations is provided
19 in this chapter. A complete presentation of the tests and of the main experimental results is included in
20 a project report (Kapulla, et al., 2015a).
21
22

23 24 **2.1 Configuration and test conditions**

25
26 The PANDA facility (Paladino and Dreier, 2012) is a multi-compartment, large-scale thermal-
27 hydraulics test rig located at the Paul Scherrer Institute (PSI), Switzerland. For these series of tests
28 only the two upper vessels were used (Fig. 1, where the large manholes at the top of the vessels are
29 also visible), which are 8 m in height and 4 m in diameter. In Fig. 1, the nominal conditions of the test
30 are indicated. The PANDA vessels and the major internal penetrations/flanges are made of stainless
31 steel. All external surfaces are insulated, and the heat losses have been experimentally determined
32 over a broad range of temperatures. The experiment mainly addresses the evolution of the thermal-
33 hydraulic variables in the vessel (injection vessel, on the left in the figure) where the initial
34 stratification was created and the steam was injected. In the injection vessel (Vessel 1), a steam jet
35 originates from a circular pipe located on the axis of the vessel and with an exit located 2 m below the
36 bottom of the helium-rich layer (which starts at 6 m). Steam is produced in the RPV vessel (scaled
37 Reactor Pressure Vessel, used for this function in integral experiments), which, for fundamental tests
38 like those in HYMERES, is configured as the steam source. The mixing is somewhat slowed down by
39 a small circular plate (20 cm in diameter) also centered on the axis and positioned 1 m above the jet
40 exit. The vessels are kept at approximately constant pressure (1.3 bar) during the test by venting the
41 fluid to the atmosphere through a nozzle at the top of Vessel 2.
42
43
44
45
46

47
48 Prior to the test, saturated steam was injected in the vessels, and the fluid and vessel walls (as well as
49 the obstruction plate) were thus heated to the target temperature, which was set to avoid wall
50 condensation during the transient. Stratified steam/helium conditions then have been created in the
51 test vessel by injecting helium above 6000 mm (Fig. 1). Just before the beginning of the test, a
52 helium-rich layer occupies the region above the elevation of 5000 mm (measured from the lowest
53
54
55
56
57
58
59
60
61
62
63
64
65

1
2
3
4
5
6
7 point on the inside of the vessel), the molar fraction of helium increasing non-linearly to about 0.22 at
8 8000 mm and above into the manhole space. The region of Vessel 1 below this layer and Vessel 2 are
9 filled with steam. The air concentrations were between 0.1 and 0.2%. The measured helium molar
10 fraction at time $t = 0$ as a function of elevation is also displayed in Fig. 1. ~~The uncertainty in the~~
11 ~~measurement of gas concentration is $\pm 1.5\%$ absolute. All concentration measurements are subject to~~
12 ~~total combined uncertainties of $<1\%$.~~The measured gas and wall temperatures immediately before the
13 start of the transient were between 105 and 108 °C (nominal value: 108 °C). These values ensure that
14 condensation (if any) could not play a role during the transient. All temperature measurements are
15 subject to an uncertainty of ± 0.7 K.

16
17
18
19 The test was started by injecting superheated steam, the flow rate and the temperature being 60 g/s
20 and 150 °C, respectively. During the test, gas and wall temperatures at several locations were
21 measured, and helium concentration was measured at 6 elevations above the injection. Moreover, PIV
22 measurements in a zone of fluid initially immersed in the helium-rich layer (far above the plate)
23 provide average velocities and turbulent quantities, and thus some information on the interaction
24 between the jet and the stratified ambient (see below).
25
26
27

28 29 **2.2 Main results**

30
31 In the experiment, the ~~time evolution~~histories of gas temperatures and helium concentrations above
32 the injection describe the progression of the erosion process (Fig 2). ~~The erosion~~which
33 is characterized, at each elevation, by helium concentration drop and temperature increase as a result of
34 the rise of the leading edge of the steam jet and associated mixing (fountain) zone to that height. A
35 visualisation of the stratification erosion process in Vessel 1 is provided by the evolution of the two-
36 dimensional spatial distributions of gas temperatures in the vertical plane containing the axis (Kapulla
37 et al., 2015a). In section 4.6, some of the calculated results for both gas temperatures and helium
38 concentrations contributed to the open benchmark will be presented.

39
40
41
42 Since the test was rather fast (within 600 s the fluid in Vessel 1 was fully mixed), and the scanning
43 rate of the mass spectrometer is necessarily low, the time history of the erosion at the various
44 elevations (which will be used to get a representative measure of the global success of the
45 simulations) was obtained from the temperature measurements (scanning rate 0.5 Hz), using a
46 threshold of 120 °C (T_{lim} in Fig. 2). This procedure for defining the “erosion times” and comparing the
47 measurements with code predictions at the various locations is clearly not accurate, especially at
48 elevations (notably the highest at 8 m) where the temperature has a slow and non-uniform increase.
49 Another option would have been to use the times of the inflection points (maximum time derivatives
50 of the temperature curves), but the results would differ from those obtained with the used procedure at
51
52
53
54
55
56
57
58
59
60
61
62
63
64
65

1
2
3
4
5
6
7 most by 50 s (at the highest elevation). The experimental values will be shown together with the
8 results of the simulations in the next section.
9

10 Mean velocity measurements were obtained by PIV in a Field of View (FOV) located between the
11 elevations of 6300 and 7000 mm. Measurements and discussion of statistical errors are included in the
12 project report (Kapulla et al., 2015a). Since the averaging period was of 409 s (centred around $t_c =$
13 326.6 s), the use of this information for comparing the simulations with the data at specific times is
14 questionable. The use of the velocity measurements for assessment purposes is reconsidered in the
15 open phase of the benchmark, for which additional data for similar conditions over a larger region
16 above the plate (between 5000 and 7000 mm) are made available. Therefore, for the sake of the open
17 benchmark, results for velocities will not be discussed.
18
19
20
21

22 3. RESULTS OF THE SIMULATIONS FOR THE BLIND BENCHMARK

23 It was mentioned above that the participants in the benchmark were requested to submit two sets of
24 results, one using the “common model” (CM) and one with the “best estimate model” (BEM). The
25 specifications for the CM (Andreani et al, 2016b) included geometry, treatment of heat transfer at the
26 walls (~~heat losses, no radiation and no condensation~~), initial and boundary conditions, and prescribed
27 use of the standard high-Reynolds number k- ϵ turbulence model. The main specifications for the CM
28 were:
29
30

- 31 • Geometry: the upper man-hole and the upper, straight section of the injection pipe
32 had to be represented. The pipe was supposed to be only a hydraulic obstruction and not to
33 participate in heat transfer processes.
- 34 • As regards walls, the model should include: the heat capacity of the walls and obstruction
35 plate; heat transfer between fluid and vessel walls and obstruction plate; heat losses from the
36 outer side of the vessel walls, assumed to be uniformly distributed over the entire outer heat
37 transfer surface of the vessel. The model (including insulation or not) shall be set to produce
38 the correct heat flux (provided in the specifications) at nominal wall temperature (107 °C).
- 39 • No condensation and no radiative heat transfer should be considered.
- 40 • Turbulence: standard high-Reynolds k- ϵ turbulence model should be used (with full treatment
41 for effect of buoyancy on turbulent kinetic energy and dissipation rate). Turbulent Schmidt
42 number: 0.8; turbulent Prandtl number: 0.9. Flat profile for velocity and turbulent intensity at
43 the exit of the injection pipe. Turbulence intensity at the pipe outlet: 4%. Molecular diffusion
44 (Diffusivity between 1 and ~3 cm²/s at p=1.3 bar and T=388 K) should also be considered.
45
46
47
48
49
50
51
52
53
54
55
56
57
58
59
60
61
62
63
64
65

- 1
2
3
4
5
6
7
8
9
10
11
12
13
14
15
16
17
18
19
20
21
22
23
24
25
26
27
28
29
30
31
32
33
34
35
36
37
38
39
40
41
42
43
44
45
46
47
48
49
50
51
52
53
54
55
56
57
58
59
60
61
62
63
64
65
- Initial and boundary conditions: initial gas and wall temperatures: 107 °C; experimental vertical distribution for gas concentrations. Experimental values for pressure, and steam mass flow rate and temperature.

The effect of buoyancy on turbulence parameters was prescribed because it is known that the effect of turbulence production due to buoyancy can be quite important for mixing transient involving large density differences (e.g. Visser et ., 2012). However, the role played by buoyancy in the dissipation rate equation is controversial in literature, and therefore no recommendation was made for the parameter entering in the equation for ϵ , also because in some codes the default cannot be easily modified by the users.

The participants were expected to deliver the times of the erosion progression, the ~~time~~ evolution histories of helium concentrations and gas temperatures at selected locations, as well as axial and transversal profiles of gas temperature and velocity at various elevations, at selected times. Moreover, the organisations delivered an accompanying document with some information on physical and numerical models.

Not all organisations submitted both sets, and two organisations submitted results with two different codes. There were thus 13 contributions with the CM and 10 with the BEM. Table 1 summarises the submissions. In table 1, only the code used the total number of cells in the mesh, the main deviations of the CM from the specifications and the differences between CM and BEM are listed.

3.1 Results with the Common Model (CM)

Table 1 shows that various codes (mostly commercial CFD codes) have been used, with a broad spectrum of meshes, from 20000 cells to more than 1 million. The CM simulations were mostly performed with models complying with the specifications, the only important deviations being those referring to initial and boundary conditions. The non-obvious effect of small differences in boundary and initial conditions was not anticipated by some users. This is a good example of the importance of the benchmarking activities for establishing CFD modelling strategies to be used for the analysis of new problems. Therefore, the comparison with data of the simulations using inaccurate values of steam injection temperature and initial helium concentration profiles is somewhat affected by this deviation in the test conditions. For these contributions, the discrepancies with the data and other simulations are easy to explain. However, also for the other contributions, a very broad variety of results has been obtained. Figure 3 shows the time history of the erosion progression and, as example of gas temperature ~~time~~ evolution histories, the results for one elevation. It can be observed that the mixing time (600 s in the experiment) is well predicted in only three simulations (AERB, IBRAE2 and PSIF), whereas most submissions exhibit either a strong underprediction or overprediction.

1
2
3
4
5
6
7 Considering the essential elements of the setups for the simulations (Table 1), but also the additional
8 information provided, it is not obvious how to associate the success of the predictions to any specific
9 difference between models. Since the physical models (and their implementation in the codes) must
10 be very similar for all simulations, the differences in the prediction can ~~only be due~~ be attributed
11 to the mesh (refinement in certain regions and mesh topology), numerical methods, and other effects and
12 modelling options not considered in the specifications (e.g. wall treatment, buoyancy effect on
13 turbulence dissipation rate). Although previous comparison exercises for basic conditions displayed
14 large difference in simulations using the same turbulence model (e.g., Gallego et al. 2007), it is
15 ~~therefore~~ surprising in this benchmark that models with largely different number of cells lead to
16 comparable predictions, and, vice versa, the use of detailed models with similar number of cells result
17 in very large differences. Although post-test analyses (see below) shed light on some of these
18 apparently puzzling results, the observed spread suggests that the set-up of a CFD simulation for a
19 new problem is not a trivial task, and requires a careful evaluation of the applicability of previous
20 experience for different geometrical configurations and physical conditions.

21
22
23
24
25
26 Another interesting observation concerns the temperature rise: in all simulations (and at all elevations)
27 this is sharper than in the experiment, with the asymptotic temperature being much higher than the
28 measured value (see Fig. 2). The temperature trend therefore reveals a systematic difficulty to predict
29 the erosion process, which is not shown in most concentrations ~~evolution histories~~ (Fig. 4) where,
30 because of the low data frequency, the calculated sudden drop seems to be always in agreement with
31 the experimental results. The temperature distribution above the plate is, in general, reasonably well
32 predicted in most simulations, where the horizontal profiles, in agreement with the experiment, show
33 low peaks along the axis. Figure 5 shows, for example, the profile at some distance downstream the
34 plate (Level G, $z=5.63$ m). However, with the exception of one simulation, the profiles are
35 systematically shifted towards higher values, indicating that some mixing and/or heat transfer
36 mechanism (convective or radiative heat transfer) is not well predicted. On the other hand, the small
37 heat losses did not play an important role on the short time scale of the experiment.

38
39
40
41
42 Indeed, it seems that most simulations over predicted the gas temperatures already in the region below
43 the plate. Figure 5 shows the temperature horizontal profile just below the plate (Level H, $z=4.97$ m)
44 at 150 s: the temperature drop between the pipe outlet and the plate along the axis is underpredicted.
45 This discrepancy, in principle, could be due to the fact that the codes predict perfectly symmetric
46 flow, whereas in the experiment the jet was not perfectly centred due to flow non-symmetry at the
47 pipe outlet, and thus the measured temperature does not represent the value (the maximum) at the jet
48 impingement point. On the other hand, the deviation could reveal unexpected difficulties in predicting
49 the broadening of the free jet. This question has been tackled in the open phase of the benchmark
50 (Section 4).
51
52
53
54
55
56
57
58
59
60
61
62
63
64
65

3.2 Results with the Best Estimate Model (BEM)

The simulations with the CM provided two main results: 1) even using very similar models (apart from the mesh) very different results can be obtained, in spite of the use of meshing strategies that could be considered “qualified” on the basis of previous experience with various tests in PANDA; 2) large discrepancies between calculated and experimental results were obtained. With respect to this second result, the agreement was expected to improve with the use of the BEM, where the participants could make use of the best modelling approach according to their experience. This mostly resulted (Table 1) in the use of a different turbulence model, the consideration of radiation heat transfer, and initializing the simulations with the experimental gas and wall temperature distribution. It is here appropriate to note that the steam in the mixture (absorbing, scattering and emitting infrared radiation) behaves as a participating medium (Abu-Romia and Tien, 1967; Howell, 1988), and therefore the radiation models consider not only heat transfer between solid surfaces, but also between gas and wall and within the gas.

Figure 6 shows the results for the erosion progression (calculated from the temperature rise) and the ~~time evolution~~ history of the helium concentration at the highest elevation. Comparing results with those shown in Figs. 3 and 4 for the simulations with the CM, it can be noted that in a few cases the BEM results are better than the CM results (especially in the case with the largest discrepancy the use of different models produce a dramatic improvement, which was discussed in Andreani et al., 2016b), but in some cases the discrepancies are larger than using the CM. Three results are rather surprising: 1) the spread of results is still quite large; 2) the “best” results are obtained with a rather coarse mesh (163000 cells); 3) two simulations with identical code and very similar models (GRS and FZJ), which using the CM exhibited very different results, are now nearly coincident. This shows that the effect of the mesh possibly depends on the interaction with other modelling choices (turbulence model, numerical methods, boundary conditions, etc.).

It is also interesting to observe that the three simulations where radiation heat transfer was modelled result in a noticeable speed-up of the erosion process, due to the generation of additional convective motions in the upper part of the vessel, which enhance the mixing (Kelm et al. 2016b). For one simulation (CIEMAT), the faster mixing is uniquely due to radiative heat transfer, since the turbulence model was not changed in the BEM with respect to the CM. Considering radiative heat transfer helped in improving the prediction of the gas temperatures at some elevations but not at other ones. Moreover, the results for wall temperatures are somewhat contradictory, because the simulations using radiative heat transfer show qualitatively different results. This indicates that the simulation of radiation heat transfer (in combination with other models, first of all turbulence) requires additional

1
2
3
4
5
6
7 investigations. The possible role played by radiation heat transfer in the process of gas mixing has,
8 among others, also been recently suggested by Filippov et al. (2017).
9

10 11 12 **3.3 Conclusions and open questions originating from blind simulations** 13

14 Both sets of submissions, i.e. those using ~~the a “common model” (CM)~~ and those using ~~the a “best~~
15 ~~estimate” model (BEM)~~, produced a large variety of results. Especially the large differences in the
16 results with the CM were not expected because, in order to establish some means for comparing the
17 results, a comprehensive set of specifications have been recommended. The open phase of the
18 benchmark was then considered necessary to provide more information on effect of meshing
19 strategies.
20
21

22
23 The comparison between predicted and experimental results, as well as between simulations, raised a
24 few questions about the actual importance of considering radiative heat transfer, the relation between
25 mesh topology and other modelling aspects (turbulence model, numerical methods, boundary
26 conditions, etc.), and the effect of some test conditions that were not modelled (e.g. non-symmetry of
27 the flow at the outlet of the pipe).
28
29
30

31 The most important difficulty in interpreting the results and finding the reason of the large deviations
32 was the lack of information on the velocity field downstream of the obstruction. In fact, the
33 interaction between the jet and the density stratification is expected to be controlled by the velocity
34 distribution at the interface between the rising jet and that interface (Paladino et al., 2013). Since the
35 velocity field changes in time, due to the upwards movement of the leading edge of the jet, a
36 meaningful comparison would require a time-dependent experimental information. Unfortunately, due
37 to the short duration of the test, only long-term averages (on the time scale of the experiment) can be
38 generated, and the comparison between the requested calculated instantaneous velocity profiles and
39 these averaged values could not provide any hint on the fidelity of the simulation. One of the main
40 difficulties to interpret the large spread of the erosion times is thus the lack of experimental
41 information on the flow field, not only because of the problems discussed above but also because this
42 is only available for a limited PIV area, which is at large distance from the obstruction. Therefore, an
43 open benchmark using only the experimental information of test HP1_6_2 would lead to little
44 progress in the understanding of the erosion process above an obstruction. The availability of velocity
45 information under quasi-steady state conditions collected in auxiliary tests (Section 4.1) without
46 helium (“zero” tests), but with the same geometrical configuration, permitted, however, to obtain new
47 information to be used in the evaluation of the calculations. In fact, although, in principle, one would
48 need information on flow patterns and temperature field below and above the plate for the specific
49
50
51
52
53
54
55
56
57
58
59
60
61
62
63
64
65

1
2
3
4
5
6
7 test, some progress in the analyses could be expected from the use of information on the extended
8 region above the plate provided in these “zero” tests.
9

10
11 It was then agreed that a meaningful open benchmark could be run, but this should include the
12 analyses of the data on flow obtained in auxiliary tests, and should be organized in a number of steps
13 (see next chapter), to gradually build confidence in the models used. [All data were available to the](#)
14 [open benchmark participants.](#)
15
16
17

20 4. THE OPEN BENCHMARK 21

22
23 To help resolve the questions resulting from the blind phase, an open phase of the benchmark was
24 conducted, where the extended data from the auxiliary “zero” tests (for similar conditions but without
25 helium layer) were provided to the participants to permit a more basic validation of their models, by
26 comparing the results for the flow downstream of the obstruction, which, in turn, are affected by the
27 accuracy in simulating the free jet below the obstruction. A “cascade” of simulations was thus
28 proposed, which aimed to separate the validation of the modelling approach for representing pure
29 fluid dynamic phenomena from the application of the selected methodology to test HPI_6_2, where
30 also heat/mass transfer effects play an equally (or even more) important role.
31
32

33
34 For each step, a summary of the contributions will be presented in tables, which include only the main
35 information on the mesh and modelling options. The tables include the equivalent CPU time using
36 one processor to provide a unified estimate of the computational overhead. A more complete list of
37 aspects considered in the simulations and details on model selection is included in the Benchmark
38 Report (2018).
39
40
41

42 4.1 The “zero” tests [and the multi-step open benchmark](#) 43 44

45
46 The two configurations (and PIV windows) for the tests with obstruction are shown in Fig. 7. In the
47 complementary, “zero”, tests, the geometry was exactly the same as for Test HPI_6_2, the only
48 difference being the initial and boundary conditions. Additionally, it is noted that for the “zero” tests
49 the zone covered by PIV measurements spans a much larger zone, extending 2 m above the
50 obstruction.
51
52
53
54
55
56
57
58
59
60
61
62
63
64
65

1
2
3
4
5
6
7 These tests were conducted injecting a constant steam flow rate in initially steam-filled vessels. In two
8 tests (HP1_6_0 and HP1_7_0), pure steam was injected in steam-filled vessels, and the pressure was
9 kept constant. The only difference was the flow rate.
10

11
12
13 These two tests, which were expected to deliver complementary information with respect to Test
14 HP1_6_2, were used for the benchmark. A third test (HP1_8_0), which was performed with air and
15 steam, and rising pressure was not used. For the two tests HP1_6_0 and HP1_7_0, the following
16 nominal conditions apply:
17
18

- 19 • Pressure: 1.3 bar
- 20 • Initial steam and wall temperature: 108 °C
- 21 • Injected steam temperature: 150 °C
- 22 • Steam flow rate: 60 g/s (HP1_6_0); 30 g/s (HP1_7_0)
- 23
- 24
- 25
- 26

27 Although test HP1_6_0 was the only with the same boundary conditions as HP1_6_2, the analysis of
28 second test was also included, because in test HP1_6_0 temperatures were not recorded.
29

30 The open phase of the benchmark thus consisted of a number of steps, aiming to separate the
31 qualification of the fluid-dynamic models from the validation of the full models for test HP1_6_2, for
32 which the success of the predictions also depend on the appropriate representation of heat and mass
33 transfer processes. The open phase of the benchmark was thus composed of four sets of results:
34

- 35 1) prediction of vertical velocity and turbulent kinetic energy (TKE) distributions for Test HP1_6_0
36 using a “common model” (CM);
37
- 38 2) prediction of vertical velocity distributions and temperatures for test HP1_7_0 using a “best-
39 estimate model” (BEM);
40
- 41 3) prediction of vertical velocity, turbulent kinetic energy and temperatures (although not measured)
42 for test HP1_6_0 using the BEM;
43
- 44 4) post-test simulation of test HP1_6_2 with BEM, including the same mesh for the plate region used
45 for Step 3
46
47

48 Additionally, also the analysis of SETH-2 test ST1_2_2 (Erkan et al., 2009; Paladino et al., 2013),
49 with the same initial and boundary conditions as for test HP_6_2, but without obstruction, was
50 included as Step 5, to verify the capability of the models to properly predict the erosion process in
51 absence of the obstacle. This step was optional for participants.
52
53
54
55
56
57
58
59
60
61
62
63
64
65

1
2
3
4
5
6
7 The test configurations, and simulation requirements for the various steps are summarized in Fig. 8.
8
9

10
11 **4.2 Step 1 (analysis with CM of test HP1_6_0, where temperatures were not measured)**
12

13
14 The first step of the open benchmark was the analysis of test HP1_6_0 (with the same flow rate, 60
15 g/s, as in test HP1_6_2), using the CM model, i.e., using a common set of recommendations regarding
16 modelling selection and initial and boundary conditions:
17

- 18
- 19 – In order to isolate possible spurious sources of deviations in the final Step 4 (post-test
20 calculation of Test HP1_6_2), also test HP1_6_0 had to be run using the full geometrical
21 model, including the straight portion of the inlet pipe
22
 - 23 – Use of prescribed I.C. and B.C.:
 - 24
 - 25 ▪ Initial fluid and wall temperature: 107 °C; Pressure and inlet flow rates: experimental
 - 26 curves. Flat pipe outlet velocity profile. Pipe exit turbulence intensity: 4%.
 - 27
 - 28 ▪ Fluid temperature at pipe outlet: 142 °C (precise value not critical, but important)
 - 29
 - 30 ▪ Obstruction plate heat capacity included.
 - 31
 - 32 ▪ Heat losses, condensation and radiative heat transfer neglected. Wall heat transfer to
 - 33 be considered: inner surface wall temperature to be prescribed (constant, at 107 °C)
34
 - 35 – Standard high-Re k-ε turbulence model with Standard wall functions
36
 - 37 – Value of y^+ in the cells below the plate between R=3 and 10 cm around 30.
38
 - 39 – Recommended simulation time: 500 s
40

41 The summary of contributions is listed in Table 2
42

43 It is noted that most organizations contributed results using a finer mesh than that used for the blind
44 benchmark, two used the same mesh, and one used a coarser mesh. Some of these choices are justified
45 in the Benchmark Report (2018). None of the submitted contributions was based on a comprehensive
46 sensitivity study aiming to obtain mesh-insensitive results.
47

48 The first variables to be considered in the comparison between data and calculated results are
49 horizontal and vertical profiles of vertical velocity, extracted from the velocity field. Figure 98 shows
50 the experimental information (averaged over 205 s), along with the elevation of the selected
51 horizontal profiles. Figure 98 also includes the experimental profiles of axial velocity, maximum of
52
53
54
55
56
57
58
59
60
61
62
63
64
65

1
2
3
4
5
6
7 the vertical velocity and difference between the maxima in the left and right half-plane in the PIV
8 window (this last being an indicator of the non-symmetry of the flow past the obstruction). Y_1 and Y_2
9 are the elevations where the vertical velocity changes sign and the maximum coincides with the axial
10 value, respectively. The former is the height of the recirculation zone (bubble) downstream of the
11 obstruction; the latter indicates the position where the flow recovers the structure of a full jet (with
12 maximum in the centre).
13
14

15 Figure 109 shows the calculated results for the vertical profiles of the axial velocity and the maximum
16 vertical velocity. The comparison of the axial profile below the plate (between 4000 and 5000 mm),
17 although no data are available for evaluating the quality of the predictions, is of some interest because
18 it shows that very large differences (also qualitative) exist between the simulations of CIEMAT and
19 BARC and the other ones. However, the differences are substantially reduced in the region
20 downstream of the plate, with maximum values being in a band of 0.25 m/s, which indicates a
21 relatively small effect of the predictions below the plate and that most differences above the plate
22 originate from the representation of the flow obstruction region. In fact, simulations showing the same
23 flow development below the plate (S/NRA/R, KAERI and FZJ), diverge above the plate. The
24 simulation of FZJ produced the highest values of the velocity at the top of the measurement region. It
25 is also interesting to observe that the velocities are still growing with distance at the top of the
26 measurement region, whereas the experimental values reach the maximum at lower elevation
27 (between 6000 and 6500 mm). Finally, the module of the minimum velocity in the “bubble” above
28 the plate is underpredicted in all simulations. The vertical distribution of the maximum velocity also
29 shows a similar spread of results, with all calculations underpredicting the distance from the plate
30 where the maximum attains its highest value. Two calculations also overpredict the highest values.
31
32
33
34
35

36 The comparison of the velocities is to some extent affected by the still slowly evolving flow field in
37 some calculations, which is well recognized in the ~~time-evolution~~ history of the maximum velocity
38 shown in the Benchmark Report (2018), which is not constant at the end of the simulation. In the
39 experiment, however, the overlapping of the long-time average central profile using the entire data set
40 with results using sub-sets indicates a practically steady-state condition. The reason for the evolving
41 flow field is the slow fluid temperature increase, possibly due to the underprediction of heat transfer
42 with the structures.
43
44
45

46 However, considering that some differences in the velocity distribution originate from the way the
47 experimentally unknown temperature field is predicted, the agreement between predictions is
48 reasonably good. The differences are larger for the Turbulent Kinetic Energy (TKE) in the
49 recirculation zone (Fig. 110), whereas in the developed flow region the simulations converge to the
50 experimental value. The large (also qualitative) differences in the distributions are thus confined to the
51 recirculation region, and decay with distance from the obstruction.
52
53
54
55
56
57
58
59
60
61
62
63
64
65

1
2
3
4
5
6
7 An important feature of the transient that could not be investigated in test HP1_6_2, but could have an
8 effect on the interaction of the jet with the density interface, was the symmetry of the flow structure
9 and the flow evolution downstream of the plate. Asymmetric flow could either be produced by the
10 impingement or directly originated at the outlet of the pipe. Whereas the flow below the obstruction
11 cannot be observed also in the “zero” tests, its structure above the plate could be characterized, and it
12 is reasonable to assume that it is representative of that produced in the reference test with helium.
13 Therefore, an important aspect of the assessment of the models using the data from the zero tests is to
14 verify whether the models correctly predict non-symmetries (if any) in the flow. For Step 1, since the
15 recommendations included the modelling of the straight section of the pipe only, the verification only
16 regards the production of non-symmetries in presence of axis-symmetric injection conditions.
17
18
19

20 Figure 124 shows the difference between the maxima in the two half-planes of the PIV window,
21 which has a maximum in the zone close to the obstruction and vanishes within half a meter
22 downstream of it. Most simulations do not display any substantial asymmetry in the flow field past
23 the plate. Only the contributions from AERB and BARC present a qualitatively important deviation
24 from symmetry, the former in the recirculation zone, the latter a slowly increasing difference with
25 distance from the plate. This asymmetry could have an effect on the erosion process, and therefore on
26 the interpretation of the results provided by AERB and BARC. Figure 124 also shows the elevation
27 where the flow recovers the jet structure (with maximum velocity in the centre). It can be observed
28 that the predictions, although obtained with the same turbulence model, are in a large band.
29 Considering the 2-D velocity maps provided by the participants (Benchmark Report, 2018), however,
30 it is presumed that at least a part of the differences could be due to the different criterion used to
31 determine the condition of “equality” between axial and maximum vertical velocity.
32
33
34
35

36 It has already been observed that large discrepancies exist in the recirculation zone between
37 calculations and experiments, and between the calculated results. This is more evident from the ~~time~~
38 evolution history of the minimum velocity (Fig. 132), which shows underprediction in all simulations.
39 It is surprising, however, that, in spite of the large differences in the velocity profile, the height of the
40 recirculation zone is well predicted in all calculations.
41
42

43 Finally, the horizontal profiles of velocity and TKE at the two elevations indicated in Fig. 110 are
44 shown in Figs. 143 and 154, respectively. With respect to velocities, at the elevation of the middle of
45 the recirculation zones, with the exception of a narrow region around the axis, the simulations are in
46 agreement with each other, and also in agreement with the measurements. A large spread of results,
47 however, is exhibited by the turbulent kinetic energies, as regards both maximum values and profiles.
48
49

50 Similar considerations also apply to the elevation at large distance from the obstruction, where the
51 velocities are in good agreement (especially outside the jet core), but the calculated TKE shows a
52 large variety of values and horizontal profile shapes.
53
54
55
56
57
58
59
60
61
62
63
64
65

1
2
3
4
5
6
7 These profiles indicate that even using the same turbulence model, the results can be quite different,
8 depending on other modelling choices. Large difference between the results obtained with GOTHIC
9 and those produced by CFD codes had to be expected because of the large differences in mesh detail
10 (Table 2). The differences between CFD codes, however, are more difficult to justify, also because no
11 correlation can be easily established between number of cells and main features of the calculated
12 profiles. These results suggest that the mesh topology (and possibly details of the numerical model)
13 could play an important role.
14
15

16 The general remark on the results of Step 1 is that even for the simplified conditions of HP1-6-0,
17 important differences are observed, which are not related to turbulence modelling (the same standard
18 $k-\epsilon$ for all) or radiation heat transfer (not considered), but probably originating mostly from the mesh
19 (and topology) and, to a lesser extent, heat transfer and implemented boundary conditions.
20
21

22 Another observation, important for the interpretation of the results for the benchmark test (HP1_6_2),
23 is that the differences in the erosion rates are likely to originate from a different prediction of the fluid
24 dynamics below the density interface, and not related to the representation of the interaction region.
25
26
27

28 **4.3 Step 2 (analysis with BEM of test HP1_7_0, where temperatures were measured)**

29
30

31 Since temperatures were not recorded for Test HP1_6_0, and models constructed for best estimate
32 simulations of the benchmark test should be validated also for their capability to properly predict fluid
33 temperatures, the analysis of test HP1_7_0 is considered, although the steam mass flow rate was the
34 half of that in test HP1_6_2 (30 g/s instead of 60 g/s).
35
36

37 In this test, the Reynolds number was thus 13500 instead of 27000. Since the effects of the Re
38 number, at least on free jet flow development, are significant up to Reynolds numbers around 10000,
39 and the TKE decay downstream of the plate is similar in the two tests, HP1_7_0 could be used for
40 developing the BEM modelling approach to be used for HP1_6_0 (and HP1_6_2). In particular, in
41 the multi-step approach for the open benchmark, the comparison of the results with test HP1_7_0 was
42 intended to provide the validation of the models with respect to representation of heat transfer.
43
44
45

46 Table 3 reports the main features of the simulations contributed to the benchmark. Unless otherwise
47 noted (FZJ and VTT), the mesh used is the ~~onesame as that~~ used for Step 1. Most users adopted the
48 SST turbulence model, one the RNG model and some retained the standard turbulence model choice.
49 With respect to Step 1, other important model modifications in some contributions were the
50 consideration of radiation and the velocity profile at the pipe exit pipe (obtained by representing the
51 straight section of the pipe or prescribed on the base of off-line calculations of the flow inside the
52
53
54
55
56
57
58
59
60
61
62
63
64
65

1
2
3
4
5
6
7 entire pipe). Buoyancy effects on turbulence parameters were included in all simulations. For codes
8 that do not offer this option in connection with certain turbulence models (e.g. SST), the buoyancy
9 term has been added using external functions. These effects are also considered for all following
10 steps.

11
12
13 Figure 165 shows the experimental flow field and the vertical velocity profiles to be used for the
14 comparison. It is noted that both the height of the recirculation bubble and the height at which the
15 flow recovers the full-jet structure are smaller than for Test HP1_6_0.

16
17 Figure 176 shows two vertical profiles of vertical velocity: the distribution along the axis and the
18 profile of the maximum velocity. The general agreement between the various simulations is similar to
19 that observed for Step 1, and, in the region above the plate, better for the simulations that exhibit a
20 close agreement below the plate (KAERI, S/NRA/R and FZJ). However, the flow evolution below the
21 plate has a minor effect on the velocity field above the plate. These results suggest that actually the jet
22 “loses the memory” above the plate.
23
24

25 Underpredictions in the far-field velocity larger than for Step 1 are observed in the results of
26 CIEMAT. Worse results were also obtained by VTT. Although the changes in modelling certainly
27 play a prevailing role, and some mesh modifications with respect to Step 1 complicate the picture, this
28 result possibly indicates that the disagreement between simulations does not depend on the jet
29 Reynolds number. Moreover, the interpretation of the results is complicated by certain instabilities
30 and large asymmetries in the velocity field which were exhibited by some simulations, but not
31 observed in the experiment (Benchmark Report, 2018). Some of the calculated asymmetries appeared
32 already at the pipe outlet, produced by bent in the lower part of the injection pipe (Figs. 1 and 7).
33 However, PIV measurements immediately above the pipe exit performed in other HYMERES
34 experiments for similar conditions (Paranjape et al., 2018) indicated that a well-developed turbulent
35 pipe profile existed at the pipe exit. Although at the higher velocity of Test HP1_6_2 the effect of the
36 bent could in principle be larger, the considerations above related to test HP1_7_0 suggested that one
37 of the open issues of the blind benchmark, namely the effect of possible non-symmetries at the pipe
38 exit the flow development above the obstruction, could be considered of minor importance for the
39 evaluation of the results of the benchmark test. Detailed discussions on these and other aspects of the
40 flow are discussed in the Benchmark Report (2018).
41
42
43
44
45

46 Concerning the fluid temperatures, the ~~time evolution histories~~ isare presented and discussed in the
47 Benchmark Report (2018). Here, we just mention that the two simulations including radiation heat
48 transfer (FZJ and BARC) correctly predict the short time required for the fluid to reach equilibrium
49 values with the structures, whereas the other predictions show still increasing temperatures at 1000 s.
50 It can be observed that these two simulations exhibit the most accurate predictions for the axial
51 temperature profile (Fig. 187). The largest deviations occur at the position close to the plate, due to
52
53
54
55
56
57
58
59
60
61
62
63
64
65

1
2
3
4
5
6
7 the difficulty to correctly predict the details of the flow within the recirculation zone (Benchmark
8 Report, 2018).
9

10 Concerning the radial profile at Level D (only this one was required in the benchmark specifications),
11 both simulations show a too narrow profile (but this is true for all simulations) and underprediction of
12 the temperatures at some distance from the axis (Fig. 187). Although the results of BARC are
13 probably somewhat biased by a large (and difficult to explain) temperature drop below the plate and
14 the radial distribution at 1000 s calculated by FZJ is affected (Benchmark Report, 2018) by a plume
15 oscillation (still of small amplitude at level D), it can be concluded that the two simulations agree with
16 each other with respect to the effect radiation heat transfer can have. Globally, these simulations can
17 also be regarded as the most successful, since the contribution of VTT (which does not model
18 radiation) also shows good agreement above the plate, but these good results are due to the lower
19 injection temperature (it can be noted in the axial temperature profile, Fig. 187).
20
21
22
23
24

25 **4.4 Step 3 (analysis with BEM of Test HP1_6_0)**

26
27
28 Step 3 was intended, in the multi-step approach of the open benchmark, to provide the participants the
29 opportunity to validate the model selection made for test HP1_7_0 for the same flow as used in Test
30 HP1_6_2, and to refine the mesh, if needed. In Step 3, additional horizontal profiles of velocity and
31 TKE at low elevations were requested.
32
33

34 The overview of contributions for Step 3 is presented in Table 4.

35
36 Figure 198 shows the axial and maximum velocity vertical profiles. For convenience, the results
37 obtained for Step 1 are also displayed using the same scales.
38

39 Two participants (BARC and CIEMAT) used the same mesh as for Step 1, whereas the other four
40 users used slightly finer meshes, adopting modifications that were suggested by the simulation of Step
41 2. Four participants used the same model settings as for Step 2, but CIEMAT and VTT used different
42 turbulence model (or corrections).
43
44

45 Figure 198 shows that differences in injection velocity for five participants (not considering the
46 contribution of CIEMAT, which for Step 1 used a too low value) are now more pronounced than for
47 Step 1, due to the different assumptions for steam injection temperature (prescribed or calculated)
48 and, possibly, details of the mesh used for the pipe. The development of the flow immediately above
49 the pipe is also affected by the use of a velocity profile at the pipe exit, so that the profiles below the
50 plate diverge more than for Step 1.
51
52
53
54
55
56
57
58
59
60
61
62
63
64
65

1
2
3
4
5
6
7 In the region above the plate, results of BARC, CIEMAT, FZJ, and VTT are very similar to those
8 obtained using the common model, and the results of S/NRA/R only show a noticeable difference for
9 the maximum velocity. These results possibly indicate that the selection of the turbulence model, for
10 these conditions, has a small impact on the prediction of the global features of the flow. The largest
11 differences between Step 1 and Step 3 regard the simulations of PSI and CIEMAT, where, in both
12 cases, the pipe exit conditions were strongly modified with respect to the calculations with the
13 common model. The calculations of PSI with the “CFD like” GOTHIC code were “worse” than with
14 the common model, but, due to the more physical representation of the pipe exit conditions (pipe exit
15 velocity and temperature profiles are considered), are the best suitable to be compared with CFD
16 codes in this benchmark.
17
18
19

20 The axial profiles of TKE (Benchmark Report, 2018) also show that the selection of the turbulence
21 model (different from the standard k- ϵ model in all calculations but that of PSI) has a strong influence
22 in the region immediately above the plate, but its effect is substantially reduced already at relatively
23 short distance from the top of the recirculation zone.
24
25

26 This consideration is especially true for the calculations of BARC, where the results with both
27 standard and RNG model are nearly coincident. This is not expected, because the RNG model was
28 developed to handle this kind of flows. The results of CIEMAT display the largest change, but for this
29 simulation are not clear whether the large difference in mesh and inlet velocity were the most
30 important effects. Finally, the radial profiles show that also the predicted axial values of S/NRA/R
31 (for which no axial profile was provided) are less sensitive to the turbulence model selection than
32 expected.
33
34
35

36 Obviously, these considerations cannot lead to the conclusion that the selection of turbulence model is
37 immaterial for the representation of the flow past the obstruction and for the erosion process in
38 transient test HP1_6_2, since an apparently small difference in the velocity and TKE distribution can
39 have a large influence on the turbulent diffusivity distribution.
40

41 Indeed, the details of the results for Step 3 are also interesting in view of their prospective importance
42 for the prediction of the benchmark test. Both velocity and TKE horizontal profiles show a large
43 spread between the various simulations, and this suggests that the differences in the flow predictions
44 could result in large differences in the erosion rate.
45
46

47 Finally, some considerations can be made on the predictions of fluid temperatures, although no
48 experimental values have been recorded. It is observed that large differences exist in the free jet
49 temperature decay (Fig. ~~2019~~), although the steam injection temperature is the same, apart from the
50 calculation of VTT. Moreover, the radial profiles, similarly to the results for Step 2, show that
51 radiation heat transfer has a strong effect on temperature spatial evolution. It is also interesting to
52
53
54
55
56
57
58
59
60
61
62
63
64
65

1
2
3
4
5
6
7
8
9
10
11
12
13
14
15
16
17
18
19
20
21
22
23
24
25
26
27
28
29
30
31
32
33
34
35
36
37
38
39
40
41
42
43
44
45
46
47
48
49
50
51
52
53
54
55
56
57
58
59
60
61
62
63
64
65

mention that the time to reach a quasi-steady-state condition is very different in the various predictions (Benchmark Report, 2018) and, for some simulations, do not appear consistent with the results (also experimental) obtained for test HP1_7_0 (Step 2). In consideration of similar differences between the various simulations observed for test HP1_7_0 (where experimental values were available), it can tentatively be concluded that the modeling of radiation also permits a better representation of the time development of the temperature field.

4.5 Step 5 (analysis with BEM of test ST1_2_2, without plate)

Before the post-test results for the benchmark test are discussed, the analyses of test ST1_2_2 are briefly illustrated. The analyses of this test (conducted with the same configuration used for HP1_6_2, with the only difference that no obstruction was present), were expected to offer the opportunity to validate/improve the mesh outside the region of the obstruction plate, also taking advantage of the PIV measurements at short distance from the pipe exit.

The configuration of test ST1_2_2 (Erkan et al., 2009; Paladino et al., 2013) is shown in Fig. 210, where the initial distribution of helium in the injection vessel is compared with that present at the start of test HP1_6_2. Figure 210 also shows the comparison of the other important boundary conditions, i.e. steam flow rate and temperature. The maximum helium concentration was slightly higher than in the benchmark test, whereas the steam injection temperature was lower. As for the steam mass flow rate, differences can be regarded as negligible.

It will be seen below that these conditions and the absence of the obstruction resulted in an about 30% faster stratification break-up.

Table 5 presents an overview of the four calculations contributed to this part of the benchmark.

Figure 224 shows the progression of the erosion, based on the gas temperature threshold of 115 °C. This limit is lower than for HP1_6_2 because the steam injection temperature was lower (Fig. 210).

The simulations of the three organizations that submitted results also for the other steps (AERB, FZJ and PSI) accurately predict the erosion process, with some differences appearing only towards the end of the transient. The good predictions of these three contributions are also confirmed by the ~~time evolution~~ histories of the helium gas concentration (Fig. 232).

The only notable discrepancy in the three simulations are the delayed helium concentration drop calculated by FZJ at level D ($z=6.3$ m), which, however, may be due to a graphical representation effect, because (see Benchmark Report, 2018) the frequency of the required data (every 5 s) does not

1
2
3
4
5
6
7 permit to display the calculated drop and recovery of the helium concentration during the time interval
8 between two measurements.
9

10 Figure 243 shows the vertical velocity axial distribution and the horizontal profile at z=5003 mm. It is
11 observed that the calculation with GOTHIC (PSI) accurately predicts the maximum velocity at short
12 distance from the pipe exit, whereas the other two simulations strongly overpredict it. The width of
13 the profile instead is better calculated by the simulations of AERB and FZJ. It could be inferred that
14 the velocity decay further up has been properly calculated in all simulations, because otherwise it
15 would not be possible to capture the erosion rate. The analysis of the results of Step 4, however, will
16 lead to different conclusions (see Section 4.6).
17
18
19

20 As regards the discrepancies at short distance from the pipe exit, although it can be presumed that
21 they can partly be due to the slightly off-center position of the jet (in the third dimension), the results
22 of AERB and FZJ suggest that either the pipe exit conditions or the near-field jet spreading is not
23 properly calculated in their simulations.
24

25 This conclusion is supported by the observation of the axial profiles of gas temperature (Fig. 254) at
26 two different times.
27

28 In both simulations of AERB and FZJ, the central temperature remains at the value of the injected
29 steam up to above 5 m, whereas the experimental value at that elevation has already dropped by more
30 than 5 K. In the calculation by PSI, however, the gas temperature drops smoothly to the lower
31 measured value. The analyses presented in the Benchmark Report (2018) show that this result is due
32 to the representation of both velocity and temperature profile at the pipe exit, due to the flow
33 development inside the pipe and heat transfer with the pipe walls. In fact, if the velocity and
34 temperature profiles are assumed flat, both axial velocity and temperature do not start decreasing
35 below 5 m.
36
37
38

39 It can be concluded that in the FZJ and AERB calculations either the entrainment in the free jet is too
40 little, which produces a too small jet broadening, or the pipe exit conditions were not properly
41 accounted for. For FZJ, the good agreement with the measurements for test HP1_7_0 (Step 2, half
42 steam flow rate) with respect to both temperature (Fig. 187) and velocity profiles (Benchmark Report,
43 2018), suggests that the predictions are affected by the Reynolds number. The comparison between
44 simulations for Test ST1_2_2 and HP1_6_2 (shown in the Benchmark Report, 2018) also indicates
45 that the jet spreading below the plate depends on the evolution of the eddy diffusivity.
46
47
48

49 The elevation where the jet is fully developed (central temperature starts decreasing) is thus predicted
50 at about 5000 mm and 5300 mm in the FZJ and AERB calculations, respectively. The
51
52
53
54
55
56
57
58
59
60
61
62
63
64
65

1
2
3
4
5
6
7 underprediction of the jet spreading in the FZJ and AERB simulations can be recognized from the too
8 narrow temperature profile, which is also present in the PSI calculation, although to a lesser extent.
9

10 This result suggests that also for Step 4 (to be discussed below) the simulations of FZJ and AERB
11 should be affected by inaccuracies in the simulation of flow field and temperatures below the plate.
12

13 The axial temperature profiles show that only the calculation (FZJ) considering radiation heat transfer
14 captures the correct level of temperature at large distance during the erosion process (time < 500s),
15 although the temperatures drop between the elevation where the jet is fully developed and the bottom
16 of the helium layer is overpredicted. In general, also the horizontal temperature profiles (Fig. 265)
17 show a better success of the FZJ simulation, although not all results seem to offer a consistent picture
18 (Fig. 276).
19
20

21 From the profiles in the mixed region below the tip of the jet (Benchmark Report, 2018) one can
22 conclude that the modelling of radiation heat transfer was necessary to correctly calculate the fluid
23 temperatures. Also at higher levels (Fig. 265 and 276), where the upwards propagation of the jet
24 produced the temperature rise and helium concentration drop, the temperatures before the mixing
25 (Level D) or during or immediately afterwards (Level C) are much better predicted by FZJ. At times
26 after the mixing has occurred (250 s at level D and especially at 500 s at level C), however, the
27 calculation of FZJ shows notable discrepancies, possibly due to the (small) asymmetry in the flow and
28 temperature field appearing shortly before the dissolution of the helium layer is completed
29 (Benchmark Report, 2018).
30
31
32

33 Some additional information can be obtained on the gas temperature-time evolution histories at the
34 required positions (not shown). First of all, the three simulations of AERB, FZJ and PSI correctly
35 predict the temperatures in vicinity to the pipe exit, which shows that the correct boundary conditions
36 were applied and no numerical diffusion corrupted the simulations from the injection elevation. The
37 best predictions were obtained by FZJ using radiation, although the results of PSI using a coarse mesh
38 and a standard correlation for convective heat transfer are nearly equally successful.
39
40
41

42 The results for off-axis positions above the initial density interface are somewhat contradictory, with
43 generally better results obtained by PSI, with the effect of radiation being to excessively reduce the
44 temperatures during the entire transient and also after the full dissolution of the helium layer. The
45 discrepancy is especially large at some positions during the erosion process. On the contrary, at lower
46 positions, the calculation with radiation permits to reproduce the correct temperature, whereas the
47 calculation with GOTHIC predicts a strong superheat, the largest differences occurring during the
48 transient compression and erosion of the helium layer, before mixing. Although it cannot be excluded
49 that convective heat transfer could also play a major role in the different predictions (since both
50
51
52
53
54
55
56
57
58
59
60
61
62
63
64
65

1
2
3
4
5
6
7 turbulence model and meshes were different), it can be presumed that the largest contribution to the
8 divergent behaviour could come from the modelling of radiation in the simulation of FZJ.
9

10 Since all positions where the discrepancies are very large are all in regions of slow velocities and even
11 in nearly stagnant zones, these results suggest that the strongest effect of radiation could be observed in
12 the zones where the temperature increase due to compression of the fluid cannot be contrasted by the
13 weak convective heat transfer but is kept low by the effect of radiation heat transfer. Moreover, the
14 results indicate that the effect of radiation heat transfer may show up more distinctly during transients
15 rather than under quasi-steady state conditions (such as those established in Test ST1_2_2 after the
16 dissolution of the stratification), which would be justified by the different time scales of the
17 convective heat transfer (which is bound to the finite propagation velocity through the fluid) and
18 radiation heat transfer (which instead has practically an immediate effect).
19
20
21
22
23

24 **4.6 Step 4 (post-test analysis of benchmark test HP1_6_2)**

25
26
27 The last step in the analysis is the post-test simulation of the benchmark test HP1_6_2. For
28 visualisation purposes, the distributions of helium concentration and gas temperatures at various times
29 calculated by one of the participants are shown in Figs. 28 and 29.
30
31

32 In accordance with the rationale for the multi-step approach, mesh around the plate and modelling
33 would be expected to be the same as for Step 3 (HP1_6_0), with some corrections to the mesh in the
34 main domain due to the knowledge gained from the analysis of Test ST1_2_2, featuring helium layer
35 erosion without obstruction. Table 6, where the overview of the contributions is presented, shows that
36 only FZJ and PSI ran all steps and followed this path in building the model used for the final
37 calculation. Also BARC and S/NRA/R submitted results with same mesh and model setting, but opted
38 not to perform the additional Step 5. It is also noted that one organization used a coarser mesh than for
39 Step 3: CIEMAT model reverted to the coarse mesh model used for the blind benchmark.
40
41

42 Also with respect to the turbulence model, in some contributions Step 4 has not been analyzed with
43 the same selection used for the other steps. As regards radiation heat transfer, it is noted that one
44 contribution (VTT) used this model only for Step 4: therefore a preliminary validation using the data
45 of HP1_7_0 and ST1_2_2 (Steps 2 and 5) was not performed.
46
47

48 Figure ~~3027~~ shows the erosion progression determined using the times at which for each location the
49 gas temperature rises to 120 °C,¹ whereas Fig. ~~3128~~ shows the helium concentration—time
50
51

52 ¹ See Section 2.2. Results up to level B (7500 mm) are confirmed by the inspection of the temperature
53 predictions. For level A (8000 mm), the “erosion time” is somewhat underestimated.
54
55
56
57
58
59
60
61
62
63
64
65

1
2
3
4
5
6
7 ~~evolution history~~ at level B ($z=7.48$ m). In these figures, the results obtained in the open phase are
8 compared with those submitted for the blind benchmark, using the best estimate model. It is noted that
9 VTT did not contribute best estimate results for the blind benchmark, and thus no comparison is
10 possible for this organization.
11

12
13 It is observed (Fig. 3128) that several organizations that participated in the blind benchmark could
14 obtain better results (especially BARC, S/NRA/R and GRS, with this third organization, however,
15 supplying the final results with a model that was not verified in Steps 1 to 5). AERB, CIEMAT and
16 FZJ, instead, practically obtained the same results as for the blind simulations. ~~This outcome of the
17 multi-step validation of the model for CIEMAT is obvious, because the final step was run with the
18 same mesh and model settings as for the blind exercise.~~ For AERB (Benchmark Report, 2018), the
19 results (using a much finer mesh) have been shown to depend on the mesh around the plate and
20 therefore on an accurate prediction of velocity field near the plate (comparing the results of sensitivity
21 studies for Step 3), overall grid size in the stratification region (Step 5), and numerical scheme. On the
22 other hand, the Realizable k- ϵ was preferred to the standard and the RNG model only for the better
23 convergence obtained with this turbulence model. For FZJ, the results could seem somewhat
24 surprising, because for all other steps the model delivered rather accurate predictions, at least at some
25 distance from the pipe exit. It has to be considered, however, that the results of the blind benchmark
26 have not been revised systematically applying the outcome of the other steps, since they used a Best
27 Estimate Model constructed on the base of a comprehensive validation experience. Numerical effects
28 were also carefully investigated by FZJ, but showed no considerable importance on global results.
29
30
31
32
33

34 A possible contribution to the discrepancy can be due to the underprediction of the jet broadening
35 below the plate, as suggested by the results of Step 5, and/or the slightly larger maximum velocity and
36 TKE at high elevations (observed in Step 3). The difference in the results can be explained neither by
37 the modelling of radiation alone (also considered by BARC, CIEMAT, GRS, and VTT), nor by mesh
38 or turbulence model or injection conditions. It is likely that a combination of all these elements finally
39 produced the large differences observed in the final results of FZJ for the transient test. Especially
40 interesting is the comparison between the calculations of FZJ and BARC, because for Step 3 the
41 results of both simulations were close to each other, the only important differences being the TKE
42 magnitude at some distance from the plate, and the elevation of the full jet recovery.
43
44

45
46 This suggests that the results for the erosion progression are strongly affected by the turbulence
47 model, and wall layer treatment of the jet impingement zone (including the best choice for the size of
48 the cell adjacent to the plate). Some additional elements to partly explain similarities and differences
49 between results will be provided by the analyses of the flow variables (see below), but only further
50 analyses and sensitivity studies by the individual organizations could bring some light on the role
51 played by mesh and modelling choice.
52
53
54
55
56
57
58
59
60
61
62
63
64
65

1
2
3
4
5
6
7 As for other simulations, the concentrations ~~time evolution~~ histories confirm that FZJ and CIEMAT
8 (and at late times also VTT) overpredict the erosion rate, whereas the others either capture or slightly
9 underpredict the mixing rate. It is also observed that in the simulation of VTT, the erosion is initially
10 slower (Level F, at $z=6$ m), probably due to the delay in the reattachment of the flow above the plate
11 (see below), which was observed for Step 2, but not for Step 3 (Benchmark Report, 2018).
12
13

14 As for the effect of modelling radiation (which, in the case of BARC lead to very accurate results, but,
15 for FZJ resulted in too fast mixing), Fig. 329 shows the comparison of the results obtained by GRS
16 (Schramm et al., 2017) and VTT (Huhtanen, 2018). For this simulation, the accelerating effect of
17 radiation is very large. In other investigations (e.g. Kelm et al., 2016b) for similar conditions,
18 radiation was shown to promote mixing due to its influence on temperature (and density) fields,
19 although its effect was not as substantial as in the simulations shown here. Additional studies on the
20 effects of radiation are presented in the Benchmark Report (2018).
21
22
23
24

25 The apparently excellent global results obtained with GOTHIC and coarse meshes are probably
26 affected by compensation of errors, as indicated by the comparison for the velocity.
27
28

29 Due to the large averaging time of the available velocity measurements, the comparison between the
30 calculated axial and horizontal velocity profiles (Fig. 330) has to be taken with some caution, as
31 shown by the large fluctuations in the measurements over a 10 s period around the central time (300 s)
32 of the averaging period. Nevertheless, it can be recognized that the velocity in the PIV window
33 calculated by PSI is far too low, which suggests that the good predictions for the erosion result from
34 the compensation of errors between the lower velocities in the far field above the plate and numerical
35 diffusion. Since the results for Step 5 in the near field (without plate) were excellent and the results
36 for Step 3 (without helium layer) were reasonably good, it can be concluded that the complexity of the
37 transient test HP1_6_2 lead to overprediction of the velocity decay between the plate and the density
38 interface. It can also be observed that the same order (from faster to slower) in the erosion timing
39 displayed by concentration and temperature traces can be found in the magnitude of the velocity: the
40 simulation of FZJ, which predicts fast erosion, also predicts the largest velocity in the PIV window.
41 Vice versa, the simulation of AERB, which underpredicts the velocity, also slightly underpredicts the
42 erosion rate.
43
44
45
46

47 A special attention deserves the simulation of VTT, which used a very detailed mesh and calculated
48 (as result from the detailed modeling of the injection pipe) an asymmetric velocity and temperature
49 profile at the pipe exit. The evolution of the calculated flow field (Benchmark Report, 2018) shows
50 for about 200 s a splitting of the velocity field above the plate (which can also be inferred from the
51 temperature distribution at 100 and 200 s in Fig. 28), and only at about 220 s the plume/jet structure is
52
53
54
55
56
57
58
59
60
61
62
63
64
65

1
2
3
4
5
6
7 recovered (see temperature distribution at 300 s in Fig. 28). Since for the same flow rate (Step 3) this
8 delay was not observed (but it was observed in test HP1_7_0, Step 2), the results suggest that the
9 density interface produced the same effect as a lower mass flow rate. No conclusive explanation could
10 be found so far for the results concerning the recirculation zone above the plate. On the other hand,
11 the simulation of BARC (taken as example, but similar behavior is displayed by FZJ and CIEMAT)
12 also show an “open” flow structure at early times, but already after 100 s the full jet/plume is
13 recovered. This behavior does not depend on the steam injection temperature (constant at 150 °C in
14 the BARC calculation).
15
16

17
18 The observation related to the VTT simulation is particularly important, because it suggests that the
19 set-up of a model based on the good results for simplified conditions can prove not to be equally
20 successful when applied to the more complex situation of a test featuring transient behavior and
21 strong density differences.
22

23
24 Some important observations can be made on the axial and horizontal temperature distributions (Figs.
25 34 and 35). Generally, the most accurate axial temperature distributions are obtained by the models
26 including radiation heat transfer, but also the simulation with GOTHIC, which accurately accounts for
27 the temperature drop between the pipe exit and the plate, displays a quite remarkable agreement. The
28 initially too large temperature difference between the elevations below and above the plate calculated
29 by VTT is related to the delay in the re-attachment of the flow (see above).
30

31
32 Due to the complexity of the phenomena, it is not possible to draw any conclusions, but it is simply
33 observed that no obvious correlation seem to exist between accuracy in the calculation of the
34 temperatures and mixing rate. The horizontal temperature profile immediately below the plate (Level
35 H) shows that all simulations predict a too narrow peak, with rather flat profile at some distance from
36 the axis. At this elevation, the most distinct difference between some simulations including radiation
37 (CIEMAT, FZJ and VTT) and those not representing this heat transfer mode is the larger temperature
38 drop between the centre of the jet/plume and the periphery of the flow. This, however, is not observed
39 in the calculation of BARC.
40
41

42
43 For the region above the plate, the results are obviously affected by the different progression of the
44 stratification erosion. It can be observed, however, that at intermediate elevations (Levels G and D)
45 most of the simulations including radiation predict better the temperature profiles, especially the
46 temperatures near the wall.
47

48
49 The results obtained with the models with radiation at the bottom of the dome (Level C) seem to be
50 less accurate than those neglecting this heat transfer mode. In fact, whereas at 250 s the top of the jet
51 has already reached that elevation in the simulations of CIEMAT, FZJ and BARC, and therefore the
52 temperature profiles are not comparable, at 500 s in all simulations the mixing has been completed at
53
54
55
56
57
58
59
60
61
62
63
64
65

1
2
3
4
5
6
7 level C, and one can observe large discrepancies with data in the simulations with radiation (again,
8 excluding BARC), of the same magnitude, though opposite in sign, as the other simulations.
9

10
11 The simulation of FZJ at 150 s, moreover, is affected by asymmetry, similar to that observed for test
12 ST1_2_2. In this case, it is easy to explain this profile with the bending and fluctuation of the plume,
13 as shown by the temperature field at various times (Benchmark Report, 2018). It is interesting to note
14 that the presence of a density interface acts on the plume as a lower flow rate. In fact, large-scale
15 oscillations were predicted for HP1_7_0 (30 g/s), but not for HP1_6_0 (60 g/s).
16

17 The comparisons of the gas temperature ~~time-evolution histories~~ at various positions (Benchmark
18 Report, 2018) permitted a better evaluation of the role played by radiation. Especially interesting is
19 the consideration of the temperature level reached during the transient, the temperature after the
20 stratification moved above a specific location, and the temperature rise time at the various locations.
21
22

23 An example of temperatures at higher locations is shown in Fig. 363. At the position along the axis
24 (Fig. 363 left), the calculations can be divided in three groups: 1) the simulations with radiation are
25 the most accurate with respect to the final values, but underpredict the times of the rise (erosion), with
26 the exception of BARC; 2) the CFD simulations without radiation overpredict the temperature; 3) the
27 results of PSI with GOTHIC are in between. Concerning the slopes of the temperature increase, the
28 results are rather sparse, with GOTHIC obtaining better results at intermediate levels, and only CFD
29 simulations with radiation (especially BARC) being able to predict the sudden rise at higher
30 elevations.
31
32

33
34 As regards the off-axis positions initially immersed in the helium layer (Fig. 363, right), the two CFD
35 simulations without radiation clearly overpredict the temperatures at all positions, whereas four of the
36 CFD simulations with radiation (CIEMAT, FZJ, GRS and VTT) underpredict the temperatures to
37 various extent. In general, the BARC simulation (also with radiation) is the most successful. The
38 calculation of PSI, however, is nearly equally accurate.
39
40

41
42 Finally, the temperatures at two positions off-axis below the initial bottom of the helium layer are
43 considered (Fig. 374). Close to the centre (325 mm from the axis), at the elevation of the recirculation
44 bubble above the plate (GH_19, z=5.3 m) the results are in a band of 15 K, with the PSI results being
45 the most accurate. Further off-axis (about 900 mm from the centre), and at the level of the injection,
46 therefore at a position weakly affected by convective motions, the CFD simulations with radiation
47 show substantially better results than the other calculations. At this position (K_17, z=4 m), and this
48 was the case also for test ST1-2-2 (Benchmark Report, 2018), the role played by radiation in nearly
49 stagnant region appear more clearly. It can also be shown that in these regions, where the heat-up is
50
51
52
53
54
55
56
57
58
59
60
61
62
63
64
65

1
2
3
4
5
6
7 initially mainly caused by compression, radiation is the only effective heat transfer process, since it
8 does not require the development of the boundary layer, which affects instead convective heat transfer
9 (Filippov et al., 2017)
10

11 It must also be remarked that the various predictions including radiation heat transfer produced
12 different results, as expected from the use of different models and methods to calculate the steam
13 absorptivity. The differences, also connected to the different time progression of the erosion, are large
14 during the mixing process, and vanish at many locations after the helium layer has been dissolved.
15
16
17
18
19
20
21

22 **5. CONCLUSIONS**

23
24 The experiment in the PANDA facility chosen for the present benchmark, test HP1_6_2, addresses
25 the stratification erosion induced by a vertical steam jet, which originates from the exit of a circular
26 pipe located below the bottom of the helium-rich layer. The mixing is somewhat slowed down by a
27 small, horizontal, circular plate above the jet source. The benchmark consisted of two phases: blind
28 and open. The results of the blind benchmark exhibited a large spread of results, some showing very
29 large discrepancies with the measured data, which was not expected, especially for the part addressing
30 the use of a “common” model. The results of the blind simulations made evident that further
31 investigations and validation studies were necessary to separate different sources of errors and avoid
32 their mutual elimination (compensating errors) in a complex model.
33
34
35

36 It was recognized that the most important difficulty in interpreting the results and finding the reason
37 of the large deviations was the lack of information on the velocity field downstream of the
38 obstruction, since only long-time averaged velocities were available in the region of the initial density
39 interface, above 6 m. It was therefore agreed that valuable information on the flow produced by the
40 interaction of the free jet with the obstruction could be obtained from auxiliary tests without helium
41 (“zero” tests), but with the same geometrical configuration and featuring an extended region above the
42 plate where velocity measurements were available.
43
44
45

46 Therefore, the open benchmark included the analyses of the data on the flow structure above the plate
47 obtained in these auxiliary tests: a “cascade” of simulations was thus proposed, which aimed to
48 separate the validation of the modelling approach for representing pure fluid dynamic phenomena
49 (using the data of the “zero” tests HP1_6_0 and HP1_7_0) from the application of the selected mesh
50 and models to the more complex test HP1_6_2, for which the success of the predictions also depend
51 on the appropriate representation of heat and mass transfer processes
52
53
54
55
56
57
58
59
60
61
62
63
64
65

1
2
3
4
5
6
7
8
9
10
11
12
13
14
15
16
17
18
19
20
21
22
23
24
25
26
27
28
29
30
31
32
33
34
35
36
37
38
39
40
41
42
43
44
45
46
47
48
49
50
51
52
53
54
55
56
57
58
59
60
61
62
63
64
65

The open phase of the benchmark thus consisted of four steps, ~~with an optional fifth step~~. Additionally, also the analysis of SETH-2 test ST1_2_2, with the same initial and boundary conditions as for test HP1_6_2, but without obstruction, was included as Step 5, to verify the capability of the models to properly predict the erosion process in absence of the obstacle, and therefore test their basic capabilities to represent the global features of the transient in the entire flow domain. Finally, also the velocity measurements at the pipe exit in two other test series were used in some comparisons to verify the appropriate representation of the injection conditions.

Since each participant was requested to submit one set (best estimate) of final results for each step and only the main sensitivity studies of some organisations were contributed to the final report, only general conclusion will be discussed, leaving the detailed answers to the questions to future publications of the individual organisations.

The simulations with a common model for the quasi-steady state conditions of test HP1_6_0 without helium (step 1) were expected to provide the opportunity to investigate the effect of mesh on the simulation of the interaction of the jet with the plate. The final results submitted exhibited notable differences, especially in relation to transversal distributions and flow development downstream of the plate. Although the simulations could be affected by numerics and the spurious effects of the calculated slow change of the thermal field, the analysis indicate that meshing strategies could not converge to produce similar results and setting an adequate mesh for representing the flow modification due to an obstacle poses a real challenge. It can be inferred that the variety of results later obtained for the full test are strongly affected by the meshes used in this region. This is somehow confirmed by the observations that the few simulations of test ST1_2_2 (Step 5) without obstacle were all reasonably successful, although performed with largely different meshes and model selections.

As regards the interaction of mesh and model selection (which produced in the blind benchmark astonishingly different results using a turbulence model but not a different one), no new information could be generated within this benchmark, due to the lack of systematic analysis and the use of similar turbulence models (all variants of $k-\varepsilon$ and $k-\omega$ models). However, comparing results for test HP1_6_0 with the “common” model and the “best-estimate” model (Steps 1 and 3, respectively), it was observed that the selection of models had a smaller effect than expected, and was seemingly less important than the mesh.

Thermal radiation heat transfer was confirmed to have an accelerating effect on the progression of the erosion process, independently of the specific model used, and a substantial part of the information obtained from the temperatures indicates that this heat transfer mode should be modelled to get the correct spatial and temporal evolution of the thermal field. However, since various simulations with

1
2
3
4
5
6
7 radiation were only performed for the final step, some results appear to be contradictory, and
8 inaccuracies (possibly compensated or enhanced by radiation) are certainly associated with the use of
9 meshes not optimised for the flow investigated (see above) and with the possible interaction with
10 other models and effects, no firm conclusion could be reached on the necessity and approach to model
11 radiation heat transfer. This issue will certainly require further investigations, both experimental and
12 numerical.
13
14

15 No definite conclusion could be reached with respect to best choice for turbulence model, as the
16 meshing appeared to be a more important issue for the conditions investigated in this benchmark.
17
18

19 The velocity and temperature distributions in the jet at the pipe exit have some effect on flow and
20 thermal variables, but this is mostly confined to the region below the obstruction. Finally, the effect of
21 numerical methods has been reported from some participants and for some contributions it can be
22 suspected to be responsible for some anomalous results and the submission of the final results with
23 meshes not optimised. However, the absence of systematic studies in most contributions show how
24 difficult is to implement in the analyses of transients requiring hundreds hours of CPU a rigorous
25 approach to guarantee mesh and time step independence.
26
27

28 The main conclusion of the open benchmark is that the step-by-step validation permitted some
29 progress with respect to some of the items identified above. However, large discrepancies with data in
30 the final analyses of the test are observed, which cannot be easily attributed to specific model
31 deficiencies. The uncertainty is partly due to the difficulty to perform exhaustive analyses for each
32 step including all effects, partly to the physical model limitations (e.g. use of RANS models for
33 turbulence), and partly to specific features of the reference test that cannot be tackled in simulations of
34 simplified conditions. On the one hand, even for the simpler fluid conditions of the tests without
35 density interface, mesh and models could not be fully assessed. On the other hand, it is clear that the
36 complexity of the physical conditions prevailing in the selected test, where the modification of the
37 flow produced by the obstacle interacts with the stratification erosion process, rendered the splitting of
38 the problem in hydrodynamic and heat/mass transfer components of lesser use than anticipated.
39
40
41
42

43 A few general considerations should be added in relation to the blind benchmark and the large,
44 unexpected, differences in the results. The spread of the results was similar, for instance, to the recent
45 OECD/NEA-PSI CFD benchmark without obstruction, although specifications for the “common”
46 model were given, which covered various aspects of the simulation (geometry, turbulence modelling,
47 initial, and boundary conditions, some fluid and flow properties, etc.). Since other aspects of the
48 simulation were not considered in the specifications (e.g. wall treatment, [buoyancy effect on](#)
49 [dissipation rate](#)), and therefore some of the differences could be due to specific code inputs as well as
50 to the numerical methods used, and the level of validation (including mesh convergence studies and
51
52
53
54
55
56
57
58
59
60
61
62
63
64
65

1
2
3
4
5
6
7
8
9
10
11
12
13
14
15
16
17
18
19
20
21
22
23
24
25
26
27
28
29
30
31
32
33
34
35
36
37
38
39
40
41
42
43
44
45
46
47
48
49
50
51
52
53
54
55
56
57
58
59
60
61
62
63
64
65

application of BPG) was different for the various contributions, it is difficult to draw any conclusions from the comparison of the requested results. However, it can be observed that, similarly to previous exercises for similar flows and configurations (but without obstruction), the present results suggest that whenever a new problem is tackled, established modelling strategies must be evaluated again. The outcome of the exercise reinforced the awareness of the spread of results that can be obtained if the adequacy of the mesh is solely evaluated on the base of previous experience and limited mesh refinement studies. In this respect, the fact that some of the best results were obtained with rather coarse meshes should not be used as argument in favour of this approach for applications, without appropriate validation. Furthermore, even the use of very detailed meshes, resulting from systematic studies (going close to the full application of the BPG) does not lead necessarily to similar results, which are possibly affected by the topology of the mesh, local refinement, details of the numerics, and other effects.

These considerations lead to a few key-findings of this comparison. First of all grid independence must be proven for each physical and geometrical model as well as set of boundary conditions and cannot be simply assumed that this can be concluded from a similar case. Small changes in the flow/setup, here the implementation of a small flow obstruction, may challenge the model validity range. This suggests that continuous validation and a backward assessment of previous results (e.g. those obtained for the OECD/NEA benchmark or other tests addressing stratification break-up) is necessary. The results furthermore highlight that the effect of user-defined numerical or physical assumptions is in the order of those of model differences.

In summary, the results highlight, for the sake of more precise conclusions, the need for proper grid convergence studies, beyond the prescriptions of the BPG (not addressing mesh topology), which possibly should be improved by including, for instance, recommendations on mesh structure for an open catalogue of simple flows. Moreover, following the practice of the V&V community (e.g. that organised by ASME), in future benchmarks more attention has to be paid to code inputs and their effects on the numerical solution of the equations.

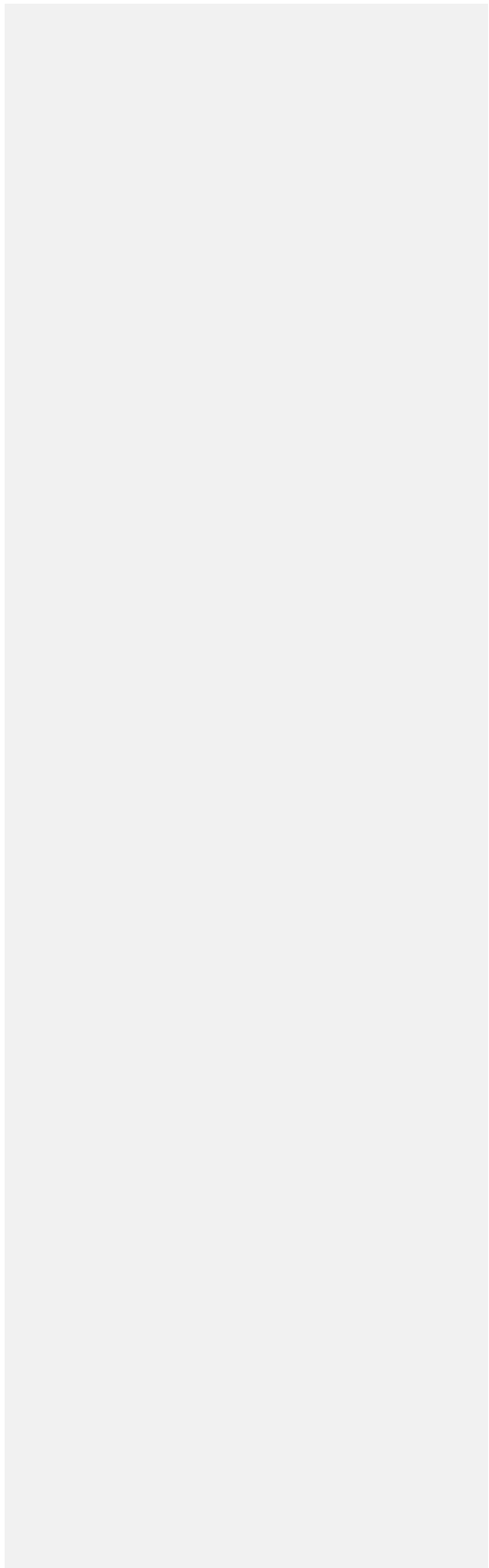
The results obtained by each participant using the best estimate models show that the combination of mesh and modelling approach again can result in a wide spread of results, with the quality of the results not always being improved using a model selection that proved to be successful for other configurations and test conditions. For instance, the use of refined turbulence models (such as SST) and considering radiative heat transfer did not result in fully satisfactory predictions, and made evident that further investigations and validation studies are necessary to separate different sources of errors and avoid their elimination (compensating errors) in a complex model.

It is important here to stress once more the importance of blind benchmarks, because they disclose the difficulty in tackling new problems for which the modelling strategy must be derived from previous

1
2
3
4
5
6
7
8
9
10
11
12
13
14
15
16
17
18
19
20
21
22
23
24
25
26
27
28
29
30
31
32
33
34
35
36
37
38
39
40
41
42
43
44
45
46
47
48
49
50
51
52
53
54
55
56
57
58
59
60
61
62
63
64
65

experience. This is true, we believe, in general, but it is more true for containment related problems, because the strict application of BPG is hindered by the long computation times associated with complex geometries, large volumes and long transients.

Finally, considering the specific configuration of the test on which it was based, the present benchmark revealed the (partly unexpected) difficulty to simulate a flow in presence of a simple obstruction. This observation suggests that in the future more experimental data and associated V&V will be required to validate the codes for more complex geometries. These issues are currently addressed in the OECD/NEA project HYMERES-2 (OECD/NEA, 2017).



1
2
3
4
5
6
7
8
9
10
11
12
13
14
15
16
17
18
19
20
21
22
23
24
25
26
27
28
29
30
31
32
33
34
35
36
37
38
39
40
41
42
43
44
45
46
47
48
49
50
51
52
53
54
55
56
57
58
59
60
61
62
63
64
65

ACKNOWLEDGMENTS

The experiment was conducted by the Experimental thermal-hydraulic group of PSI, composed by three of the authors - R. Kapulla, S. Paranjape and D. Paladino – and G. Mignot, M. Fehlmann, L. Ryan and S. Suter. The authors gratefully acknowledge the support of all the countries participating in the OECD/NEA HYMERES project and the OECD/NEA secretariat. The authors would like to thank all the members of the Management Board and the Programme Review Group of the HYMERES project for their help in defining the test programme and evaluating the test results.

REFERENCES

Abe, S., Studer, E., Ishigaki, M., Sibamoto, Y., and Yonomoto, T. (2018) “Stratification Breakup by a Diffuse Buoyant Jet: The MISTRA HM1-1 and 1-1bis Experiments and their CFD Analysis”, *Nucl. Eng. Design*, **331**, pp. 162–175.

Abu-Romia, M.M. and Tien, C.L (1967) “Appropriate Mean Absorption Coefficients for Infrared Radiation of Gases”, *Journal of Heat Transfer*, **89**(4), 321-327.

Allelein, H.-J., Fischer, K., Vendel, J., Malet, J., Studer, E., Schwarz, S., Houkema, M., H. Paillère, H., Bentaib, A. (2007). International Standard Problem ISP-47 on Containment Thermal Hydraulics. Nuclear Energy Agency, Committee on the Safety of Nuclear Installations, Final Report NEA/CSNI/R(2007)10, 2007.

Allein, H.-J., Reinecke, E.-A., Belt, A., Broxtermann, P., and Kelm, S. (2012) “Combined Analytical and Experimental Investigations for LWR Containment Phenomena”, *Nucl. Eng. Technol.*, **44**(3), 249-260.

Andreani, M., Badillo, A., and Kapulla, R. (2016a) “Synthesis of the OECD/NEA-PSI CFD Benchmark Exercise”, *Nucl. Eng. Design*, **299**, 59-80

Andreani, M., Daqiang, Y., Gaikwad, A.J., Ganju, S., Gera., B., Grigoryev, S., Herranz, L.E., Huhtanen, R., Kanaev, A., Kelm, S., Kim, J., Nishimura, T., Schramm, B., Sharabi, M., and Paladino, D. (2016b) “Synthesis of a blind CFD benchmark exercise based on a test in the PANDA facility addressing the stratification erosion by a vertical jet in presence of a flow obstruction”,

1
2
3
4
5
6
7 OECD/NEA 6th Workshop on Computational Fluid Dynamics for Nuclear Reactor Safety
8 (CFD4NRS-6), MIT, Cambridge, MA-USA, 13-15 September, 2016.
9

10 Andreani, M. and Paladino D., (Benchmark Report, 2018), prepared by PSI (with appendices
11 contributed by AERB, FZJ and VTT) (2018) “OECD/NEA HYMERES project: synthesis of results of
12 the benchmark on PANDA test HPI_6_2”, PSI Technical Note AN-42-17-07 Rev.1, Project report
13 HYMERES-P-17-48, May 2018.
14
15

16 Bentaib, A., Meynet, N., and Bleyer, A. (2015) “Overview on Hydrogen Risk Research and
17 Development Activities: Methodology and Open Issues”, *Nucl. Eng. Technol.*, **47**, 26-32.
18
19

20 Breitung, W. and Royl, P. (2000) “Procedure and Tools for Deterministic Analysis and Control of
21 Hydrogen Behavior in Severe Accidents”. *Nucl. Eng. Design*, **202**, 249-268.
22
23

24 Chan, C.K. and Jones, S.C. (1997) “Gas Mixing Experiments in a Large Enclosure”, Proc. of the 18th
25 Annual Conf. of the Canadian Nuclear Society
26
27

28 Choi, Y.-S., Lee, U.-J., and Park, G.-C. (2001) “Study on local hydrogen behaviors in a
29 subcompartment of the NPP containment”, *Nucl. Eng. Design*, **208**, 99-116.
30
31

32 Deri, E., Cariteau, B., and Abdo D. (2010) “Air fountains in the erosion of gaseous stratifications”,
33 *Int. J. Heat and Fluid Flow*, Volume **31**, Issue 5, Pages 935–941.
34
35

36 Erkan, N., Mignot, G., Kapulla, R., Paladino, D., Zboray, R., Strassberger, H.J., Bissels, W. and
37 Fehlmann, M. (2009) “OECD SETH-2 PANDA Test ST1_2_2 Quick-Look Report”, PSI internal
38 technical report TM-42-09-07-0, April 2009.
39
40

41 Filippov, A.S., Grigoryev, S.Yu., O.V. Tarasov, O.V. (2017) “On the possible role of thermal
42 radiation in containment thermal–hydraulics experiments by the example of CFD analysis of
43 TOSQAN T114 air–He test”, *Nucl. Eng. Design*, **310**, 175-186.
44
45
46

47 [Gallego E., Migoya E., Martín-Valdepeñas, J.M., Crespo, A., García, J., Venetsanos, A.,](#)
48 [Papanikolaou, E., Kumar, S., Studer, E., Dagba, Y., Jordan, T., Jahn, W., Høiset, S., Makarov, D.,](#)
49 [Piechna, J., \(2007\) “An intercomparison exercise on the capabilities of CFD models to predict](#)
50 [distribution and mixing of H₂ in a closed vessel”.](#) *International Journal of Hydrogen Energy*, **32**, 2235
51 [– 2245](#)
52
53
54
55
56
57
58
59
60
61
62
63
64
65

1
2
3
4
5
6
7 Gupta, S. (2015) “Experimental Investigations Relevant for Hydrogen and Fission Product Issues
8 Raised by the Fukushima Accident”, *Nucl. Eng. Technol.*, **47**, 11-25.

9
10
11 Howell, J.R. (1988) “Thermal Radiation in Participating Media: The Past the Present, and Some
12 Possible Futures”, *Journal Heat Transfer*, **110**, 1220-1229.

13
14 Huhtanen, R. (2018), Private Communication.

15
16
17 Kapulla, R., Mignot, G., Paranjape, S., Suter, S., Fehlmann, M., and Paladino, D. (2015a)
18 “OECD/NEA HYMERES Project: Jet/Plume interacting with flow obstruction HP1 Series. Test Series
19 Report”, PSI internal report TM-42-15-16, Rev.0, Project report HYMERES-P-15-26, Nov. 2015
20 (report restricted to project participants).
21

22
23
24 Kapulla, R., Paranjape, S., Mignot, G., Suter, S., Fehlmann, M., and Paladino D. (2015b)
25 “OECD/NEA HYMERES Project: PANDA Tests HP1_6_0, HP1_7_0, HP1_8_0, and HP1_678_Disk
26 Data Report”, PSI internal report TM-42-15-13 Rev. 0, Project report HYMERES-P-15-25, October
27 2015 (report restricted to project participants).
28

29
30
31 Karwat, H. et al. (1999) “State-of-the-Art Report on Containment Thermal-hydraulics and Hydrogen
32 Distribution”, OECD/NEA group of experts, CSNI/R(99)-16 (1999).
33

34
35 Kelm, S., Ritterath, M., Prasser, H.-M., and Allelein, H.J. (2016a) "Application of the MINIPANDA
36 Test Case ‘Erosion of a Stratified Layer by a Vertical Jet’ for CFD Validation”, *Nucl. Eng. Design*,
37 **299**, 124-135.
38

39
40 Kelm, S., Müller, H., and Allelein, H.-J. (2106b) “Importance of thermal radiation heat transfer
41 modeling in containment typical flows”, Paper submitted for presentation at the CFD4NRS-6, MIT,
42 Cambridge, MA, USA, September 13-15.
43

44
45
46 Liang, R. et al., (2015) “Status Report on Hydrogen Management and Related Computer Codes“,
47 NEA/CSNI/R(2014)8,
48

49
50
51
52
53
54
55
56
57
58
59
60
61
62
63
64
65

1
2
3
4
5
6
7 Lopez-Alonso E., Papini D., and Jimenez G. (2017) "Hydrogen Distribution and Passive
8 Autocatalytic Recombiner (PAR) Mitigation in a PWR-KWU Containment Type", *Annals of Nuclear
9 Energy*, **109**, pp. 600-611.

10
11
12 Mahaffy, J., et al. (2015). Best Practice Guidelines for the Use of CFD in Nuclear Reactor Safety
13 Applications - Revision" NEA/CSNI/R(2014)11.

14
15
16 Noutsopoulos, G.C. and Yannopoulos, P.C. (1989) "Axial Dilution in Obstructed Round Buoyant Jet",
17
18 *Journal of Hydraulic Engineering*, **115**(1), pp. 71-81.

19
20 Nishimura, T., Hoshi, H. and Hotta, A. (2015) "Current Research and Development Activities on
21 Fission Products and Hydrogen Risk after the Accident at Fukushima Daiichi Nuclear Power Station",
22
23 *Nucl. Eng. Technol.*, **47**, 1-10

24
25 OECD/NEA HYMERES-2 project (2017-2021).

26
27 OECD/NEA THAI Project (2010) "Hydrogen and Fission Product Issues Relevant for Containment
28 Safety Assessment under Severe Accident Conditions" Final Report, 22 June 2010, Report
29
30 NEA/CSNI/R(2010)3.

31
32
33 Paladino, D. and Dreier, J. (2012) "PANDA a Multi Purposes Integral Test Facility", *Science and
34 Technology of Nuclear Installations*, **2012**, Article ID 239319, doi:10.1155/2012/239319.

35
36
37 Paladino, D., Mignot, G., Kapulla, R., Zboray, R., Andreani, M., Tkatschenko, I., Studer, E., and
38 Brinster, J. (2013) "OECD/SETH-2 Project: PANDA and MISTRA Experiments addressing Key
39 Safety Issues for Water Reactor Containment", Proceedings of the 15th International Topical Meeting
40 on Nuclear Reactor Thermal-hydraulics (NURETH-15), paper 106, Pisa, Italy, 12-17 May 12-17,
41
42 2013.

43
44
45 Paladino, D., Andreani, M., Guentay, S., Mignot, G., Kapulla, R., Paranjape, S., Sharabi, M.,
46 Kisselev, A., Yudina, T., Filippov, Kamnev, M., Khizbullin, A., Tyurikov, O., Liang, Z., Daniele
47 Abdo, D., Brinster, J., Dabbene, F., Kelm, S., Klauck, M., Götz, L., Gehr, R., Malet, J., Bentaib, A.,
48 Bleyer, A., Lemaitre, P., Porcheron, E., Benz, S., Jordan, T., Xu, Z., Boyd, C., Siccama, A., Visser, D.
49 (2016) "Outcomes from the EURATOM-ROSATOM ERCOSAM SAMARA projects on
50
51

Formatted: Font: (Default) Times New Roman

Formatted: Line spacing: 1.5 lines

1
2
3
4
5
6
7
8
9
10
11
12
13
14
15
16
17
18
19
20
21
22
23
24
25
26
27
28
29
30
31
32
33
34
35
36
37
38
39
40
41
42
43
44
45
46
47
48
49
50
51
52
53
54
55
56
57
58
59
60
61
62
63
64
65

containment thermal-hydraulics for severe accident management”. *Nuclear Eng. and Design*, **308**, 103–114.

Paranjape, S., Kapulla, R., Mignot, G. and Paladino D. (2018) “Gas Redistribution Caused by Interacting Heat Sources in the Presence of a Vertical Condenser,” 12th International Topical Meeting on Nuclear Reactor Thermal-Hydraulics, Operation and Safety (NUTHOS-12), Qingdao, China, October 14-18, 2018.

Sarikurt, F.S. and Hassan, Y.A. (2017) “Large Eddy Simulations of Erosion of a Stratified Layer by a Buoyant Jet”, *Int. J. of Heat and Mass Transfer*, Vol. **112**, p. 354-365.

Schramm, B., Stewering, J., and Sonnenkalb M. (2017) “Einsatz von CFD-Codes für die Simulation von unfalltypischen Phänomenen im Sicherheitseinschluss: Validierung und gezielte Modellerweiterung”, Anschlussbericht RS1526, 2017 GRS-472, ISBN 978-3-946607-55-7.

Schwarz, S., Fischer, K., Bentaib, A., Burkhardt, J., Lee, J.-J., Duspiva, J., Visser, D., Kyttala, J., Royl, P., Kim, J., Kostka, P. and Liang, R. (2011) “Benchmark on Hydrogen Distribution in a Containment based on the OECD-NEA THAI HM-2 Experiment”, *Nucl. Technol.*, **175**(3), 594–603.

Smith B.L. (2009) “Identification and Prioritization of Generic Nuclear Safety Problems Requiring CFD Analysis”, Proc. 17th Int. Conf. on Nuclear Engineering (ICONE-17), Paper 75482, Brussels, Belgium, July12-16, 2009.

Studer, E., Brinster, J., Tkatschenko, I., Mignot, G., Paladino, D., and Andreani, M. (2012) “Interaction of a light gas stratified layer with an air jet coming from below: Large scale experiments and scaling issues”, *Nucl. Eng. Design*, **253**, 406-412.

Visser, D.C., Houkema, M., Siccama, N.B., and Komen, E.M.J. (2012) “Validation of a FLUENT CFD model for hydrogen distribution in a containment”, *Nuclear Engineering and Design*, **245**, 161–171.

Formatted: Font: (Default) Times New Roman, Italic

Formatted: Font: (Default) Times New Roman

Formatted: Font: (Default) Times New Roman, Bold

Formatted: Font: (Default) Times New Roman

1
2
3
4
5
6
7
8
9
10
11
12
13
14
15
16
17
18
19
20
21
22
23
24
25
26
27
28
29
30
31
32
33
34
35
36
37
38
39
40
41
42
43
44
45
46
47
48
49
50
51
52
53
54
55
56
57
58
59
60
61
62
63
64
65

LIST OF TABLES

Table 1: Summary of submissions for the blind benchmark

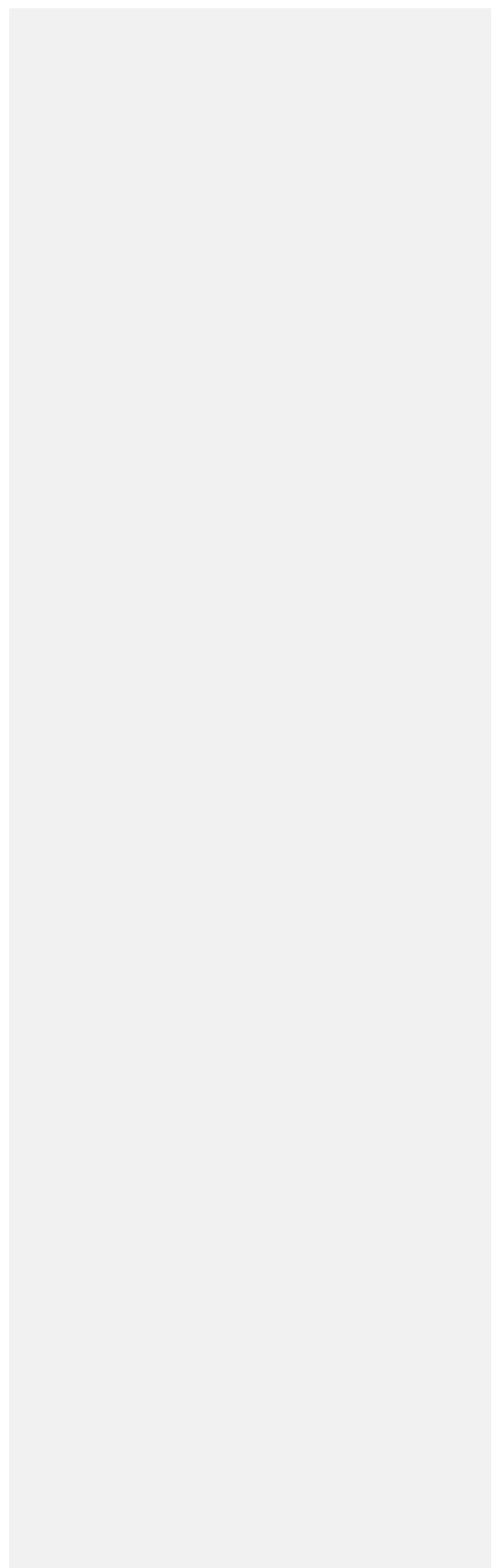
Table 2: Overview of contributions for Step 1 ([Exp. HP1_6_0](#)) of the open benchmark

Table 3: Overview of contributions for Step 2 ([Exp. HP1_7_0](#)) of the open benchmark

Table 4: Overview of contributions for Step 3 ([Exp. HP1_6_0](#)) of the open benchmark

Table 5: Overview of simulations performed for Step 5 ([Exp. ST1_2_2](#)) of the open benchmark

Table 6: Overview of contributions for Step 4 ([Exp. HP1_6_2](#)) of the open benchmark



1
2
3
4
5
6
7
8
9
10
11
12
13
14
15
16
17
18
19
20
21
22
23
24
25
26
27
28
29
30
31
32
33
34
35
36
37
38
39
40
41
42
43
44
45
46
47
48
49
50
51
52
53
54
55
56
57
58
59
60
61
62
63
64
65

Table 1: Summary of submissions for the blind benchmark

	CM			BEM
Organi- sation Contri- bution*	Code	<u>Num- ber of cells</u> x10 ³	Main deviations from specifications	Differences from CM
AERB	FLUENT 16	163	-	RNG k-ε
BARC	CFD- ACE+	164	Injected steam temperature	RNG k-ε
CIEMAT	FLUENT 15	135	-	radiative heat transfer (<u>Discrete Ordinates Method</u>) included
FZJ	CFX-15	565	Constant pressure	SST, condensation and radiative heat transfer included (<u>Monte Carlo Method</u>). Initial gas and wall T distribution.
GRS	CFX-15	1412	-	Slightly refined mesh (1.7 million cells), SST, radiative heat transfer (<u>Discrete Transfer Model</u>) included
IBRAE <i>IBRAE</i>	CFX-12	110	No man-hole, injected steam temperature	Different code (CABARET)
IBRAE <i>IBRAE2</i>	FLUENT 14.5.7	355	No man-hole, plate thickness=0	RSM
KAERI	OpenFOAM 2.3.1	158	Square pipe and plate	
S/NRA/R	FLUENT 15	655	-	SST, pre-conditioning phase (He injection) simulated
PSI <i>PSIF</i>	FLUENT 15	560	Half vessels, no man-hole	
PSI <i>PSIG</i>	GOTHIC 8.1	20	Square plate	Initial gas and wall T distribution. Enhanced HTC at the walls
SPICRI	CFX-13	1284	Initial T and X _{He} . No wall heat capacity	SST
VTT	FLUENT 16	2872		

*for multiple contributions from the same organisation

1
2
3
4
5
6
7
8
9
10
11
12
13
14
15
16
17
18
19
20
21
22
23
24
25
26
27
28
29
30
31
32
33
34
35
36
37
38
39
40
41
42
43
44
45
46
47
48
49
50
51
52
53
54
55
56
57
58
59
60
61
62
63
64
65

Table 2: Overview of contributions for Step 1 (Exp. HP1_6_0) of the open benchmark

Organi- sation	Code	Number of Cells x10 ³ (Nr. Cells for Blind simulations) (U=unstructured mesh)	Reported deviations from specifications	Size of cells below obstruction (m)	Equivalent CPU time on one core (h)
AERB	FLUENT V.16	240 (163)	Constant Pressure B.C.	0.03 y+=40-125	1500
BARC	CFD-ACE+ Version 2011	690 (U) (164)	Constant Pressure B.C.	0.03 y+=30-50	848
CIEMAT	FLUENT 16.2	256 (U) (135)	350 s transient time	(V=9.4e-7 m ³) ³ √V~0.01	24
FZJ	CFX-17	570 (565)	-	0.005 y+~30	1606
KAERI	OpenFOAM 2.4X	260 (158)	-	0.04	375
S/NRA/R	FLUENT V15.0	843 (U) (655)	-	0.0036	696
PSI	GOTHIC 8.1	41 (20)	-	0.01 y+~17-38	768
VTT	FLUENT V16.0	2214 (2872)	Enhanced wall treatment	0.0125	2500

1
2
3
4
5
6
7
8
9
10
11
12
13
14
15
16
17
18
19
20
21
22
23
24
25
26
27
28
29
30
31
32
33
34
35
36
37
38
39
40
41
42
43
44
45
46
47
48
49
50
51
52
53
54
55
56
57
58
59
60
61
62
63
64
65

Table 3: Overview of contributions for Step 2 (Exp. HP1 7 0) of the open benchmark

Organisa- tion	Code	Number of Cells $\times 10^3$ (Step 1)	Turbulence model	Thermal B.C. at the vessel wall Heat transfer	Radiation	Annotatio ns	Equival- ent CPU time on one core (h)
AERB	FLUENT V.16	240 (240)	Standard k- ϵ Standard wall functions	Heat loss: heat flux B.C. No Rad	No Rad	Constant pressure B.C. Lower steam injection temperatu re	1500
BARC	CFD-ACE+ Version 2011	690 (690)	RNG k- ϵ Non-equil. wall function	Heat losses: considered (heat flux B.C.) Rad.: Discrete Ordinate (DO) Method	Discrete Ordinate (DO) Method	Constant pressure B.C.	1536
CIEMAT	FLUENT 16.2	256 (256)	Standard k- ϵ Standard wall functions	Heat losses: considered No radiation	No Rad	Lower steam injection temperatu re Constant pressure B.C.	44
FZJ	CFX-17	660 (570)	SST, production limiter for TKE, Low Re corrections Automatic wall treatment	Heat losses: considered using effective HTC on outer surface and average steel T. Rad.: Monte Carlo method with $\kappa=1\text{ m}^{-1}$ (gray-gas)	Monte Carlo (MC) method Gray gas Absorption coefficient: $\kappa=1\text{ m}^{-1}$	Cell size below plate: 0.0005 m; y+~4 (Mesh refined around plate to match requireme nt of SST turbulence model) Inlet V profile Different from Step 1 due to modelling straight part of pipe	2932

Formatted: English (United States)

Formatted: English (United States)

Formatted: English (United States)

Formatted: Left

1
2
3
4
5
6
7
8
9
10
11
12
13
14
15
16
17
18
19
20
21
22
23
24
25
26
27
28
29
30
31
32
33
34
35
36
37
38
39
40
41
42
43
44
45
46
47
48
49
50
51
52
53
54
55
56
57
58
59
60
61
62
63
64
65

KAERI	OpenFOAM 2.4X	260 (260)	Standard k-ε Standard wall functions	No Rad. No heat losses. Fix wall temperature	No Rad.	Flat V profile at pipe exit	672
S/NRA/R	FLUENT V15.0	843	k-ω SST, Kato-Launders, Low Re corrections	No Rad. Constant Wall temp.	No Rad.	Constant Pressure B.C. Inlet V profile	928
PSI	GOTHIC 8.2a	42 (41) Injection pipe modeled	Standard k-ε Standard wall functions	Heat losses: heat flux B.C. No Rad.	No Rad.	Inlet V and T profiles obtained modelling the injection pipe (tuning the vessel inlet T) New version of the code (8.2)	444
VTT	FLUENT V16.0	2388 (2872) Finer than for Step 1	k-ω SST, Production Kato-Launders, Production Limiter, low-Re correction Near-wall treatment	No Rad. Constant Wall temp.	No Rad.	Grid includes injection pipe with heat structures. Experimental Mass inflow and temperature defined into the inlet pipe.	N/A

1
2
3
4
5
6
7
8
9
10
11
12
13
14
15
16
17
18
19
20
21
22
23
24
25
26
27
28
29
30
31
32
33
34
35
36
37
38
39
40
41
42
43
44
45
46
47
48
49
50
51
52
53
54
55
56
57
58
59
60
61
62
63
64
65

Table 4: Overview of contributions for Step 3 (Exp. HP1_6_0) of the open benchmark

Organi- sation	Code	Number of cells	Turbulence model	Thermal B.C. at the vessel wallHeat transfer	Radiation	Annotations	Equivalent CPU time on one core (h)
		x10 ³ (used for steps 1 and 2)	(choice for Step 2)				
BARC	CFD- ACE+ Version 2011	690 (690/ 690)	RNG k-ε Non-equil. wall function (same)	Heat losses: considered (heat flux B.C.) Rad: DO method	<u>DO method</u>	Constant pressure B.C.	904
CIEMAT	FLUENT 17.1	429 (256/ 256)	SST k-ω Standard wall functions (Standard k-ε)	Heat losses: considered Rad: DO method	<u>DO method</u>	Mesh refined Min/Maxim um volume (m ³): 1.1424e-07/ 1.4587e-02 cell below plate ≈7.3e- 07 New version of the code used	412
FZI	CFX-17	660 (570/ 660)	SST Automatic wall treatment. (same)	Heat losses: <u>considered</u>	<u>MC</u> method <u>Gray gas.</u> <u>Absorption</u> coefficient: <u>κ=1 m⁻¹</u>	Cell size below plate: 0.0005 m; y+~4 (same as for Step 2)	2882
S/NRA/R	FLUENT V15.0	843 (843/ 843)	SST,Kato- Launder, low Re corrections (same)	No Rad. Constant Wall temp.	<u>No Rad.</u>	Cell size below plate: 0.0036 m. No Cond./Rad. Inlet V profile	480

Formatted: English (United States)
Formatted: English (United States)

1
2
3
4
5
6
7
8
9
10
11
12
13
14
15
16
17
18
19
20
21
22
23
24
25
26
27
28
29
30
31
32
33
34
35
36
37
38
39
40
41
42
43
44
45
46
47
48
49
50
51
52
53
54
55
56
57
58
59
60
61
62
63
64
65

PSI	GOTHIC 8.2	42 (41/42)	Standard k-ε Standard wall functions (same)	Heat losses: heat flux B.C. No Radiation	No Radiation <u>No Radiation</u>		755
VTT	FLUENT V16.0	2311 (2214, 2378)	SST k-ω, Production Kato-Launder, Production Limiter, low Re corrections Near wall treatment (same)	No Radiation Constant Wall temp.	No Radiation <u>No Radiation</u>	Grid includes injection pipe with heat structures. Experimental Mass inflow and temperature defined into the inlet pipe	N/A

1
2
3
4
5
6
7
8
9
10
11
12
13
14
15
16
17
18
19
20
21
22
23
24
25
26
27
28
29
30
31
32
33
34
35
36
37
38
39
40
41
42
43
44
45
46
47
48
49
50
51
52
53
54
55
56
57
58
59
60
61
62
63
64
65

Table 5: Overview of simulations performed for Step 5 (Exp. ST1 2 2) of the open benchmark

Organi- sation	Code	Number of cells	Turbulence model	Thermal B.C. at the vessel wallHeat transfer	Radiation	Annotations	Equiva- lent time one c (h)
		x10 ³ (Steps 2/3)	(Steps 2/3)				
AERB	FLUENT V.16	895 (240)	Realizable k-ε Non-equilibrium wall functions (Standard k-ε, standard wall functions)	Heat loss: heat flux B.C. No Radiation	No Radiation	Straight part of Injection pipe modelled to get velocity profile. Constant pressure B.C.	2160
FZJ	CFX-16.1	560 (660)	SST Automatic wall treatment	Heat loss: heat flux B.C. Radiative heat transfer considered. Gray gas. Absorption coefficient: 1 m ⁻¹	MC method Gray gas Absorption coefficient: κ=1 m ⁻¹	Straight part of Injection pipe modelled to get velocity profile (w/o heat transfer) Constant pressure B.C.	2660
PSI	GOTHIC 8.2a	42	Standard k-ε Standard wall functions	Heat losses: heat flux B.C. No Radiation	No Radiation	Same mesh as for other steps (including denser mesh at 5 m)	755
SPICRI	cosCYCAS 1.0	5.5	Standard k-ε Standard wall functions	Wall heat transfer considered	No Radiation	Axis- symmetric model	27.9

Formatted: English (United States)
Formatted: English (United States)
Formatted: English (United States)
Formatted: English (United States)
Formatted: English (United States)

1
2
3
4
5
6
7
8
9
10
11
12
13
14
15
16
17
18
19
20
21
22
23
24
25
26
27
28
29
30
31
32
33
34
35
36
37
38
39
40
41
42
43
44
45
46
47
48
49
50
51
52
53
54
55
56
57
58
59
60
61
62
63
64
65

Table 6: Overview of contributions for Step 4 (Exp. HP1 6 2) of the open benchmark

Organi- sation	Code	Nr.	Turbulence model	Thermal B.C. at the vessel wallHeat transfer	Radiation	Annotations	Equivalent CPU time on one core (h)
		Cells x10 ³ (Steps 1, 2, 3 and 5)	(steps 2,3,5)				
AERB	FLUENT V16.1	899 (240, 240, N/A, 894)	Realizable k- ε (standard) Non-equil. wall function (standard)	Heat losses: heat flux B.C. No Rad.	No Rad.	Straight part of Injection pipe modelled to get velocity profile. Constant pressure B.C.	1730
BARC	CFD-ACE+ Version 2011	690 (690). 690, 690, N/A)	RNG k-ε Non-equil. wall function (same)	Heat losses: heat flux B.C. No Cond. Rad: DO method	<u>DO method</u>	Cell size below plate: 0.03 m; y+ between 30 and 50. Constant pressure B.C.	1536
CIEMAT	FLUENT 17.1	133 (260, 260, 420, N/A)	Standard k-ε Standard wall functions (SST)	Heat losses: Considered No Cond. Radiation: DO method	<u>DO method</u>	Submitted results using the same model as for BEM blind simulation	188 1920 for the BEM blind simulation
FZI	CFX-17	660 (570, 660, 660, 550)	SST Automatic wall treatment (same)	Radiative heat transfer: Monte Carlo: Gray gas; absorption coefficient: 1 m⁻¹	<u>MC method.</u> <u>Gray gas</u> <u>Absorption</u> <u>coefficient:</u> <u>κ=1 m⁻¹</u>	Cell size below plate: 0.0005 m; y+~4	5551

Formatted: English (United States)
Formatted: English (United States)
Formatted: English (United States)
Formatted: English (United States)
Formatted: English (United States)

Formatted: Space After: 10 pt

1
2
3
4
5
6
7
8
9
10
11
12
13
14
15
16
17
18
19
20
21
22
23
24
25
26
27
28
29
30
31
32
33
34
35
36
37
38
39
40
41
42
43
44
45
46
47
48
49
50
51
52
53
54
55
56
57
58
59
60
61
62
63
64
65

GRS	CFX-17	7000	SST, Including buoyancy turbulence terms automatic wall treatment	Radiative heat transfer: DTM (64 rays), gray gas, absorption coefficient 1 m^{-1} (from RS1500 correlation)	DTM (64 rays) Gray gas absorption coefficient 1 m^{-1} (from RS1500 correlation)	Straight part of injection pipe modelled to get velocity profile	17700
S/NRA/R	FLUENT	843	SST, Kato-Lauder, low Re corrections no wall treatment	No Cond. No Rad. Constant Wall temp.	No Rad.	Cell size below plate: 0.0036 m. Constant P Inlet V profile	208
	V15.0	(843, 843, 843, N/A)	(same)				
PSI	GOTHIC 8.2	42 (41,42,42,42)	Standard k-ε Standard wall functions (same)	Heat losses: heat flux B.C. Rad: not considered	No Rad.	Contrarily to BEM simulation for the blind benchmark, the low initial values of the wall temperature at the top of the dome were not used for a large part of the dome, and Standard convective HTC correlation were used (no enhancement factor)	768

Formatted: English (United States)
Formatted: English (United States)
Formatted: English (United States)
Formatted: English (United States)
Formatted: English (United States)

1
2
3
4
5
6
7
8
9
10
11
12
13
14
15
16
17
18
19
20
21
22
23
24
25
26
27
28
29
30
31
32
33
34
35
36
37
38
39
40
41
42
43
44
45
46
47
48
49
50
51
52
53
54
55
56
57
58
59
60
61
62
63
64
65

VTT	FLUENT V16.2	3313 (2214, 2378, 2311, N/A)	k- ω SST, Production Kato- Launder, Production Limiter Near wall treatment	Constant vessel wall temperature No Cond Rad: P1 method with WSGG model for gas absorptivity Absorption coefficient between 0.38 and 0.393 m⁻¹	P1 method with WSGG model for gas absorptivity Absorption coefficient between 0.38 and 0.393 m⁻¹	No low-Re correction Grid used for the other steps is refined in plume area above 5.9m. Boundary- layer cells on walls (2 cells). Grid includes injection pipe with heat structures. Experimenta l mass inflow and temperature defined into the inlet pipe. Cell size below plate: 0.0125 m	8400
-----	-----------------	--	--	--	--	--	------

1
2
3
4
5
6
7 **LIST OF FIGURES**
8
9

10 Figure 1: Cutaway drawing of the vessels (left), configuration for the experiment (middle), and initial
11 helium concentration vertical profile in Vessel 1 (right).
12

13 Figure 2: ~~Time Evolution histories~~ of helium concentrations (left) and gas temperatures (right) at
14 various elevations along axis of Vessel 1.
15

16 Figure 3: Blind benchmark: Erosion progression (right) calculated with the CM and ~~evolution time~~
17 ~~history~~ (left) of gas temperature at position B20 ($z=7500$ mm), shown as an example. The dashed line
18 shows how the erosion time at each elevation (e.g. at the elevation of position B20) is derived.
19
20

21 Figure 4: Blind benchmark: Helium concentration ~~evolution time histories~~ at elevation A (left) and B
22 (right) calculated with the “Common Model” (CM)
23

24 Figure 5: Blind benchmark: Gas temperature horizontal profile at level G at 300 s (left) and at level H
25 at 150 s (right) calculated with the CM. Square marks show the experimental data.
26

27 Figure 6: Blind benchmark: Erosion progression (left) and helium concentration ~~evolution time history~~
28 at Level B (right) calculated with the BEM.
29
30

31 Figure 7: (top) vertical section (plane 315° - 135°) and horizontal section of Vessel 1 showing the
32 locations of the concentration and gas temperature measurements and the Field of View (FOV) for
33 PIV measurements used for HP1_6_2 (Vessel 2 and IP are not shown); (bottom) position of the
34 combined PIV window used for Tests HP1_X_0.
35

36 Figure 8: Experiments and models used in the five steps of the open benchmark.
37

38 Figure ~~98~~: Open benchmark, Step 1: Average experimental flow field (left) measured in Test
39 HP1_6_0, and vertical velocity profiles used in the comparisons with calculated results (right).
40

41 Figure ~~109~~: Open benchmark, Step 1: Axial profile of the vertical velocity (left) and vertical profile of
42 the maximum vertical velocity (right).
43

44 Figure ~~110~~: Open benchmark, Step 1: Measured distribution of Turbulent Kinetic Energy (left) and
45 comparison between experimental and calculated axial profile
46
47

48 Figure ~~124~~: Open benchmark, Step 1: Difference of the maximum velocity in the two half planes (left)
49 and position (Y2) of the full jet recovery (right).
50

51 Figure ~~132~~: Open benchmark, Step 1: ~~Evolution Time history~~ of the minimum vertical velocity (left)
52 and elevation (Y1) of the top of the recirculation zone (right).
53
54
55
56
57
58
59
60
61
62
63
64
65

1
2
3
4
5
6
7 Figure 143: Open benchmark, Step 1: Horizontal profiles of the vertical velocity at the elevation of
8 the middle of the recirculation zone (left) and at an elevation in the flow developed region (right).

9
10 Figure 154: Open benchmark, Step 1: Horizontal profiles of the TKE at the elevation of the middle of
11 the recirculation zone (left) and at an elevation in the flow developed region (right).

12
13 Figure 165: Open benchmark, Step 2: Average experimental flow field (left) measured in Test
14 HP1_7_0, and vertical velocity profiles used in the comparisons with calculated results (right).

15
16 Figure 176: Open benchmark, Step 2: Axial profile of the vertical velocity (left) and vertical profile of
17 the maximum vertical velocity (right).

18
19 Figure 187: Open benchmark, Step 2: Temperature radial profile at 6.276 m (left) and axial
20 temperature distribution (right).

21
22 Figure 198: Open benchmark, Step 3: Axial velocity and maximum velocity vertical profiles for Step
23 3, compared with results for Step 1.

24
25 Figure 2049: Open benchmark, Step 3: Axial temperature profile and horizontal profile at 6.3 m.

26
27 Figure 210: Open benchmark, Step 5: Configuration for SETH-2 test ST1_2_2, and important initial
28 and boundary conditions of test ST1_2 and repetition test ST1_2_2 compared with those used for Test
29 HP1_6_2.

30
31 Figure 224: Open benchmark, Step 5: Progression of erosion along the axis in test ST1_2_2, using
32 gas temperature rise times.

33
34 Figure 232: Open benchmark, Step 5: Helium concentration ~~evolutiontime-histories~~
35 at various elevations along the axis of Vessel 1.

36
37 Figure 243: Open benchmark, Step 5: Vertical velocity axial profile (left) and horizontal profile at
38 z=5003 mm (1 m above pipe exit)

39
40 Figure 254: Open benchmark, Step 5: Axial temperature profile at two times.

41
42 Figure 265: Open benchmark, Step 5: horizontal profiles at 6.3 m at 150 s (before mixing) and 300 s
43 (after mixing)

44
45 Figure 276: Open benchmark, Step 5: horizontal profiles at 6.93 m at 250 s (during mixing or
46 immediately after) and 500 s (after mixing)

47
48 Figure 28: Open benchmark, Step 4: Calculated sequence of spatial distributions of helium
49 concentrations at various times (contribution of VTT).

50
51
52
53
54
55
56
57
58
59
60
61
62
63
64
65

1
2
3
4
5
6
7
8
9
10
11
12
13
14
15
16
17
18
19
20
21
22
23
24
25
26
27
28
29
30
31
32
33
34
35
36
37
38
39
40
41
42
43
44
45
46
47
48
49
50
51
52
53
54
55
56
57
58
59
60
61
62
63
64
65

Figure 29: Open benchmark, Step 4: Calculated sequence of spatial distributions of gas temperatures at various times (contribution by VTT).

Figure 3027: Open benchmark, Step 4: Erosion progression calculated in the open phase (left), compared with best estimate results contributed to the blind benchmark.

Figure 3128: Open benchmark, Step 4: Helium concentration ~~evolutiontime-history~~ at $z=6.48$ m calculated in the open phase (left), compared with best estimate results contributed to the blind benchmark.

Figure 3229: Open benchmark, Step 4: Example of results obtained using the model for radiation or neglecting it: helium concentration ~~evolutiontime-histories~~ calculated at 8 m (left, GRS, Schramm et al., 2017) and at 7.5 m (right, VTT, Huhtanen, 2018).

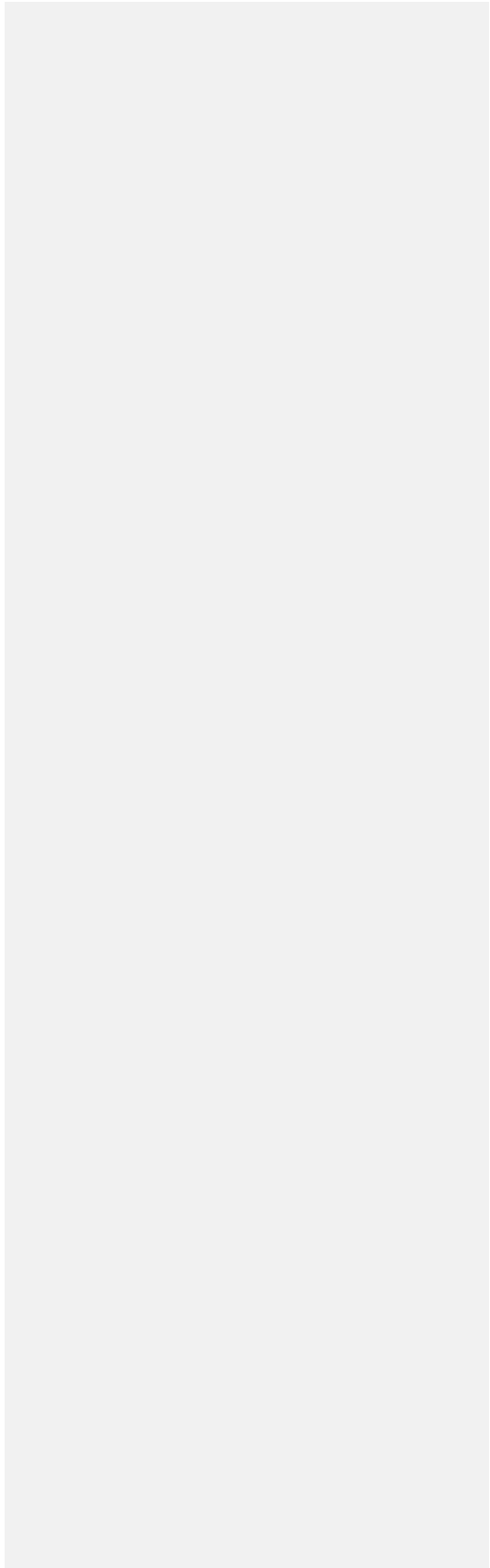
Figure 330: Open benchmark, Step 4: Vertical velocity averaged axial and horizontal profiles in the PIV window.

Figure 344: Open benchmark, Step 4: Axial gas temperature distributions at two times

Figure 352: Open benchmark, Step 4: Gas temperature horizontal profiles at various elevations and two times.

Figure 363: Open benchmark, Step 4: Gas temperature ~~evolutiontime-histories~~ at two positions (left: on the axis; right: at 570 mm from the wall) at 6.5 m.

Figure 374: Open benchmark, Step 4: Off-axis ($r: \pm 325$ mm) gas temperature ~~evolutiontime-histories~~ at two positions below the initial bottom of the helium layer ($z: 5301$ and 4000 mm, respectively)



1
2
3
4
5
6
7
8
9
10
11
12
13
14
15
16
17
18
19
20
21
22
23
24
25
26
27
28
29
30
31
32
33
34
35
36
37
38
39
40
41
42
43
44
45
46
47
48
49
50
51
52
53
54
55
56
57
58
59
60
61
62
63
64
65

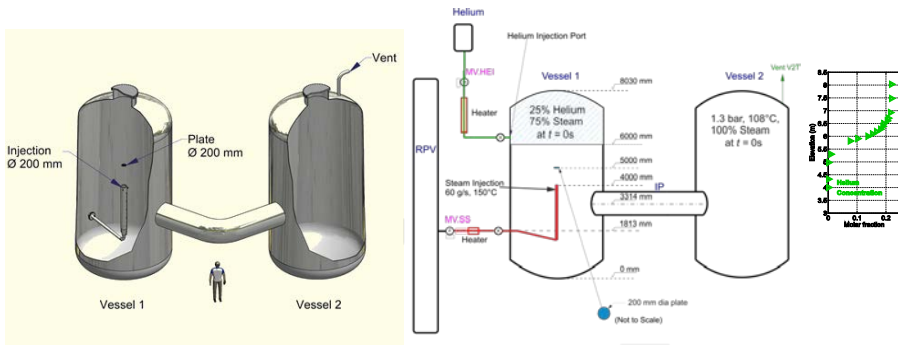


Figure 1: Cutaway drawing of the vessels (left), configuration for the experiment (middle), and initial helium concentration vertical profile in Vessel 1 (right).

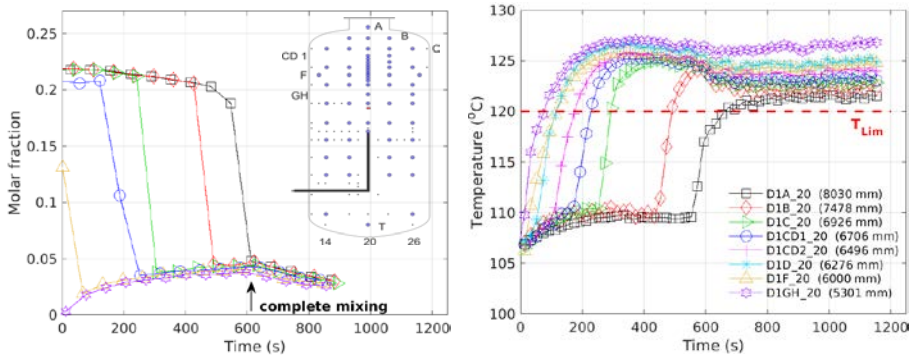


Figure 2: EvolutionTime-histories of helium concentrations (left) and gas temperatures (right) at various elevations along axis of Vessel 1.

1
2
3
4
5
6
7
8
9
10
11
12
13
14
15
16
17
18
19
20
21
22
23
24
25
26
27
28
29
30
31
32
33
34
35
36
37
38
39
40
41
42
43
44
45
46
47
48
49
50
51
52
53
54
55
56
57
58
59
60
61
62
63
64
65

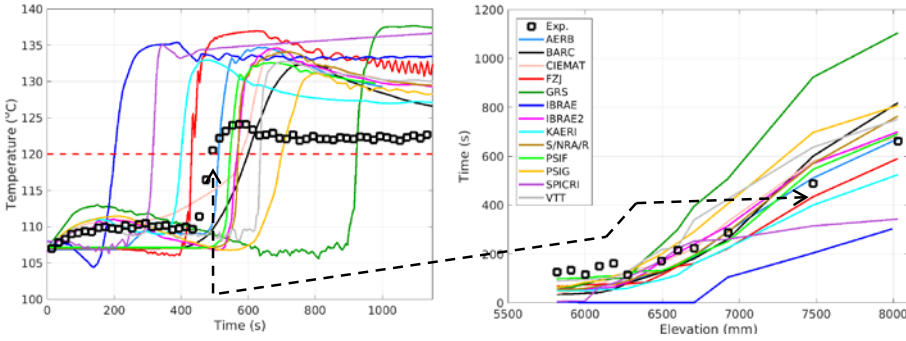


Figure 3: Blind benchmark: erosion progression (right) calculated with the CM and evolution time history (left) of gas temperature at position B20 ($z=7500$ mm), shown as an example. The dashed line shows how the erosion time at each elevation (e.g. at the elevation of position B20) is derived.

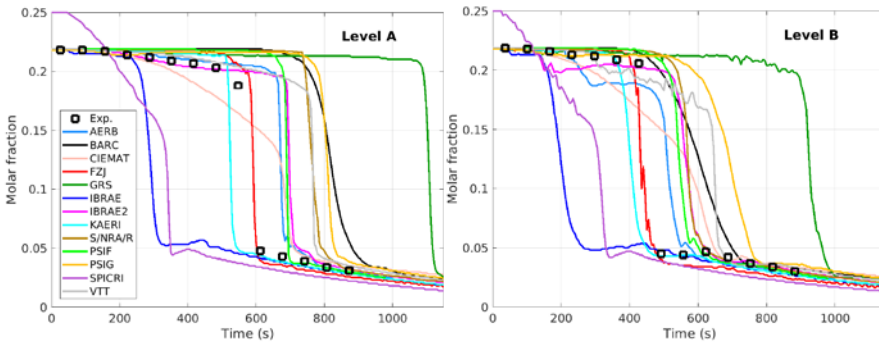
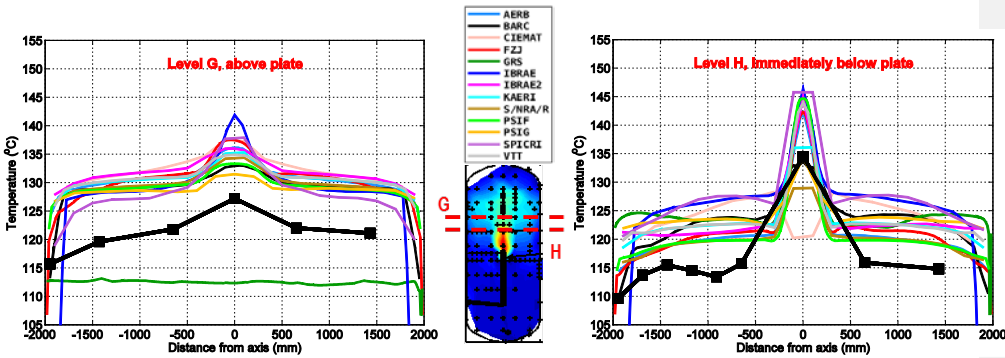


Figure 4: Blind benchmark: Helium concentration evolution time histories at elevation A (left) and B (right) calculated with the "Common Model" (CM).



1
2
3
4
5
6
7
8
9
10
11
12
13
14
15
16
17
18
19
20
21
22
23
24
25
26
27
28
29
30
31
32
33
34
35
36
37
38
39
40
41
42
43
44
45
46
47
48
49
50
51
52
53
54
55
56
57
58
59
60
61
62
63
64
65

Figure 5: Blind benchmark: Gas temperature horizontal profile at level G at 300 s (left) and at level H at 150 s (right) calculated with the CM. Square marks show the experimental data.

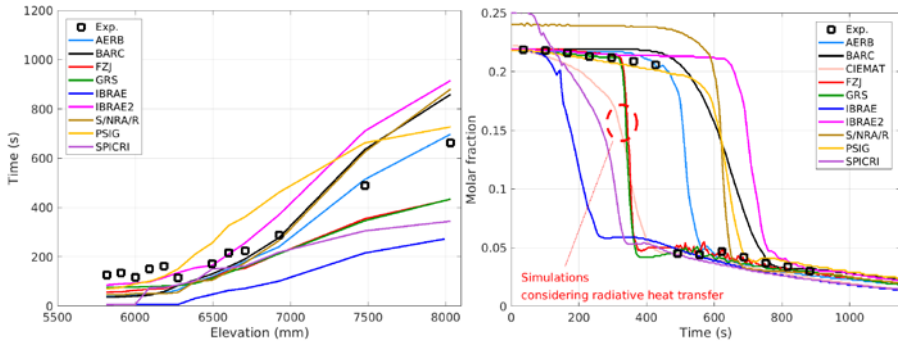
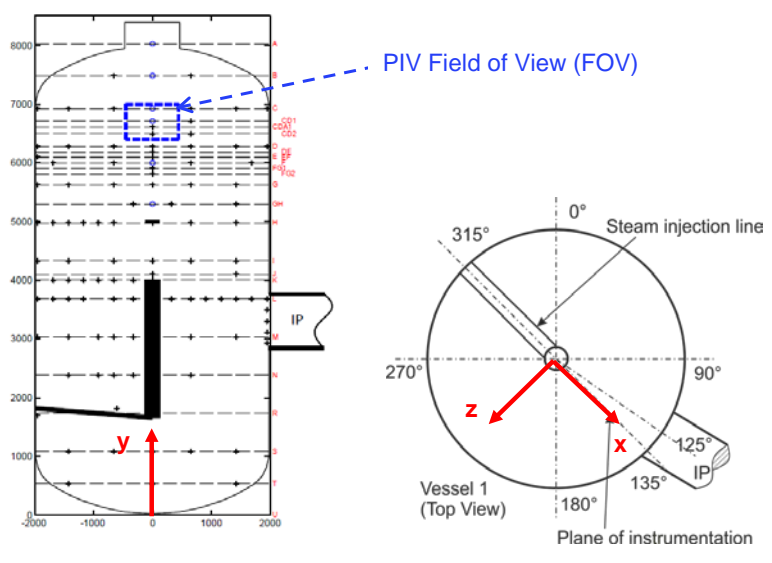


Figure 6: Blind benchmark: Erosion progression (left) and helium concentration ~~evolution~~ ~~time~~ ~~history~~ at Level B (right) calculated with the BEM.



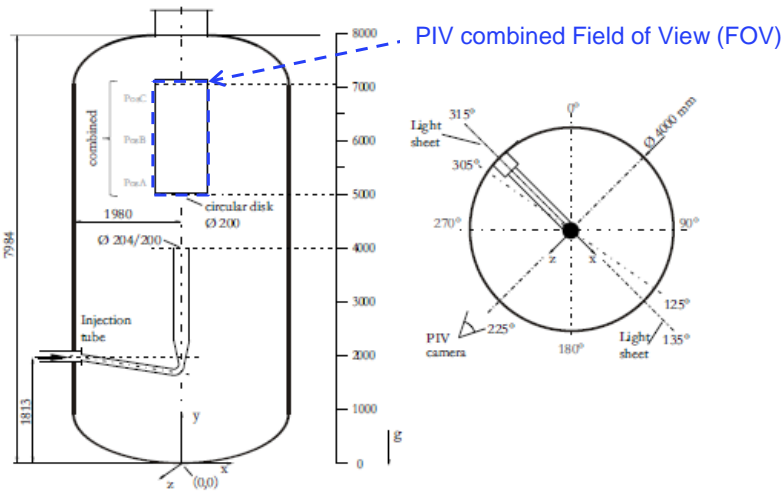


Figure 7: (top) vertical section (plane 315°-135°) and horizontal section of Vessel 1 showing the locations of the concentration and gas temperature measurements and the Field of View (FOV) for PIV measurements used for HP1_6_2 (Vessel 2 and IP are not shown); (bottom) position of the combined PIV window used for Tests HP1_X_0.

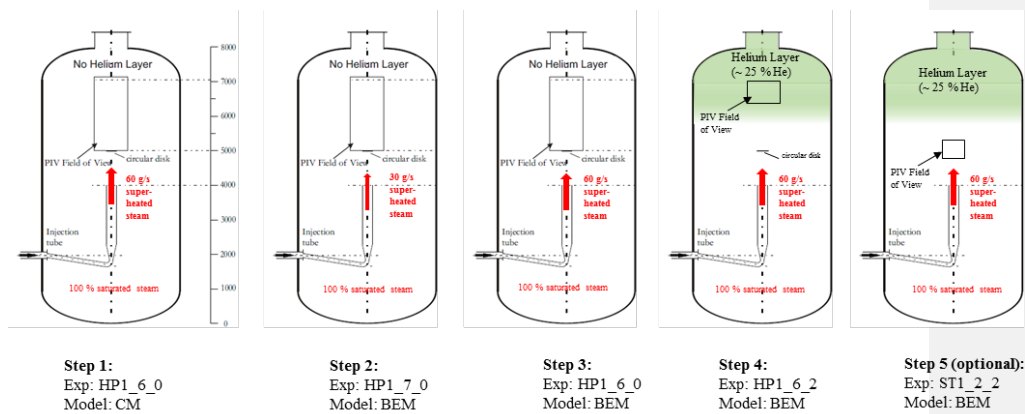


Figure 8: Experiments and models used in the five steps of the open benchmark.

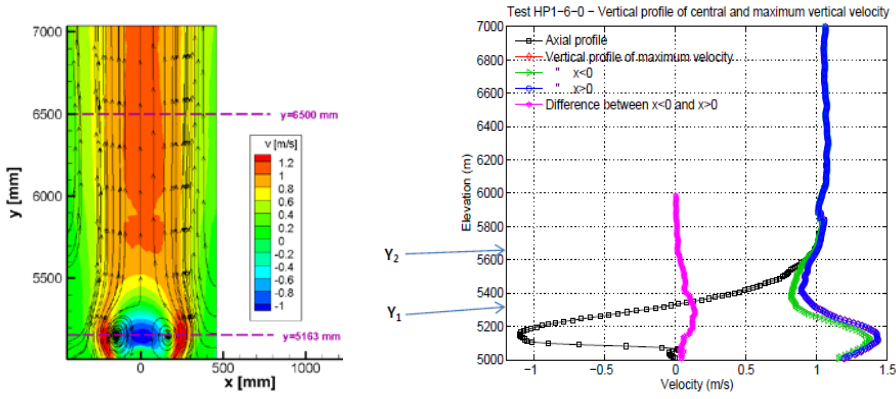


Figure 98: Open benchmark, Step 1: Average experimental flow field (left) measured in Test HP1_6_0, and vertical velocity profiles used in the comparisons with calculated results (right).

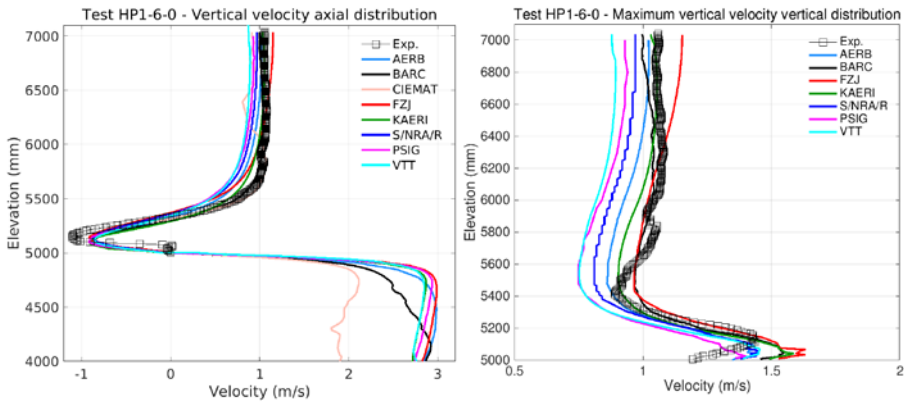


Figure 109: Open benchmark, Step 1: Axial profile of the vertical velocity (left) and vertical profile of the maximum vertical velocity (right).

1
2
3
4
5
6
7
8
9
10
11
12
13
14
15
16
17
18
19
20
21
22
23
24
25
26
27
28
29
30
31
32
33
34
35
36
37
38
39
40
41
42
43
44
45
46
47
48
49
50
51
52
53
54
55
56
57
58
59
60
61
62
63
64
65

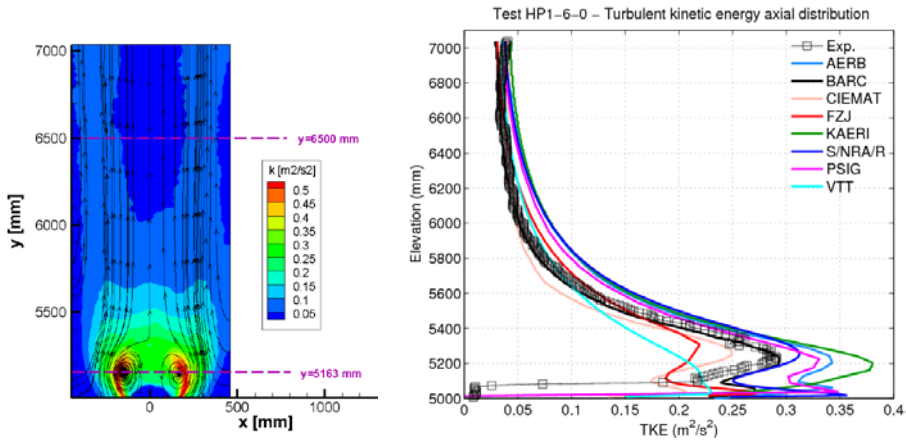


Figure 110: Open benchmark, Step 1: Measured distribution of Turbulent Kinetic Energy (left) and comparison between experimental and calculated axial profile.

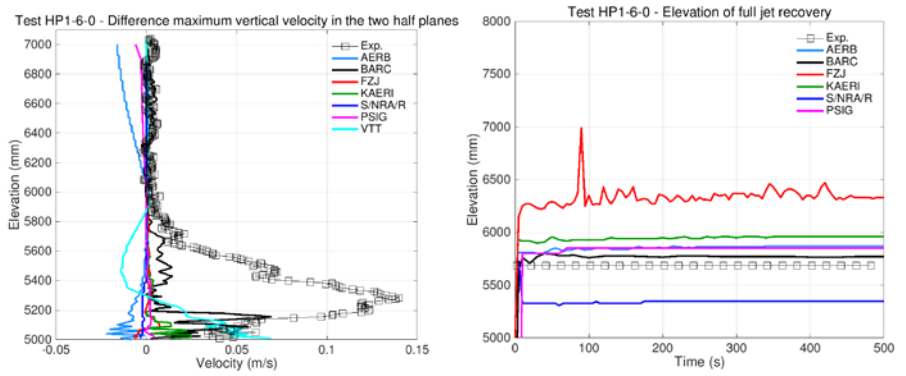


Figure 124: Open benchmark, Step 1: Difference of the maximum velocity in the two half planes (left) and position (Y2) of the full jet recovery (right).

1
2
3
4
5
6
7
8
9
10
11
12
13
14
15
16
17
18
19
20
21
22
23
24
25
26
27
28
29
30
31
32
33
34
35
36
37
38
39
40
41
42
43
44
45
46
47
48
49
50
51
52
53
54
55
56
57
58
59
60
61
62
63
64
65

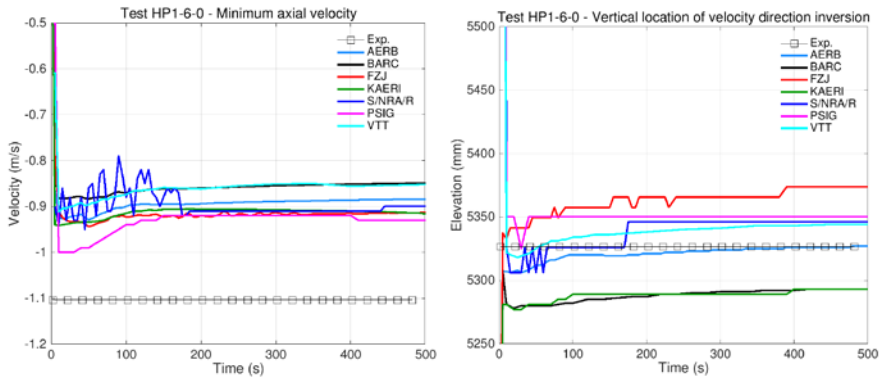


Figure 132: Open benchmark, Step 1: EvolutionTime history of the minimum vertical velocity (left) and elevation (Y1) of the top of the recirculation zone (right).

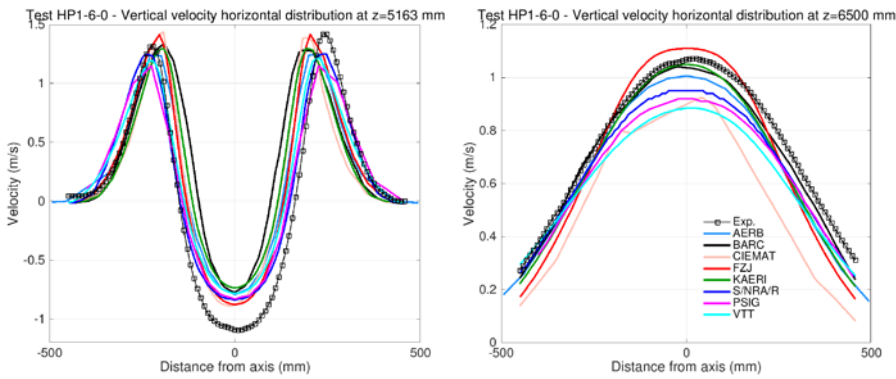


Figure 143: Open benchmark, Step 1: Horizontal profiles of the vertical velocity at the elevation of the middle of the recirculation zone (left) and at an elevation in the flow developed region (right).

1
2
3
4
5
6
7
8
9
10
11
12
13
14
15
16
17
18
19
20
21
22
23
24
25
26
27
28
29
30
31
32
33
34
35
36
37
38
39
40
41
42
43
44
45
46
47
48
49
50
51
52
53
54
55
56
57
58
59
60
61
62
63
64
65

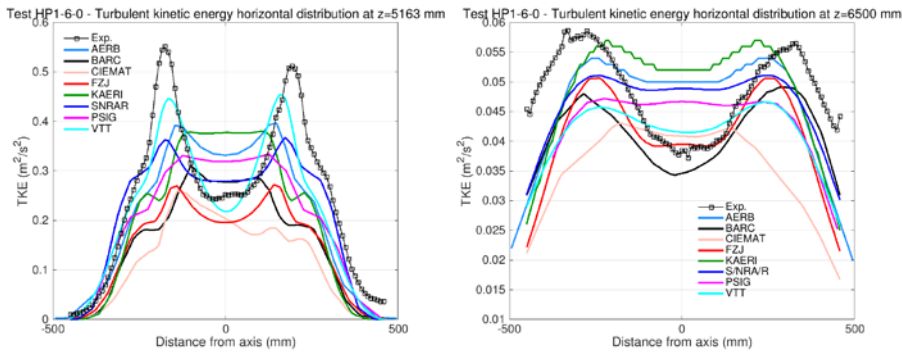


Figure 154: Open benchmark, Step 1: Horizontal profiles of the TKE at the elevation of the middle of the recirculation zone (left) and at an elevation in the flow developed region (right).

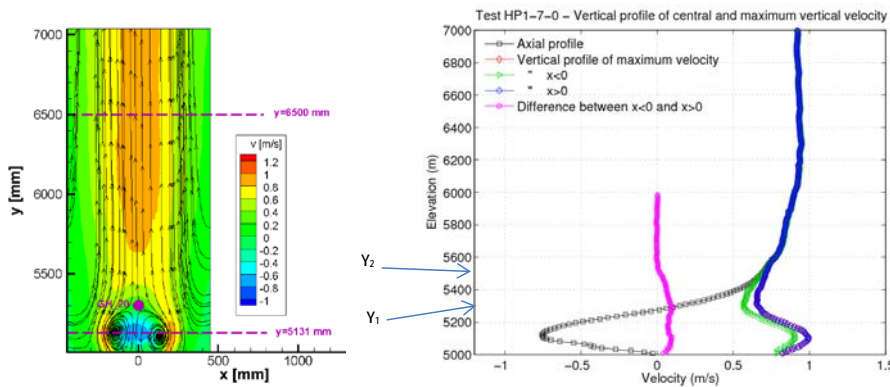


Figure 165: Open benchmark, Step 2: Average experimental flow field (left) measured in Test HP1_7_0, and vertical velocity profiles used in the comparisons with calculated results (right).

1
2
3
4
5
6
7
8
9
10
11
12
13
14
15
16
17
18
19
20
21
22
23
24
25
26
27
28
29
30
31
32
33
34
35
36
37
38
39
40
41
42
43
44
45
46
47
48
49
50
51
52
53
54
55
56
57
58
59
60
61
62
63
64
65

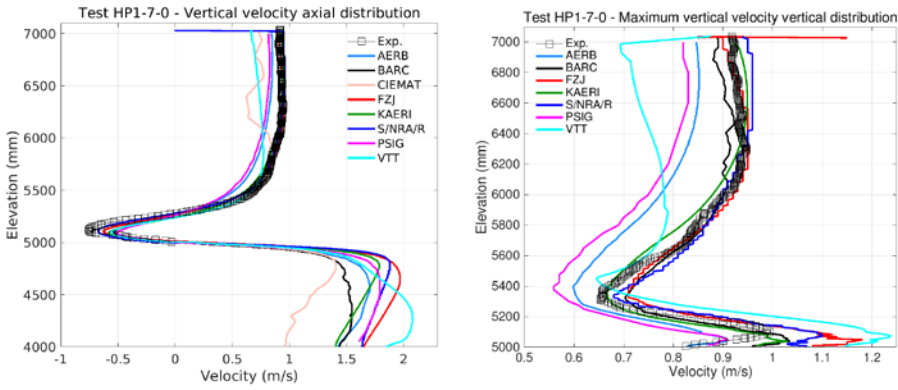


Figure 176: Open benchmark, Step 2: Axial profile of the vertical velocity (left) and vertical profile of the maximum vertical velocity (right).

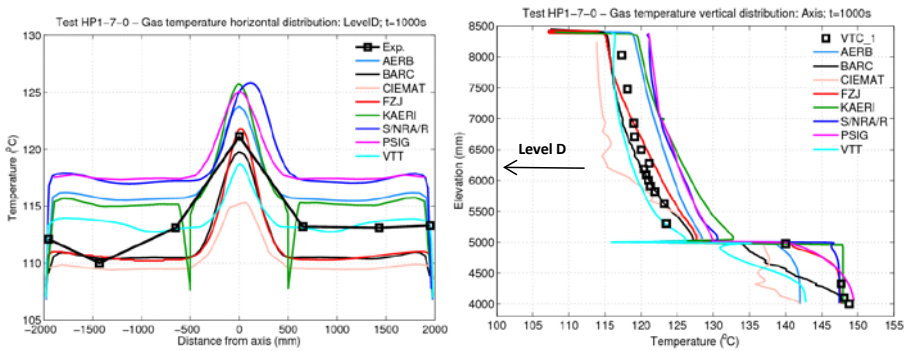


Figure 187: Open benchmark, Step 2: Temperature radial profile at 6.276 m (left) and axial temperature distribution (right).

1
2
3
4
5
6
7
8
9
10
11
12
13
14
15
16
17
18
19
20
21
22
23
24
25
26
27
28
29
30
31
32
33
34
35
36
37
38
39
40
41
42
43
44
45
46
47
48
49
50
51
52
53
54
55
56
57
58
59
60
61
62
63
64
65

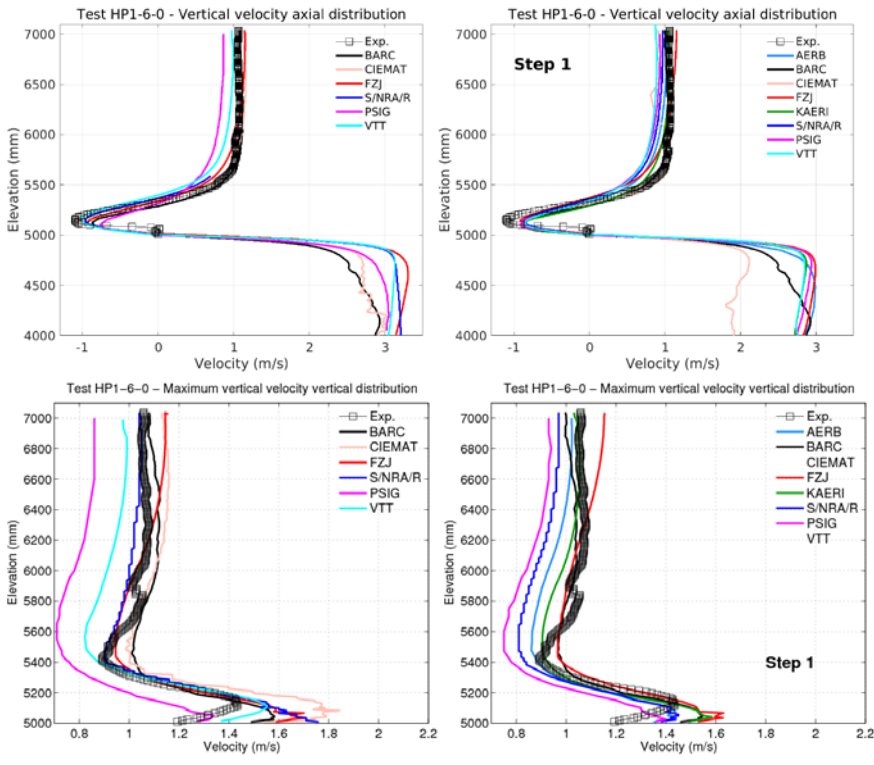


Figure 198: Open benchmark, Step 3: Axial velocity and maximum velocity vertical profiles for Step 3, compared with results for Step 1.

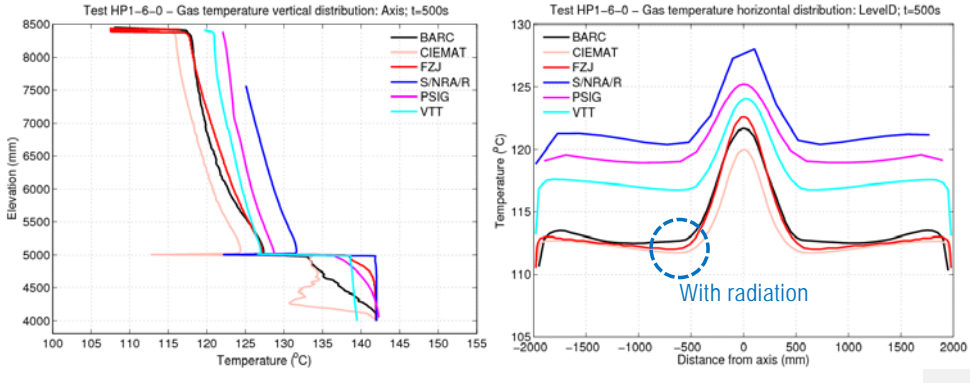


Figure 2049: Open benchmark, Step 3: Axial temperature profile and horizontal profile at 6.3 m.

1
2
3
4
5
6
7
8
9
10
11
12
13
14
15
16
17
18
19
20
21
22
23
24
25
26
27
28
29
30
31
32
33
34
35
36
37
38
39
40
41
42
43
44
45
46
47
48
49
50
51
52
53
54
55
56
57
58
59
60
61
62
63
64
65

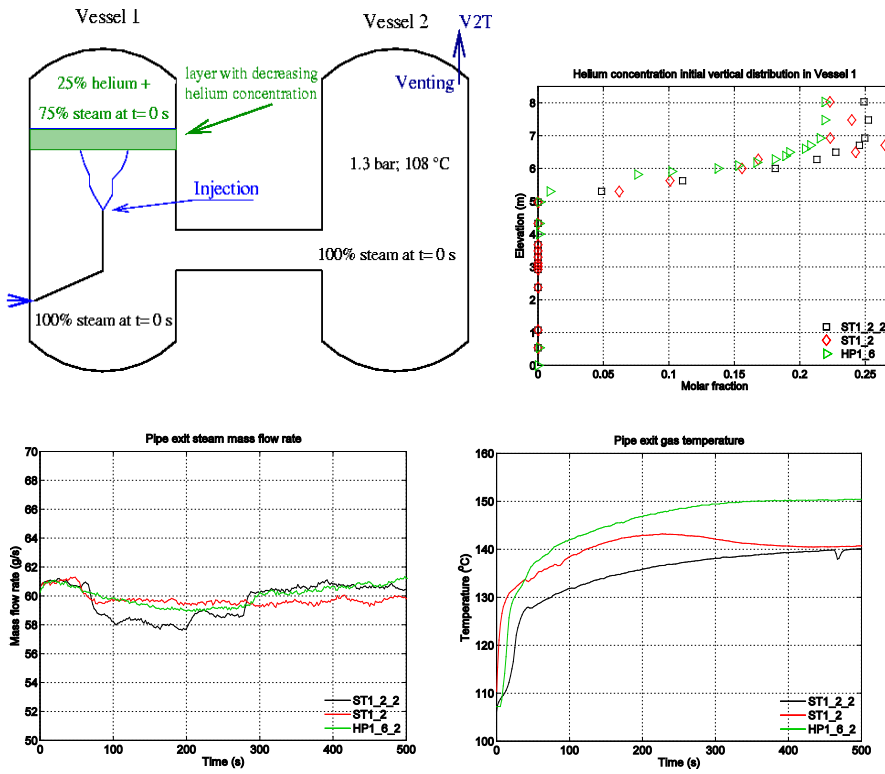


Figure 219: Open benchmark, Step 5: Configuration for SETH-2 test ST1_2_2, and important initial and boundary conditions of test ST1_2 and repetition test ST1_2_2 compared with those used for Test HP1_6_2.

1
2
3
4
5
6
7
8
9
10
11
12
13
14
15
16
17
18
19
20
21
22
23
24
25
26
27
28
29
30
31
32
33
34
35
36
37
38
39
40
41
42
43
44
45
46
47
48
49
50
51
52
53
54
55
56
57
58
59
60
61
62
63
64
65

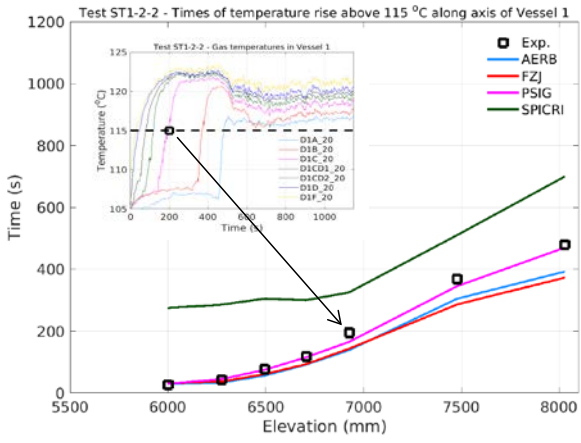


Figure 224: Open benchmark, Step 5: Progression of erosion along the axis in test ST1_2_2, using gas temperature rise times.

1
2
3
4
5
6
7
8
9
10
11
12
13
14
15
16
17
18
19
20
21
22
23
24
25
26
27
28
29
30
31
32
33
34
35
36
37
38
39
40
41
42
43
44
45
46
47
48
49
50
51
52
53
54
55
56
57
58
59
60
61
62
63
64
65

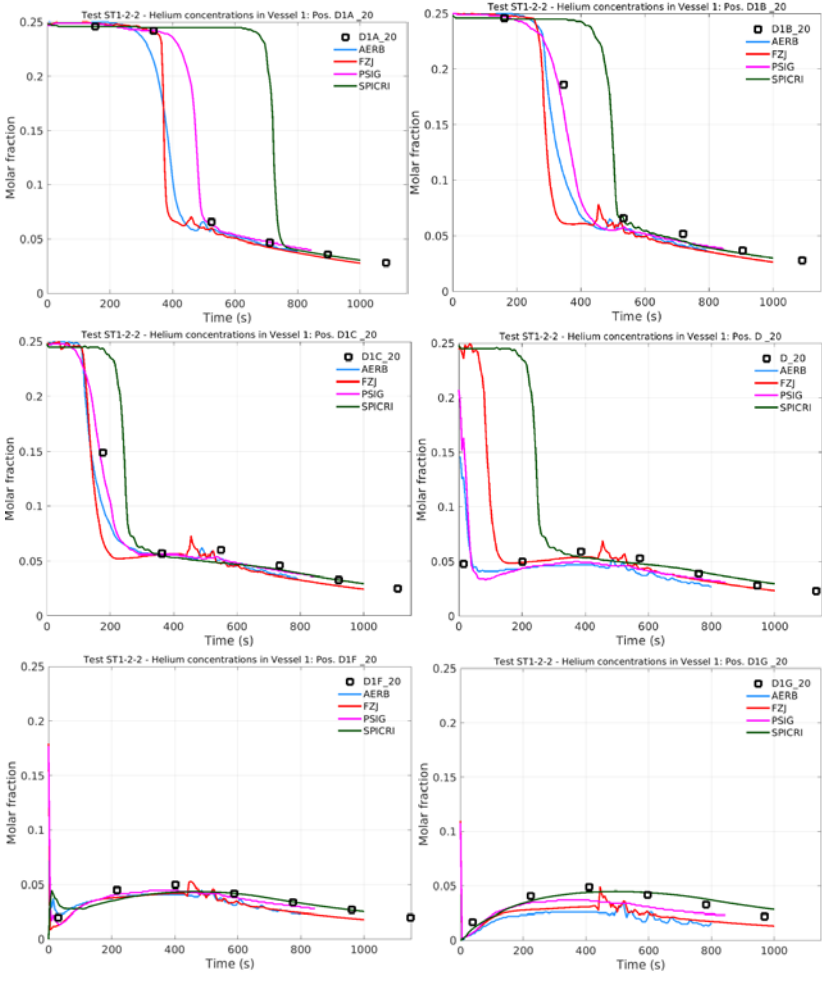


Figure 232: Open benchmark, Step 5: Helium concentration ~~evolutiontime histories~~ at various elevations along the axis of Vessel 1.

1
2
3
4
5
6
7
8
9
10
11
12
13
14
15
16
17
18
19
20
21
22
23
24
25
26
27
28
29
30
31
32
33
34
35
36
37
38
39
40
41
42
43
44
45
46
47
48
49
50
51
52
53
54
55
56
57
58
59
60
61
62
63
64
65

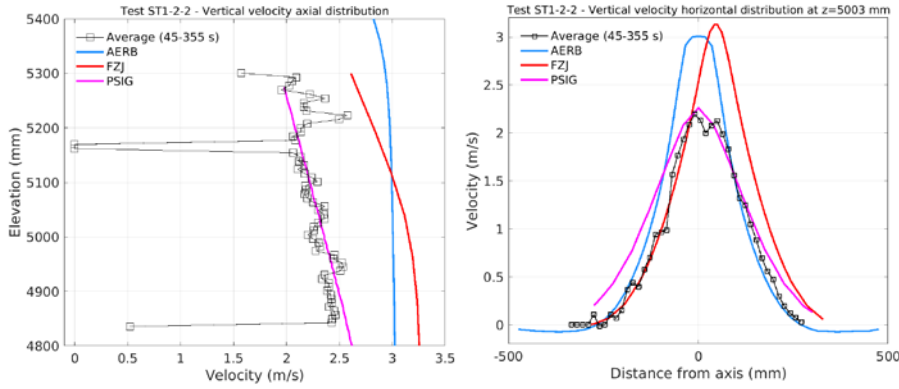


Figure 243: Open benchmark, Step 5: Vertical velocity axial profile (left) and horizontal profile at $z=5003$ mm (1 m above pipe exit)

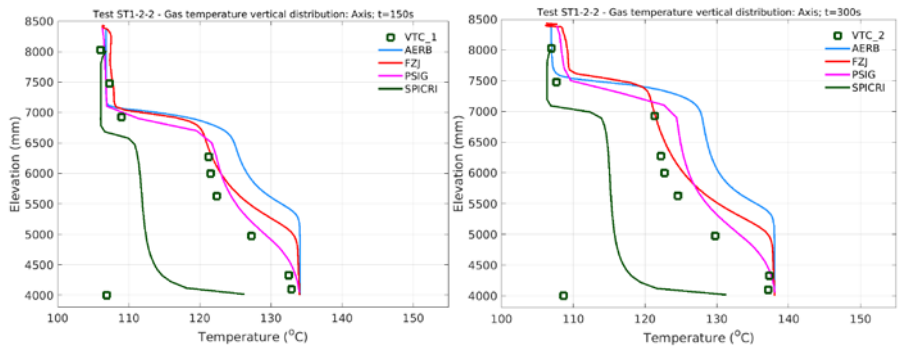


Figure 254: Open benchmark, Step 5: Axial temperature profile at two times.

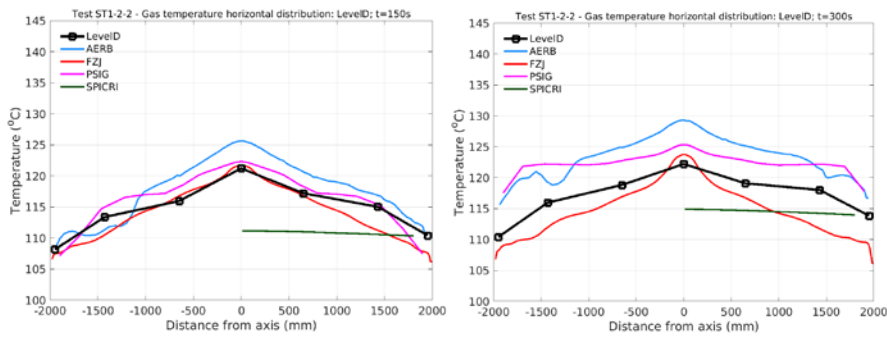


Figure 265: Open benchmark, Step 5: Horizontal profiles at 6.3 m at 150 s (before mixing) and 300 s (after mixing)

1
2
3
4
5
6
7
8
9
10
11
12
13
14
15
16
17
18
19
20
21
22
23
24
25
26
27
28
29
30
31
32
33
34
35
36
37
38
39
40
41
42
43
44
45
46
47
48
49
50
51
52
53
54
55
56
57
58
59
60
61
62
63
64
65

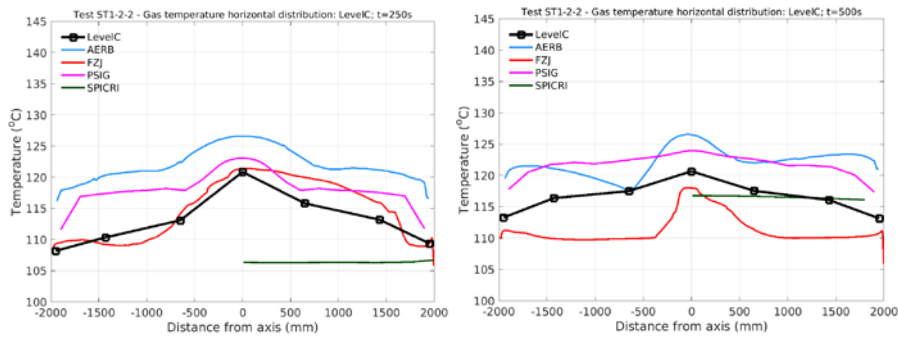


Figure 276: Open benchmark, Step 5: Horizontal profiles at 6.93 m at 250 s (during mixing or immediately after) and 500 s (after mixing)

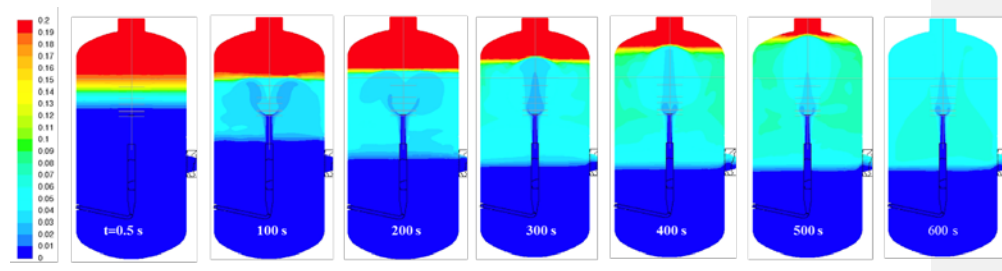


Figure 28: Open benchmark, Step 4: Calculated sequence of spatial distributions of helium concentrations at various times (contribution of VTT).

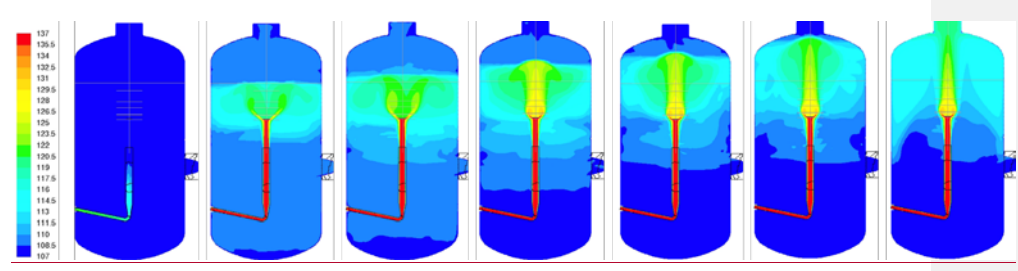


Figure 29: Open benchmark, Step 4: Calculated sequence of spatial distributions of gas temperatures at various times (contribution by VTT).

1
2
3
4
5
6
7
8
9
10
11
12
13
14
15
16
17
18
19
20
21
22
23
24
25
26
27
28
29
30
31
32
33
34
35
36
37
38
39
40
41
42
43
44
45
46
47
48
49
50
51
52
53
54
55
56
57
58
59
60
61
62
63
64
65

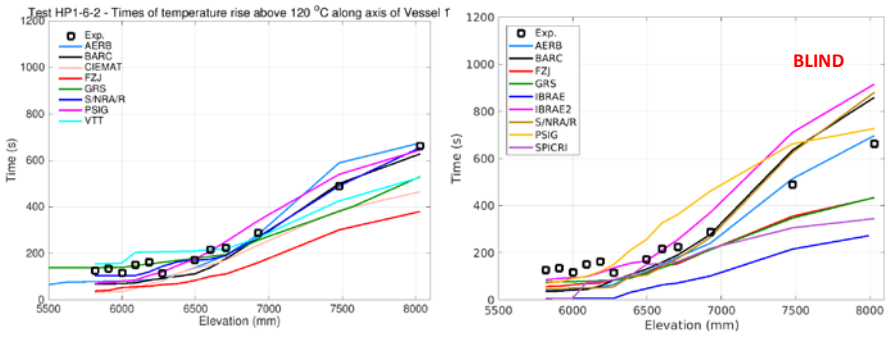


Figure 3027: Open benchmark, Step 4: Erosion progression calculated in the open phase (left), compared with best estimate results contributed to the blind benchmark.

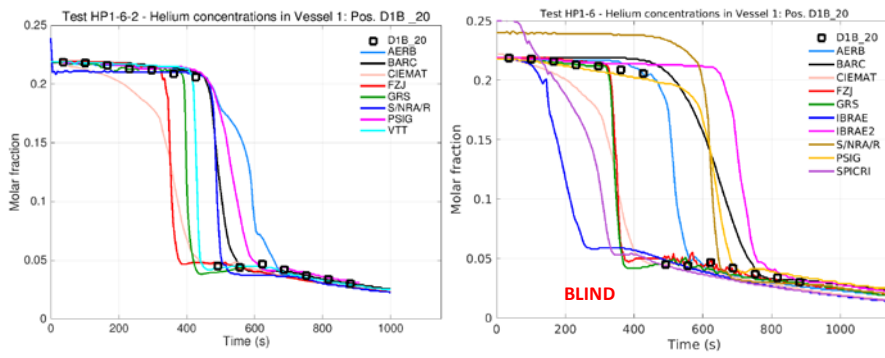
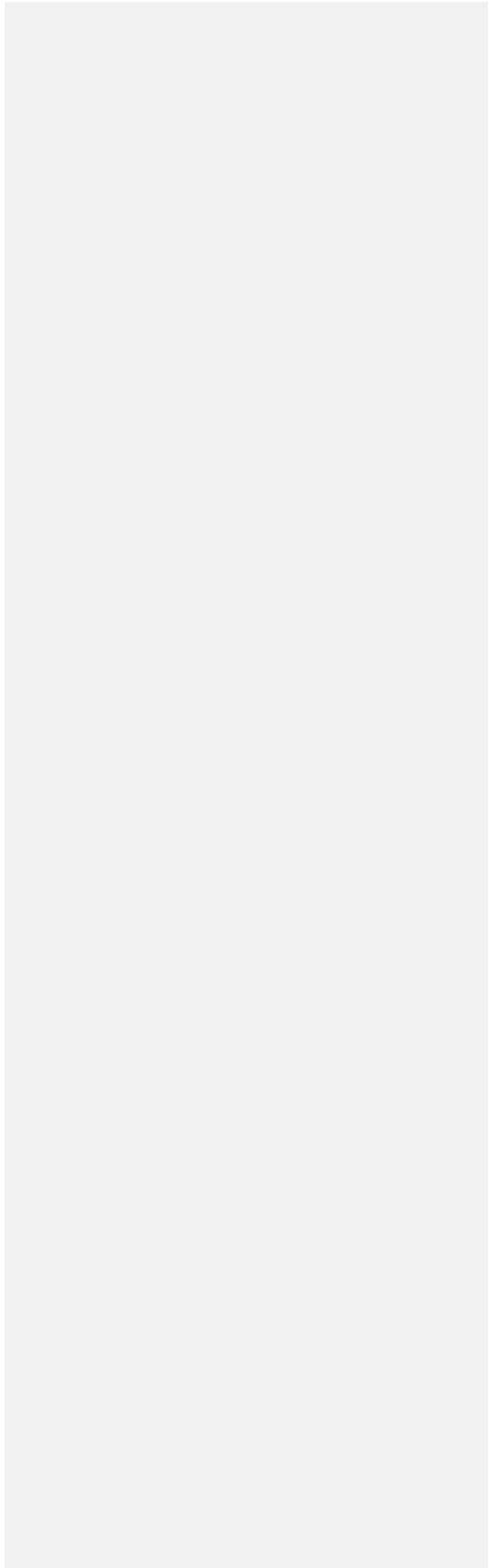
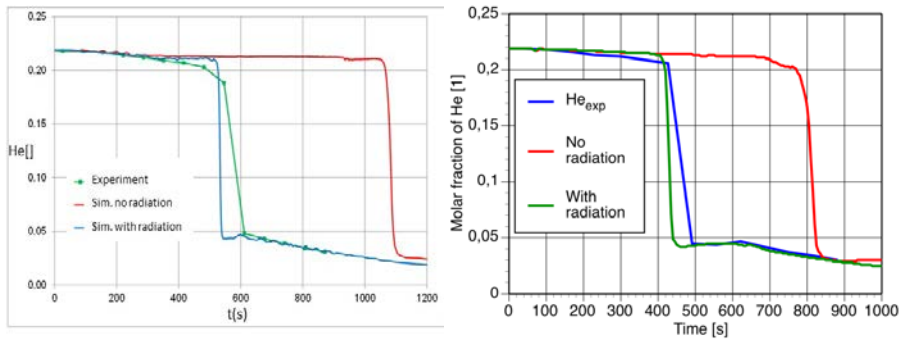


Figure 3128: Open benchmark, Step 4: Helium concentration evolutiontime-history at z=6.48 m calculated in the open phase (left), compared with best estimate results contributed to the blind benchmark.



1
2
3
4
5
6
7
8
9
10
11
12
13
14
15
16
17
18
19
20
21
22
23
24
25
26
27
28
29
30
31
32
33
34
35
36
37
38
39
40
41
42
43
44
45
46
47
48
49
50
51
52
53
54
55
56
57
58
59
60
61
62
63
64
65

Figure 3229: Open benchmark, Step 4: Example of results (helium concentration ~~evolution~~ ~~time~~ ~~histories~~) obtained at 8 m (left) by GRS (Schramm et al., 2017) and at 7.5 m (right) by VTT (Huhtanen, 2018) using the model for radiation or neglecting it.

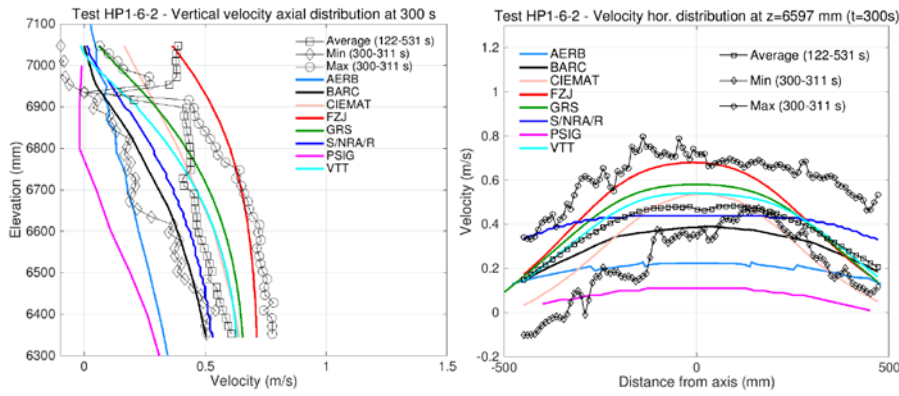


Figure 330: Open benchmark, Step 4: Vertical velocity averaged axial and horizontal profiles in the PIV window.

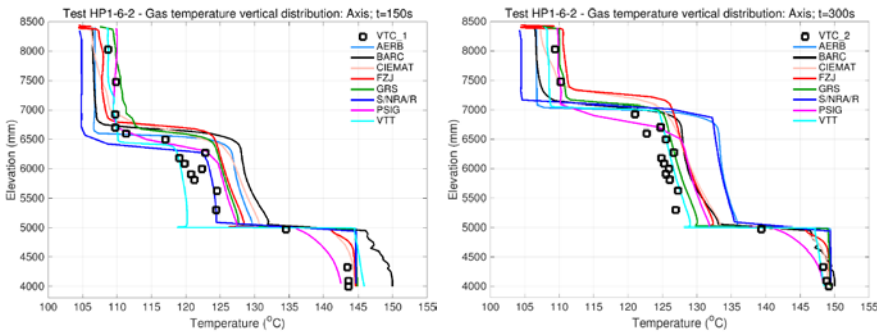
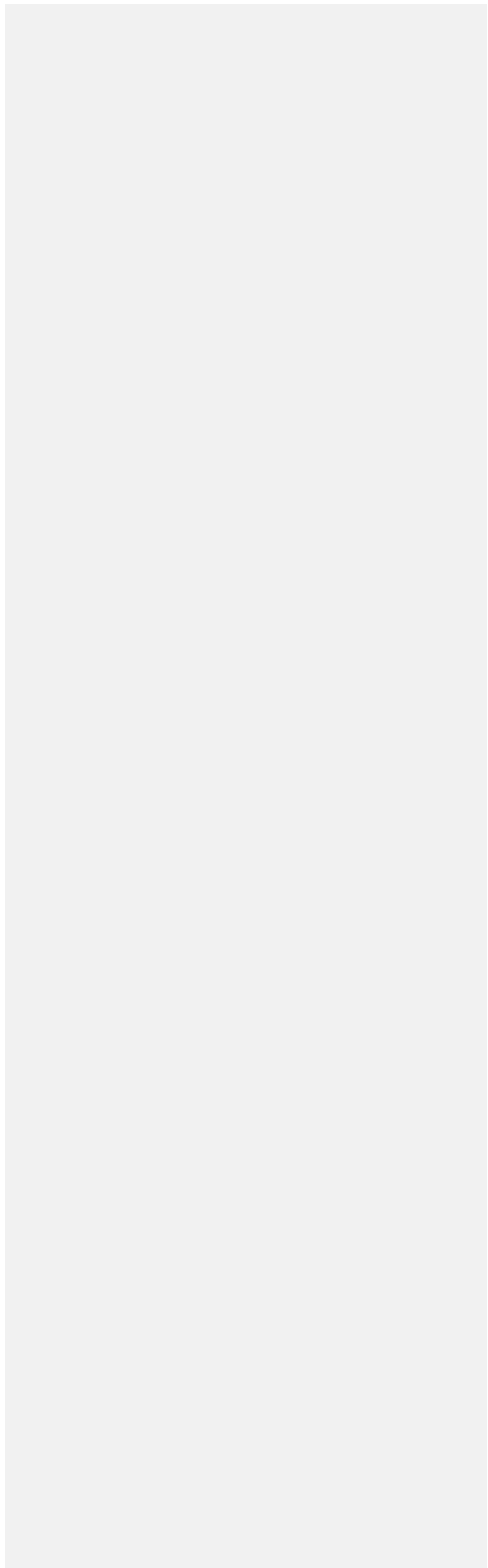
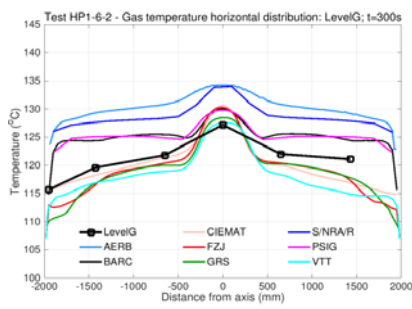
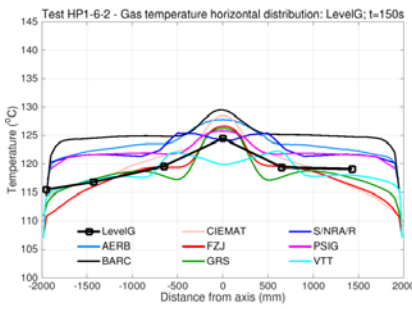
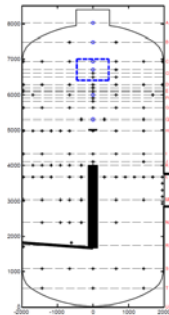
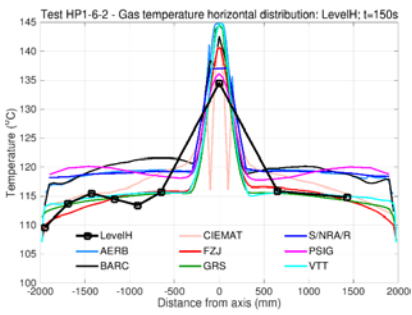


Figure 344: Open benchmark, Step 4: Axial gas temperature distributions at two times.

1
2
3
4
5
6
7
8
9
10
11
12
13
14
15
16
17
18
19
20
21
22
23
24
25
26
27
28
29
30
31
32
33
34
35
36
37
38
39
40
41
42
43
44
45
46
47
48
49
50
51
52
53
54
55
56
57
58
59
60
61
62
63
64
65



1
2
3
4
5
6
7
8
9
10
11
12
13
14
15
16
17
18
19
20
21
22
23
24
25
26
27
28
29
30
31
32
33
34
35
36
37
38
39
40
41
42
43
44
45
46
47
48
49
50
51
52
53
54
55
56
57
58
59
60
61
62
63
64
65

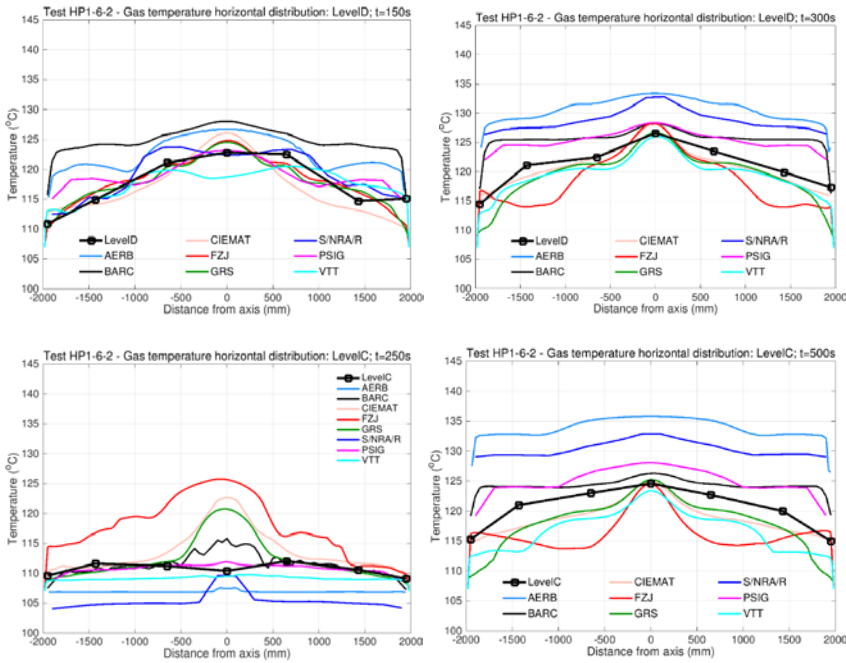


Figure 352: Open benchmark, Step 4: Gas temperature horizontal profiles at various elevations and two times.

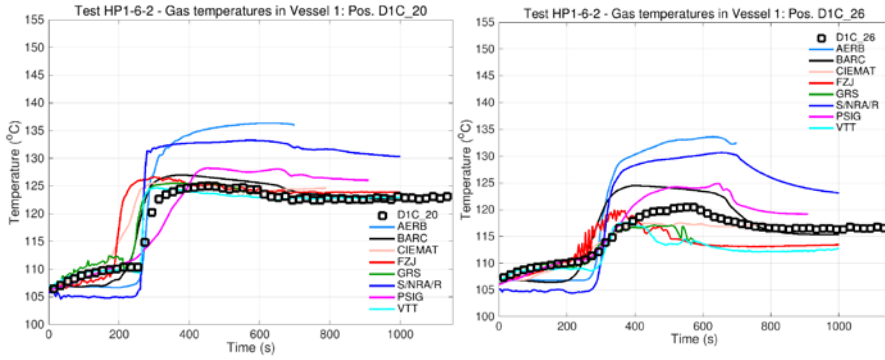


Figure 363: Open benchmark, Step 4: Gas temperature evolutiontime histories at two positions (left: on the axis; right: at 570 mm from the wall) at 6.5 m.

1
2
3
4
5
6
7
8
9
10
11
12
13
14
15
16
17
18
19
20
21
22
23
24
25
26
27
28
29
30
31
32
33
34
35
36
37
38
39
40
41
42
43
44
45
46
47
48
49
50
51
52
53
54
55
56
57
58
59
60
61
62
63
64
65

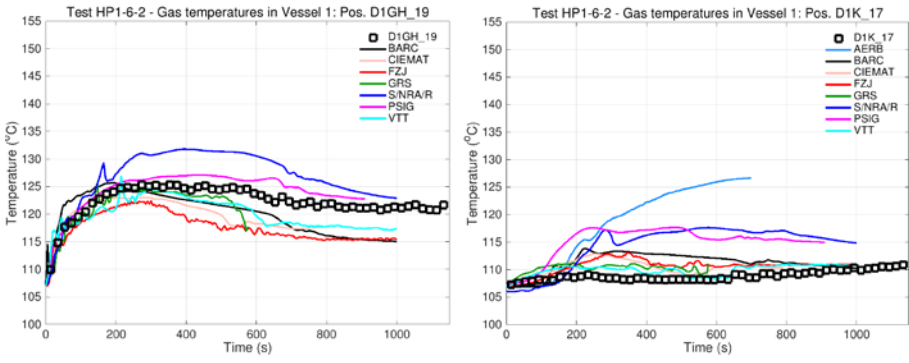
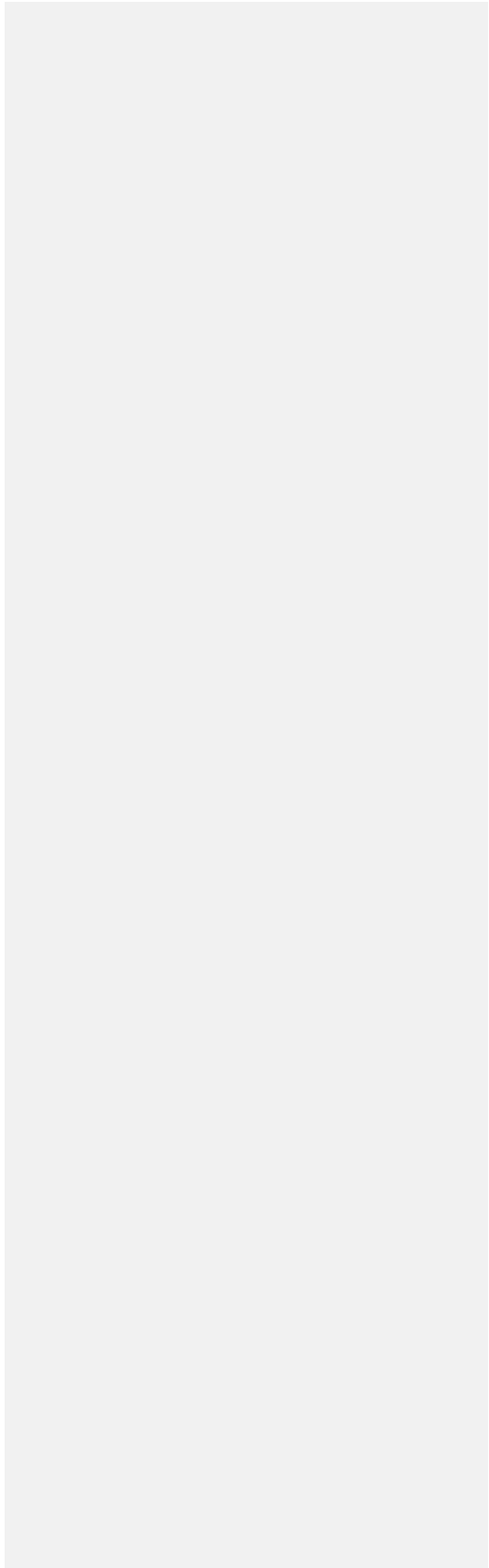


Figure 374: Open benchmark, Step 4: Off-axis ($r: \pm 325$ mm) gas temperature ~~evolution~~time histories at two positons below the initial bottom of the helium layer ($z: 5301$ and 4000 mm, respectively)



REFERENCES

Abe, S., Studer, E., Ishigaki, M., Sibamoto, Y., and Yonomoto, T. (2018) “Stratification Breakup by a Diffuse Buoyant Jet: The MISTRA HM1-1 and 1-1bis Experiments and their CFD Analysis”, *Nucl. Eng. Design*, **331**, pp. 162–175.

Abu-Romia, M.M. and Tien, C.L (1967) “Appropriate Mean Absorption Coefficients for Infrared Radiation of Gases”, *Journal of Heat Transfer*, **89**(4), 321-327.

Allelein, H.-J., Fischer, K., Vendel, J., Malet, J., Studer, E., Schwarz, S., Houkema, M., H. Paillère, H., Bentaib, A. (2007). International Standard Problem ISP-47 on Containment Thermal Hydraulics. Nuclear Energy Agency, Committee on the Safety of Nuclear Installations, Final Report NEA/CSNI/R(2007)10, 2007.

Allein, H.-J., Reinecke, E.-A., Belt, A., Broxtermann, P., and Kelm, S. (2012) “Combined Analytical and Experimental Investigations for LWR Containment Phenomena”, *Nucl. Eng, Technol.*, **44**(3), 249-260.

Andreani, M., Badillo, A., and Kapulla, R. (2016a) “Synthesis of the OECD/NEA-PSI CFD Benchmark Exercise”, *Nucl. Eng. Design*, **299**, 59-80

Andreani, M., Daqiang, Y., Gaikwad, A.J., Ganju, S., Gera., B., Grigoryev, S., Herranz, L.E., Huhtanen, R., Kanaev, A., Kelm, S., Kim, J., Nishimura, T., Schramm, B., Sharabi, M., and Paladino, D. (2016b) “Synthesis of a blind CFD benchmark exercise based on a test in the PANDA facility addressing the stratification erosion by a vertical jet in presence of a flow obstruction”, OECD/NEA 6th Workshop on Computational Fluid Dynamics for Nuclear Reactor Safety (CFD4NRS-6), MIT, Cambridge, MA-USA, 13-15 September, 2016.

Andreani, M. and Paladino D., (Benchmark Report, 2018), prepared by PSI (with appendices contributed by AERB, FZJ and VTT) (2018) “OECD/NEA HYMERES project: synthesis of results of the benchmark on PANDA test HP1_6_2”, PSI Technical Note AN-42-17-07 Rev.1, Project report HYMERES-P-17-48, May 2018.

Bentaib, A., Meynet, N., and Bleyer, A. (2015) “Overview on Hydrogen Risk Research and Development Activities: Methodology and Open Issues”, *Nucl. Eng. Technol.*, **47**, 26-32.

Breitung, W. and Royl, P. (2000) “Procedure and Tools for Deterministic Analysis and Control of Hydrogen Behavior in Severe Accidents”. *Nucl. Eng. Design*, **202**, 249-268.

Chan, C.K. and Jones, S.C. (1997) “Gas Mixing Experiments in a Large Enclosure”, Proc. of the 18th Annual Conf. of the Canadian Nuclear Society

Choi, Y.-S., Lee, U.-J., and Park, G.-C. (2001) “Study on local hydrogen behaviors in a subcompartment of the NPP containment”, *Nucl. Eng. Design*, **208**, 99-116.

Deri, E., Cariteau, B., and Abdo D. (2010) “Air fountains in the erosion of gaseous stratifications”, *Int. J. Heat and Fluid Flow*, Volume **31**, Issue 5, Pages 935–941.

Erkan, N., Mignot, G., Kapulla, R., Paladino, D., Zboray, R., Strassberger, H.J., Bissels, W. and Fehlmann, M. (2009) “OECD SETH-2 PANDA Test ST1_2_2 Quick-Look Report”, PSI internal technical report TM-42-09-07-0, April 2009.

Filippov, A.S., Grigoryev, S.Yu., O.V. Tarasov, O.V. (2017) “On the possible role of thermal radiation in containment thermal–hydraulics experiments by the example of CFD analysis of TOSQAN T114 air–He test”, *Nucl. Eng. Design*, **310**, 175-186.

Gallego E., Migoya E., Martín-Valdepeñas, J.M., Crespo, A., García, J., Venetsanos, A. Papanikolaou, E., Kumar, S., Studer, E., Dagba, Y., Jordan, T., Jahn, W., Høiset, S., Makarov, D., Piechna, J., (2007) “An intercomparison exercise on the capabilities of CFD models to predict distribution and mixing of H₂ in a closed vessel”, *International Journal of Hydrogen Energy*, **32**, 2235 – 2245

Gupta, S. (2015) “Experimental Investigations Relevant for Hydrogen and Fission Product Issues Raised by the Fukushima Accident”, *Nucl. Eng. Technol.*, **47**, 11-25.

Howell, J.R. (1988) “Thermal Radiation in Participating Media: The Past the Present, and Some Possible Futures”, *Journal Heat Transfer*, **110**, 1220-1229.

Huhtanen, R. (2018), Private Communication.

Kapulla, R., Mignot, G., Paranjape, S., Suter, S., Fehlmann, M., and Paladino, D. (2015a) "OECD/NEA HYMERES Project: Jet/Plume interacting with flow obstruction HP1 Series. Test Series Report", PSI internal report TM-42-15-16, Rev.0, Project report HYMERES-P-15-26, Nov. 2015 (report restricted to project participants).

Kapulla, R., Paranjape, S., Mignot, G., Suter, S., Fehlmann, M., and Paladino D. (2015b) "OECD/NEA HYMERES Project: PANDA Tests HP1_6_0, HP1_7_0, HP1_8_0, and HP1_678_Disk Data Report", PSI internal report TM-42-15-13 Rev. 0, Project report HYMERES-P-15-25, October 2015 (report restricted to project participants).

Karwat, H. et al. (1999) "State-of-the-Art Report on Containment Thermal-hydraulics and Hydrogen Distribution", OECD/NEA group of experts, CSNI/R(99)-16 (1999).

Kelm, S., Ritterath, M., Prasser, H.-M., and Allelein, H.J. (2016a) "Application of the MINIPANDA Test Case 'Erosion of a Stratified Layer by a Vertical Jet' for CFD Validation", *Nucl. Eng. Design*, **299**, 124-135.

Kelm, S., Müller, H., and Allelein, H.-J. (2016b) "Importance of thermal radiation heat transfer modeling in containment typical flows", Paper submitted for presentation at the CFD4NRS-6, MIT, Cambridge, MA, USA, September 13-15.

Liang, R. et al., (2015) "Status Report on Hydrogen Management and Related Computer Codes", NEA/CSNI/R(2014)8,

Lopez-Alonso E., Papini D., and Jimenez G. (2017) "Hydrogen Distribution and Passive Autocatalytic Recombiner (PAR) Mitigation in a PWR-KWU Containment Type", *Annals of Nuclear Energy*, **109**, pp. 600-611.

Mahaffy, J., et al. (2015). Best Practice Guidelines for the Use of CFD in Nuclear Reactor Safety Applications - Revision" NEA/CSNI/R(2014)11.

Noutsopoulos, G.C. and Yannopoulos, P.C. (1989) "Axial Dilution in Obstructed Round Buoyant Jet", *Journal of Hydraulic Engineering*, **115**(1), pp. 71-81.

Nishimura, T., Hoshi, H. and Hotta, A. (2015) “Current Research and Development Activities on Fission Products and Hydrogen Risk after the Accident at Fukushima Daiichi Nuclear Power Station”, *Nucl. Eng. Technol.*, **47**, 1-10

OECD/NEA HYMERES-2 project (2017-2021).

OECD/NEA THAI Project (2010) “Hydrogen and Fission Product Issues Relevant for Containment Safety Assessment under Severe Accident Conditions” Final Report, 22 June 2010, Report NEA/CSNI/R(2010)3.

Paladino, D. and Dreier, J. (2012) “PANDA a Multi Purposes Integral Test Facility”, *Science and Technology of Nuclear Installations*, **2012**, Article ID 239319, doi:10.1155/2012/239319.

Paladino, D., Mignot, G., Kapulla, R., Zboray, R., Andreani, M., Tkatschenko, I., Studer, E., and Brinster, J. (2013) “OECD/SETH-2 Project: PANDA and MISTRA Experiments addressing Key Safety Issues for Water Reactor Containment”, Proceedings of the 15th International Topical Meeting on Nuclear Reactor Thermal-hydraulics (NURETH-15), paper 106, Pisa, Italy, 12-17 May 12-17, 2013.

Paladino, D., Andreani, M., Guentay, S., Mignot, G., Kapulla, R., Paranjape, S., Sharabi, M., Kisselev, A., Yudina, T., Filippov, Kamnev, M., Khizbullin, A., Tyurikov, O., Liang, Z., Daniele Abdo, D., Brinster, J., Dabbene, F., Kelm, S., Klauck, M., Götz, L., Gehr, R., Malet, J., Bentaib, A., Bleyer, A., Lemaitre, P., Porcheron, E., Benz, S., Jordan, T., Xu, Z., Boyd, C., Siccama, A., Visser, D. (2016) “Outcomes from the EURATOM–ROSATOM ERCOSAM SAMARA projects on containment thermal-hydraulics for severe accident management”, *Nuclear Eng. and Design*, **308**, 103–114.

Paranjape, S., Kapulla, R., Mignot, G. and Paladino D. (2018) “Gas Redistribution Caused by Interacting Heat Sources in the Presence of a Vertical Condenser,” 12th International Topical Meeting on Nuclear Reactor Thermal-Hydraulics, Operation and Safety (NUTHOS-12), Qingdao, China, October 14-18, 2018.

Sarikurt, F.S. and Hassan, Y.A. (2017) “Large Eddy Simulations of Erosion of a Stratified Layer by a Buoyant Jet”, *Int. J. of Heat and Mass Transfer*, Vol. **112**, p. 354-365.

Schramm, B., Stewering, J., and Sonnenkalb M. (2017) “Einsatz von CFD-Codes für die Simulation von unfalltypischen Phänomenen im Sicherheitseinschluss: Validierung und gezielte Modellerweiterung”, Anschlussbericht RS1526, 2017 GRS-472, ISBN 978-3-946607-55-7.

Schwarz, S., Fischer, K., Bentaib, A., Burkhardt, J., Lee, J.-J., Duspiva, J., Visser, D., Kytala, J., Royl, P., Kim, J., Kostka, P. and Liang, R. (2011) “Benchmark on Hydrogen Distribution in a Containment based on the OECD-NEA THAI HM-2 Experiment”, *Nucl. Technol.*, **175**(3), 594–603.

Smith B.L. (2009) “Identification and Prioritization of Generic Nuclear Safety Problems Requiring CFD Analysis”, Proc. 17th Int. Conf. on Nuclear Engineering (ICONE-17), Paper 75482, Brussels, Belgium, July12-16, 2009.

Studer, E., Brinster, J., Tkatschenko, I., Mignot, G., Paladino, D., and Andreani, M. (2012) “Interaction of a light gas stratified layer with an air jet coming from below: Large scale experiments and scaling issues”, *Nucl. Eng. Design*, **253**, 406-412.

Visser, D.C., Houkema, M., Siccama, N.B., and Komen, E.M.J. (2012) “Validation of a FLUENT CFD model for hydrogen distribution in a containment”, *Nuclear Engineering and Design*, **245**, 161–171.